THE VISCOSITY OF DACITIC LIQUIDS MEASURED AT CONDITIONS RELEVANT TO EXPLOSIVE ARC VOLCANISM: DETERMINING THE INFLUENCE OF TEMPERATURE, SILICATE COMPOSITION, AND DISSOLVED VOLATILE CONTENT

A Thesis presented to the Faculty of the Graduate School
University of Missouri-Columbia

In Partial Fulfillment
of the Requirements for the Degree

Masters of Science

---

by
BRIDGET M. HELLWIG

Dr. Alan G. Whittington, Thesis Supervisor

May 2006

The undersigned, appointed by the Dean of the Graduate School, have examined the thesis entitled:

THE VISCOSITY OF DACITIC LIQUIDS MEASURED AT CONDITIONS RELEVANT TO EXPLOSIVE ARC VOLCANISM: DETERMINING THE INFLUENCE OF TEMPERATURE, SILICATE COMPOSITION, AND DISSOLVED VOLATILE CONTENT

Presented by Bridget M. Hellwig

a candidate for the degree of Master of Science

And hereby certify that in their opinion it is worthy of acceptance.

_____

Alan G. Whittington

_____

Peter I. Nabelek

_____

Wouter Montfrooij

ACKNOWLEDGMENTS

I would like to thank Alan Whittington for his support, guidance, and patience throughout this project (and for being understanding when something broke). Thank you for giving me such a great opportunity. Next, I would like to thank Peter Nabelek and Wouter Montfrooij for being on my thesis committee. Thank you to Harald Behrens, Bastian Joachim and André Stechern at the Institut fur Mineralogie in Hannover, Germany for preparing my hydrous samples and to Bastian and Andre who also ran several of my hydrous samples on the parallel plate. I would also like to thank Oto Matias and Julio Cornejo for guiding us around Santiaguito and making the trip so enjoyable and memorable. ¡Usted es maravilloso! Thank you to Eddy Sanchez at INSIVUMEH for helping to make this trip possible. To the helicopter pilots who flew us around Santiaguito Dome Complex, thank you for showing us such a spectacular view of Santiaguito. I acknowledge the National Science Foundation for providing the funding for this project. I would like to thank Jackie Getson for spending so much quality time in the lab with me. It would have been dull without you. Finally, thank you to my parents and family, for always supporting and encouraging me to follow my dreams wherever they take me (even active volcanoes). And to Jason, thanks for your encouragement and for putting up with me through this whole project. I couldn't have done it without you!

TABLE OF CONTENTS

LIST OF FIGURES

LIST OF TABLES

THE VISCOSITY OF DACITIC LIQUIDS MEASURED AT CONDITIONS RELEVANT TO EXPLOSIVE ARC VOLCANISM: DETERMINING THE INFLUENCE OF TEMPERATURE, SILICATE COMPOSITION, AND DISSOLVED VOLATILE CONTENT

Bridget M. Hellwig

Dr. Alan G. Whittington **Thesis Advisor**

ABSTRACT

Viscosity is a major control on magma transport, differentiation, and eruptive style. Silicate liquid viscosity varies by orders of magnitude as a function of temperature, composition and dissolved volatiles. There is no predictive model for the viscosity of hydrous dacitic liquids, and these compositions play an important role in explosive volcanism. This study investigated the effects of variable bulk composition and water content on anhydrous and hydrous dacites.

Ten iron-free dacitic glasses were synthesized, with varying degrees of silicate polymerization. Five hydrous samples were made for two of the different anhydrous base compositions, with water contents varying from nominally anhydrous to about 5 wt.%. The viscosity of all samples was measured using parallel plate viscometry in the glass transition range (10^9 to $10^{12.5}$ Pa.s). Anhydrous samples were measured by concentric cylinder viscometry at super-liquidus temperatures ($10^{1.2}$ to 10^5 Pa.s). TVF equations, of the form $\log \eta = A + B/(T-C)$, allow liquid viscosities at magmatic temperatures and water contents to be estimated.

At 1100 K, the viscosity of anhydrous dacitic liquids decreases from 10^{10} to 10^{9} Pa.s with decreasing melt polymerization. At 1100K, liquids containing 1 and 5 wt.% dissolved water are about 5 and 7 orders of magnitude less viscous than anhydrous liquids, respectively. The results demonstrate that varying polymerization state of the liquids affects viscosity to a much lesser degree than water content and temperature. At magmatic temperatures of 1100K and water contents greater than 0.5 wt.%, dacite liquids are less viscous than either rhyolites or andesites.

CHAPTER 1 - INTRODUCTION

1.1 Overview

The purpose of this study is to determine the rheological effects of bulk composition, water and fluorine content on the viscosity of dacite and rhyodacite melts. Chapter 1 will discuss the background behind this study including the statement of purpose, the theoretical background, and the geological applications. The theoretical background will include outlining the general importance of viscosity in igneous processes, explore problems with current predictive models of viscosity, and summarize the results of previous studies of the effects of water and fluorine on the viscosity of silicate melts.

Chapter 2 will discuss the various methods used in this study. These methods include glass synthesis, including the addition of water and fluorine for some samples, density measurements, parallel plate and concentric cylinder viscometry. Chapter 3 will show the results of the measurements taken throughout this study and compare these results to those obtained in previous work. Chapter 4 will then discuss modeling the viscosity of hydrous melts, water speciation and solubility, and implications of the viscosity of hydrous dacites and rhyodacites for igneous processes in arc settings. Lastly, Chapter 5 will summarize the main findings of this study.

1.2 Introduction

Volcanism is a common, but fascinating geologic process that can have catastrophic effects on human populations, the environment, and climate. Volcanic activity in some settings can be fairly predictable, but the majority of the time, no one truly knows what is going to happen or if an eruption is imminent. There are a variety of

eruptive volcanic styles which occur throughout the world. These can range from effusive basaltic flows at shield volcanoes, to explosive stratovolcanoes, to very large (eruptive) caldera forming events. Subduction zones are the cause of arc volcanism, which can have a large impact on all aspects of life. The "Ring of Fire" includes the geologically significant margins, made up of a series of convergent plate boundaries, which surround the Pacific Ocean. It is known as the "Ring of Fire" because of the high abundance of active volcanoes. There have been many famous and significant volcanic eruptions associated with subduction zones including Vesuvius (79 A.D), Krakatoa (1883), Mt. Pelée (1902), Mt. St. Helens (1980), and Pinatubo (1991) (Figure 1.1).

In order to gain an understanding of the mechanics of volcanism, it is important to explore and examine the processes involved. These processes include magma formation by partial melting, magma transport, assimilation, fractional crystallization, and eruption style or emplacement as an intrusion. The key to understanding these volcanic processes is determining the dynamics behind them, including the thermodynamic and rheological properties of magmas. There are many parameters controlling volcanic activity, but viscosity is one of the most important parameters affecting the evolution and eruption style of silicate melts. Temperature, pressure, volatile content, chemical composition, bubble content, and crystal content are the main controlling factors on magma viscosity, and though viscosity is so important, it is still not well enough understood to be able to make reliable predictive models (Dingwell et. al., 1993). A better understanding of viscosity and its controlling factors needs to be developed in order to understand eruptive processes better. A good starting point for magma viscosity is to examine the liquid viscosity instead, because the physical effects of crystals can

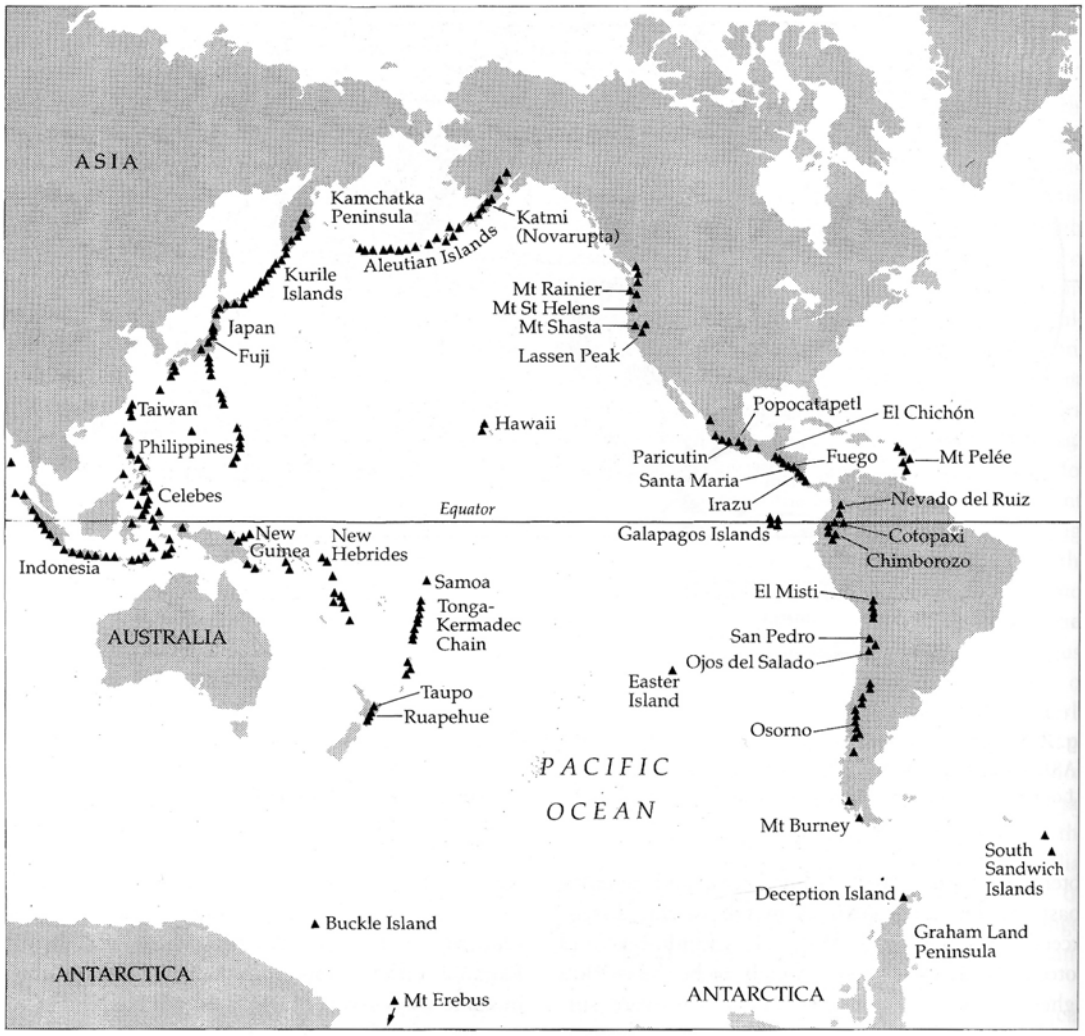

Figure 1.1. A map of the "Ring of Fire" and the volcanoes which surround it (Francis and Oppenheimer, 2004).

be accounted for with the Einstein-Roscoe equation (Marsh, 1981) and the rheological effects of bubbles are generally small, at least at low to moderate strain rates (Spera, 1974, 2000).

The purpose of this project was to analyze the effects of bulk composition, water and fluorine content on the viscosity of dacite and rhyodacite liquids. A variety of samples ranging from basalts to rhyolites have been studied previously, but there is a major gap between andesites and rhyolites, with virtually no data on dacite and

rhyodacite compositions. These compositions are important because they are a dominant component of explosive volcanism. Volatile bearing compositions are very important because dissolved volatiles greatly reduce magma viscosity, and volatile exsolution and subsequent bubble expansion is the driving force for explosive activity. The Santiaguito Dome Complex of Santa Maria Volcano in Guatemala was chosen as the ideal locality to examine first hand active explosive volcanism and also rhyodacite/dacite block lava flows, a feature which is extremely rare to witness. The compositions synthesized for this study were based on the compositions found at this locality.

1.3 Theoretical Background

1.3.1 Viscosity

There are many parameters which control volcanic activity, but viscosity is one of the most important. The viscosity of silicate melts exerts a strong control on many volcanic processes including the formation of magma, transport style, crystallization, fragmentation and most importantly, eruptive style. The main factors which control viscosity are temperature, pressure, volatile content, chemical composition, crystal content, and bubble content (Dingwell et al., 1993). Temperature, chemical composition, and volatile content have been found to have the greatest effect on viscosity and are thus the most significant to be measured and quantified because any small change in any of these factors may lead to changes in viscosity of several orders of magnitude. Even though viscosity is so important, it is still not well enough understood to be quantitatively predictable. Relatively reliable empirical models are available for hydrous rhyolitic liquids, but the viscosity of other compositions must be experimentally determined.

Silicate liquid viscosity has a non-Arrhenian behavior. This has been shown by measurements taken at low temperatures near the glass transition and measurements at high temperatures above the liquidus. Two methods have been used to measure the low temperature range in viscosity: the parallel plate and micropenetration viscometry techniques. The difference between the techniques is that the parallel plate measures the bulk deformation of a cylinder while the micropenetration measures the penetration of a rod into the surface layer of the sample. High temperature measurements can be performed using concentric cylinder viscometry for anhydrous samples at room pressures and the falling sphere method for volatile bearing liquids at high pressure. It is necessary to measure both the high and low temperature ranges because viscosity acts with a non-Arrhenian behavior and because most volcanic processes actually occur at intermediate temperatures, between the glass transition and the liquidus. By having measurements on both ends of the spectrum, the intermediate range can easily be interpolated rather than extrapolated, achieving better accuracy.

Many different equations have been used to relate viscosity to temperature. The simplest is the Arrhenian equation. It is a two parameter equation based on a constant activiation enthalpy for viscous flow (Shaw, 1972):

$$\log\eta = A + \frac{B}{T} \qquad (1.1)$$

A and B ($=\Delta H_\eta$) are both constants specific to individual compositions and water contents, T is the temperature and η is the viscosity of the melt. This equation works well for limited temperature ranges, but typically does not reproduce viscosity data well over a wide temperature range because silicate liquid viscosity has a non-Arrhenian behavior (i.e. it is non-linear with inverse temperature).

The Tammann-Vogel-Fulcher (TVF) equation (Tammann and Hesse, 1926; Fulcher, 1925; Vogel, 1921) is an empirical equation that is very commonly used for viscosity because it incorporates non-Arrhenian behavior:

$$\log\eta = A + \frac{B}{(T - C)} \qquad (1.2)$$

This equation is a three parameter equation where A, B and C are constants that vary with melt composition and water content. It is a good equation to fit non-Arrhenian behavior, but it is empirical in nature with no physical basis. The TVF equation works especially well for low temperature work. This equation also implies that there is a temperature at which viscosity would be infinite (Richet, 1984). The success of the TVF equation lies in its similarity to the Adam-Gibbs equation, described below (Russell et al., 2003)

A third equation for viscosity is based on the Adam-Gibbs configurational entropy theory (Adam and Gibbs, 1965). This theory allows for the derivation of the relationship between temperature and viscosity of a liquid by considering that viscous flow involves configurational changes (Richet, 1984):

$$\log\eta = A + \frac{B}{(TS^{conf})} \qquad (1.3)$$

where A and B are constants and S^{conf} is the configurational entropy at temperature T. S^{conf} can be obtained using equation 1.4:

$$S^{conf}(T) = S^{conf}(T_g) + \int_{Tg}^{T} \frac{C_p^{conf}}{T} dT \qquad (1.4)$$

where T_g is the glass transition temperature and C_p^{conf} is the configurational heat capacity. The C_p^{conf} is calculated by:

$$C_p^{conf} = C_{pL}(T) - C_{pg}(T_g) \qquad (1.5)$$

where C_{pL} is the heat capacity of a liquid at a specific temperature and C_{pg} is the heat capacity of the glass at the glass transition temperature (T_g). Glasses cannot undergo configurational changes, so the residual entropy of a glass at 0 K is its configurational entropy, which remains constant up to the glass transition (Neuville and Richet, 1991). Above T_g, the liquid can access more configurational states with increasing temperatures. From this theory, it can be determined that derivations from an Arrhenian behavior increase with the dependence of S^{conf} on temperature (Richet, 1984). The Adams-Gibbs theory provides a very simplified framework in which the dependence of viscosity on both temperature and composition can be understood and potentially modeled (Neuville and Richet, 1991). The problem with the theory is the requirement to know C_p^{conf} (T) for hydrous liquids. This remains generally unknown, although the first measurements have recently been made (Bouhifd et al., 2006).

As can be seen, the current viscosity equations cannot predict viscosity for hydrous dacite and rhyodacite compositions. By studying the effect of water content on the viscosity, a new model has the potential to emerge that is more accurate and reliable. New measurements directly applicable to volcanology may help to construct a thermodynamic model for the viscosity of hydrous silicate liquids.

1.3.2 Effect of Water

Volatiles can significantly affect both the chemistry and physical properties of silicate melts, and play a vital role in magmatic and volcanic processes (Huppert et al., 1982; Carroll and Holloway, 1994). Water content in particular is known to have a strong effect on the physical properties of both polymerized and depolymerized silicate melts. Bowen (1928) described water in magmatic systems as a “Maxwell demon” because as

he put it, it can do whatever it wants to. Water can specifically have effects on properties including phase equilibra, kinetics, density, and, importantly for this study, viscosity. Many geologic processes are therefore affected by the influence of water including formation of magma, transport style, crystallization, and eruptive style. The effects of water depend on both the amount of dissolved water in the melt and the anhydrous melt composition. Studying the effects of water can be difficult due to a wide range of water contents relevant to natural magmas, the dissolution mechanisms of water, the high pressure required to actually dissolve the water in a sample, and the difficulty in quenching depolymerized melts (Mysen and Richet, 2005).

How water affects melt composition has been investigated in detail and it has been found that water exists as at least 2 different water species in silicate melts: hydroxyl (OH^-) groups and molecular H_2O (Scholze, 1956). Stolper (1982) studied water speciation using infrared spectroscopy and deduced that the proportions of OH^- and molecular water vary systematically with the total amount of water within the sample. The principal solution mechanism described by this equilibrium is:

$$H_2O \text{ (molecular)} + O^{2-} \text{ (melt)} \leftrightarrow 2OH^- \text{ (melt)} \qquad (1.6)$$

This original model of Stolper (1982) has been refined and the equilibrium constant for this reaction is known to be a function of the composition of the melt, temperature, pressure, and total water content. The model shows that when water is added to the melt, it enters first as OH^-, which coincides with a dramatic decrease in melt viscosity. As more water is added, then the water goes into the melt mostly as molecular water, which has a smaller effect on the viscosity of a melt. Speciation measured *in situ* shows that

the proportion of OH^- increases at high temperatures in the melt (Nowak and Behrens, 1995; Shen and Keppler, 1995).

In the past, measurements using falling sphere viscometry (Shaw, 1963; Periskov et al., 1990) in an internally heated pressure chamber were made to determine the effects of water, but these experiments were restricted to low viscosities which could be measured using the falling sphere method, without any measurements at subliquidus temperatures or the glass transition. The glass transition is a range over which a glass will transform from a brittle condition (glass) to a plastic or viscous (liquid) condition. In order to truly understand dissolved water effects, observations are needed near the glass transition for two reasons. First, variations in viscosity due to minor compositional differences between samples are greater at lower temperatures. Secondly, at high temperatures, the water is exsolved readily at atmospheric pressures, so accurate measurements on hydrous samples cannot be taken. Developments were made when it was determined that near the glass transition the water exsolution within a sample is slow and water can be kept dissolved metastably at room pressure in the supercooled liquid. This allowed for accurate measurements to be performed at room pressure on water bearing silicate liquids (Lejeune et al., 1994; Richet et al.,1996).

Since then, many experiments have been run in order to quantify the effects of water. Experiments have been run on three main types of compositions, each having its own purpose. The first types of composition examined are those with simple mineral end-member compositions. Some examples of these include $NaAlSi_3O_8$ (albite) and $CaAl_2Si_2O_8$ (anorthite). The purpose of looking at these is to gain insight on the effects of different components within the melt and their effect on viscosity. These studies have

led to the development of both empirical and theoretical models including the configurational entropy model of Neuville and Richet (1991) for $(Ca,Mg)_3Al_2Si_3O_{12}$ and $(Ca,Mg)SiO_3$ liquids, models on hydrous $NaAlSi_3O_8$ (Romano et al, 2001; Whittington et al., 2004) and others which apply to granites (e.g. Baker and Vaillancourt, 1995; Baker, 1998; Holtz et al., 1999).

The second type of compositions examined are synthetic glass compositions which are based on a specific type of magma composition. Synthetic samples are made with a few important components, but Fe is typically left out because of its promotion of crystallization within the sample. Several studies have been conducted on simple $(SiO_2$-$NaAlSi_3O)_8$-$KAlSi_3O_8$ (haplogranite) compositions (Dingwell et al. 1996; Schulze et al., 1996; Dingwell et al., 1998a, 1998b; Schulze et al., 1999).

Other less polymerized melts have also been examined including andesites (Richet et al., 1996; Liebske et al., 2003), tephrites and foidites (Whittington et al., 2000), phonolites (Whittington et al, 2001), and trachytes (Whittington et al., 2001). The amount of depolymerization within a sample can be indicated by the NBO/T ratio which is a calculated ratio of the non-bridging oxygens to the tetrahedrally coordinated cations within a melt structure and approximates the actual structural state of a liquid (Mysen, 1988). The silicic compositions mentioned above tend to have low NBO/T values indicating that they are highly polymerized, while the more depolymerized compositions have higher NBO/T values.

The last type of compositions which have been examined are natural samples, collected from either a pluton or lava flow. These samples are more difficult to examine due to their crystal content and bubble content in determining their viscosity, so these

studies are typically conducted on remelted samples. Some natural sample experiments include rhyolites from various locations (Stevenson et al, 1998; Zhang et al., 2003), phonolites from Tenerife (Giordano et al., 2000), basalts from Etna (Giordano and Dingwell, 2003a) leucogranites from the Himalayas (Scaillet et al, 1996; Whittington et al., 2004), and trachytes (Romano et al., 2003; Giordano et al., 2004).

Even though there have been many different studies on various melt compositions described above, there is an important gap in our present knowledge of hydrous melt viscosity between granitic or rhyolitic compositions and the andesite of Richet et al. (1996). One major gap in our current knowledge for silicic melts is dacite and rhyodacite compositions and this is why they were chosen for this study.

Though these studies have provided a lot of useful information about the properties of silicate melts and their viscosities, they are still limited. Various empirical models have been proposed from previous results, but they are limited because most experiments have been restricted to anhydrous compositions (Bottinga and Weill, 1972; Giordano and Dingwell, 2003b). Other restrictions include that most liquids have been measured only at high temperatures, and only narrow compositional ranges are measured. Viscosities near the glass transition need to be measured because viscosity varies non-linearly with temperature, so that extrapolations from high temperature data are unreliable. Due to these limitations, there is no model which can reliably predict the viscosity of hydrous silicate melts over the wide range of magmatic compositions, temperatures and water contents found in nature. Models that have been developed (Bottinga and Weill, 1972; Shaw, 1972; Giordano and Dingwell, 2003) are all empirical

fits to data. A comprehensive model based in configurational entropy theory will require many years more work to measure heat capacities and other data.

Water content will cause the largest decrease in viscosity when the first 2 wt.% is added to the melt. There is a further decrease in viscosity when more than 2 wt.% water is added, but it is much less drastic and the decrease tends to level off at water contents greater than about 4% (Dingwell et al., 1996 and Richet et al.,1996). As an example, Figure 1.2 shows the strong effects of water on the viscosity of synthetic hydrous trachytes (Whittington et al., 2001). At a constant temperature, tremendous viscosity reduction can be easily observed with added water (Figure 1.3). The effects of water on the trachytes are expected to be quantitatively similar to what the dacite and rhyodacite will experience because they have broadly similar compositions.

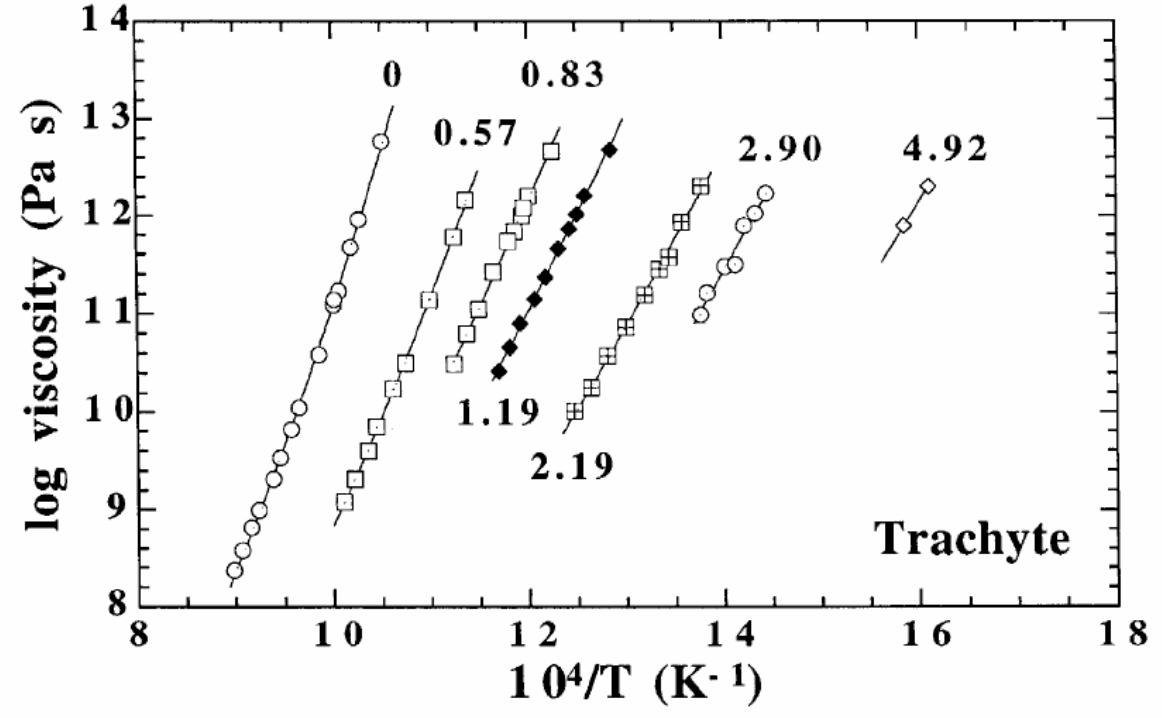

Figure 1.2. The effect of water on the viscosity of trachytes (Whittington et al., 2001).

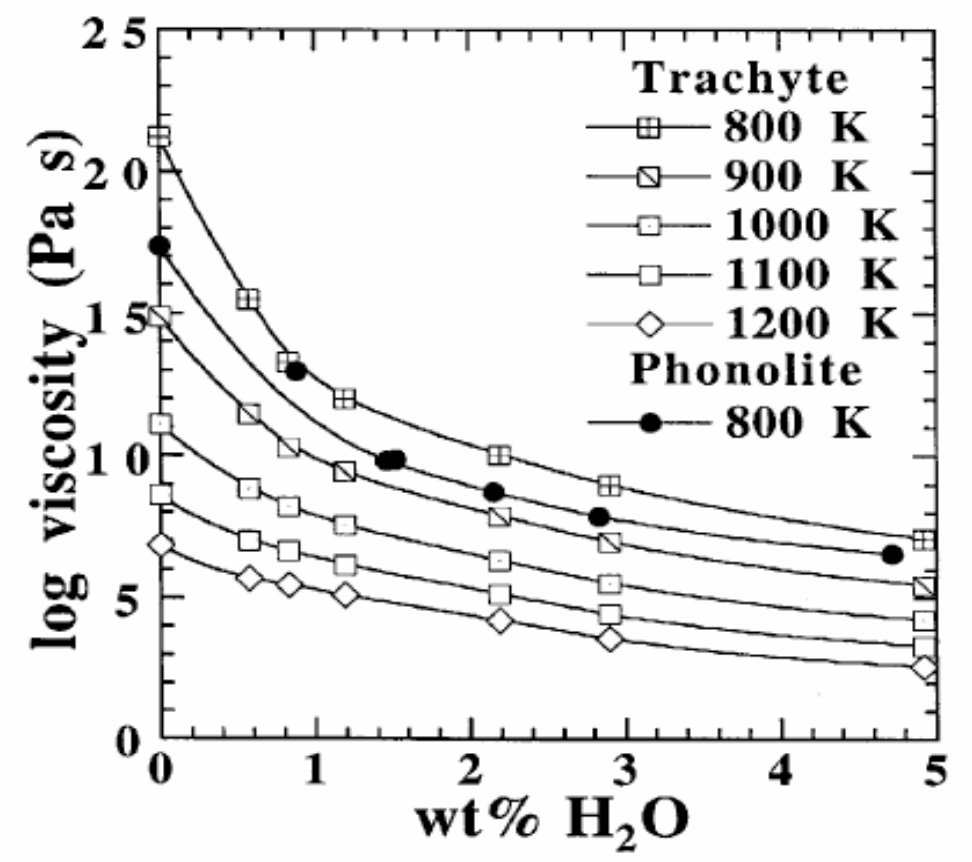

Figure 1.3. The viscosity of hydrous trachytes at constant temperatures with varying water content (Whittington et al., 2001).

Highly polymerized silicate melts tend to show a larger and non-linear viscosity decrease with increasing water content, while basalts and other depolymerized liquids show a less drastic and more linear decrease with increasing water content, indicating that silicic melts are more affected by water, at least at low temperatures near the glass transition (Figure 1.4). This change appears gradational, but a significant change can be observed around an NBO/T of 0.2, where compositions are more depolymerized (andesite, trachytes and phonolite). A significant observation can also be made in the fact that at low temperatures (<850 K) and moderate water contents (> about 1.5 wt.% H_2O) silicic liquids like the granite and rhyolite can become less viscous than the more

depolymerized liquids like basalt. This observation contradicts the common assumption that rhyolites are always much more viscous than basalts, an assumption which does hold true for anhydrous liquids.

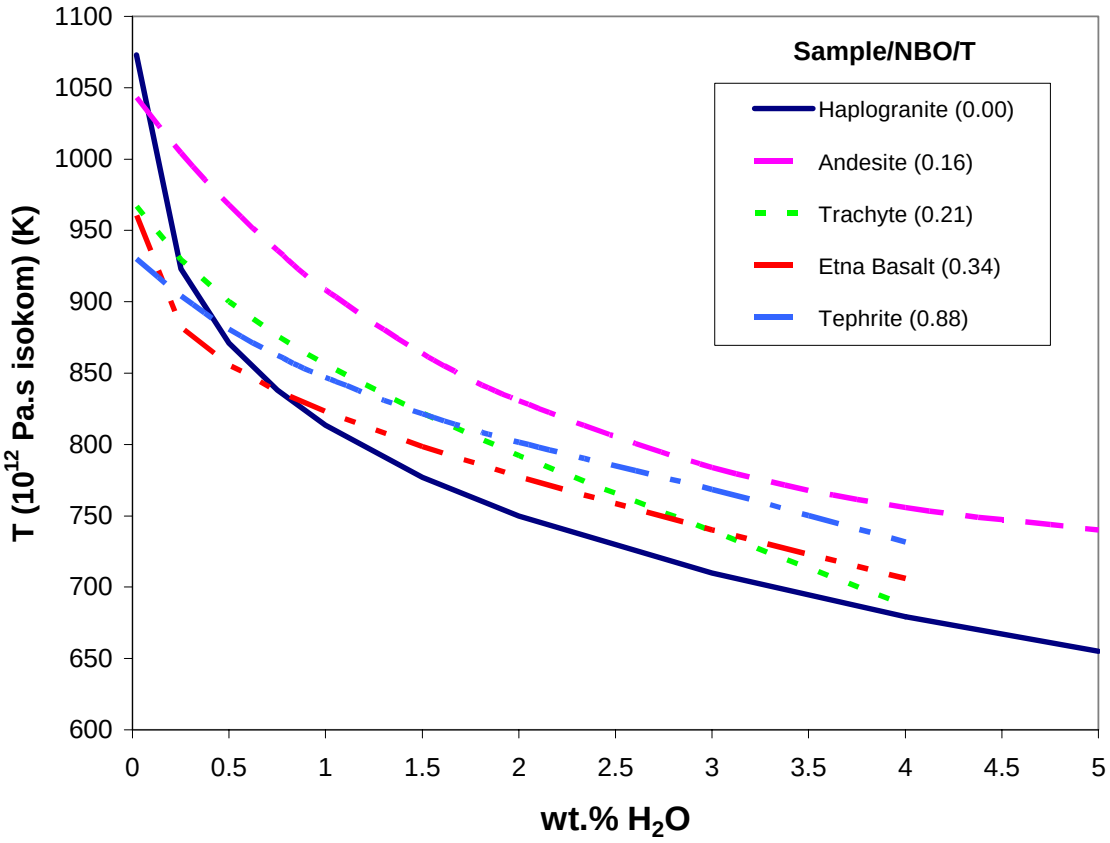

Figure 1.4. Various 10^{12} Pa-s temperatures of different silicate liquids as a function of water content. The lines are fitted to T^{12} calculated from TVF equations for each composition and water content from: Haplogranite (Dingwell et al. 1996), Andesite (Richet et al., 1996), Tephrite (Whittington et al. 2000), Trachyte (Whittington et al., 2001), and Etna Basalt (Giordano and Dingwell, 2003).

Water in silicate melts also tends to have less of an effect at higher temperatures, but studies cannot be performed at high temperatures due to limited water solubility, unless high pressure is applied. Besides decreasing the viscosity, water can also cause the temperature dependence of viscosity to move further away from Arrhenian behavior, i.e. becoming more fragile at higher water content (Dingwell et al., 1996 and Richet et

al., 1996) . Water was found to reduce the glass transition temperature similarly for intermediate magmas with a similar structural character, not dependent upon the exact nature of the network modifiers (Whittington et al., 2001) (Figure 1.5).

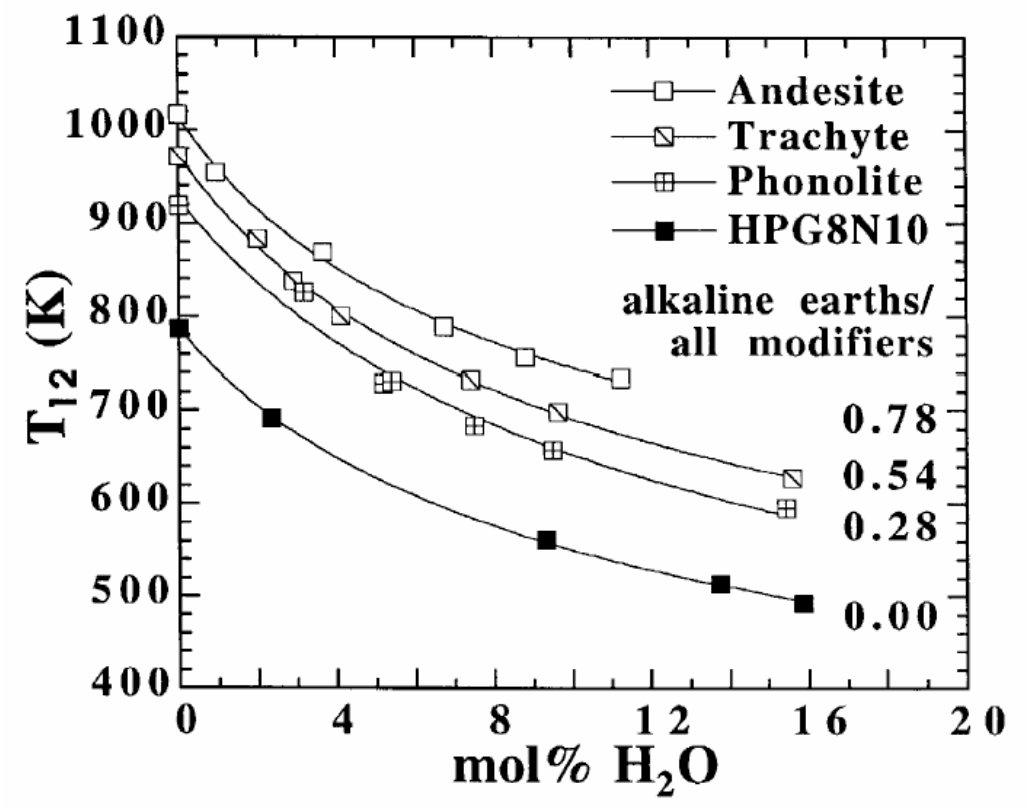

Figure 1.5. The glass transition temperatures of intermediate magmas with different alkali/alkaline earth ratios as function of water content. The experimental data is from Whittington et al. (2001) and Dingwell et al. (1998b) (figure by Whittington et al., 2001).

As described above, there is an important subset of polymerized compositions for which no data currently exists. Both dacites and rhyodacite compositions are extremely important because they are associated with explosive volcanic eruptions. These liquids can also form intrusive rocks such as granodiorites. Therefore, this study was designed to examine the effect of water on the viscosities of dacites and rhyodacites.

1.3.3 Effect of Fluorine

Water is not the only volatile that can have effects on the viscosity of silicate melts. Other volatiles which are important include F, CO_2, and Cl, among others. Fluorine has many known effects including increasing the solubility of water in a melt (Holtz et al., 1993), increasing diffusivities (Dingwell, 1987a), decreasing the density (Dingwell et al., 1993), and modifying the temperature of the glass transition in melts (Dingwell and Webb, 1992; Lange, 1994). The effects of fluorine depend on the specific silicate composition and become less important the more depolymerized the silicate melt (Dingwell et al., 1985; Dingwell, 1989). Dissolved fluorine will also cause a depression of the liquidus temperature resembling that caused by water (Wyllie and Tuttle, 1961; van Groos and Wyllie,1967; Luth, 1988a).

Fluorine is one of the most important volatiles in evolved volcanic suites and in late stage granitic systems (Giordano et al., 2004). Some examples of fluorine rich silicic magmas include topaz bearing rhyolites from Spor Mountain (Burt et al., 1982), Honeycomb Hills, Utah (Congdon and Nash, 1991), the macusanites from Peru (Pichavant et al., 1987) and hypabyssal and intrusive rocks with fluorine up to 5 wt% or higher (Bailey, 1977; Congdon and Nash, 1988; Kortemeier and Burt, 1988; Carroll and Webster, 1994). Fluorine has also been found in mafic igneous rocks up to 2 wt% (Aoki et al., 1981).

Few studies have measured the effects of fluorine on concentrations of up to 2 wt.% on the viscosity of silicate melts. Studies have been conducted at high temperatures on anhydrous fluorine-bearing phonolites to rhyolites and show that the reduction of the viscosity by fluorine increases with SiO_2 content of the melt (Dingwell et al., 1985).

Dingwell (1989) found that fluorine has almost no effect on the viscosity of diopside melts. Other studies include Persikov (1991) on hydrous granites with fluorine increasing the viscosity, on albite liquids where water was shown to have slightly larger effects in decreasing the viscosity than fluorine (Dingwell and Mysen, 1985; Baker and Vaillancourt, 1995), and on rhyolites (haplogranites) where the effect of fluorine is also slightly smaller than that of water (Giordano et al., 2004). Luth (1988) suggested that fluorine may slightly increase the viscosity of highly depolymerized liquids. Hess et al. (1995), using infrared spectroscopy, concluded that if the fraction of water inferred to be present as molecular water is subtracted, then water dissolved as OH^- has a much larger effect on decreasing the viscosity than fluorine. Most studies that have been conducted determined that fluorine, like water, will decrease the viscosities of both highly polymerized and moderately depolymerized melts by several orders of magnitude (Dingwell et al., 1985, 1993; Dingwell, 1989; Dingwell and Hess, 1998).

Currently, there is a debate on whether fluorine is dissolved within the silicate framework by substituting with oxygen or if it is isolated from the network to form complexes with other cations (Mysen and Cody, 2001; Giordano et al., 2004). Various types of fluorine complexes have been proposed. One involves the possible breakage of bridging oxygen bonds as interpreted by Raman spectroscopy (Yamamoto et al., 1983; Duncan et al., 1986). The exchange reaction can be written:

$$F_2O_{-1} + O^{2-} \leftrightarrow 2F^- \qquad (1.7)$$

Mysen and Virgo (1985) used Raman spectroscopy on SiO_2-NaF and SiO_2-AlF_3 glasses and concluded that a portion of dissolved fluorine exists as Si-F bonds, and more importantly as NaF or AlF_3 bonds. Spectroscopy studies therefore suggest that several

dissolution mechanisms of fluorine in silicate melts exist, depending on the melt composition. Each of these would affect the melt structure differently, some causing depolymerization, with others causing polymerization (Carroll and Webster, 1994). These may be expected to decrease and increase melt viscosity, respectively.

The first mechanism occurs when fluorine substitutes for oxygen forming Si-F bonds. In this scenario, one bridging bond is broken and replaced by two fluorine atoms, causing depolymerization (Mysen and Virgo, 1985a). This process is analogous to OH^- replacing a bridging oxygen in silicate melts when water is added (Mysen and Richet, 2005). Mysen and Virgo (1985b) showed that fluorine seems to be attracted to Na and Al more than to Si and proposed that fluorine may form charge-balanced complexes with Na and Al outside the silicate network, causing depolymerization.

Four different types of fluorine complexes have been discovered to occur in Al-bearing silicate glasses, which are relevant to magmatic compositions. Mysen et al. (2004) identified these using Raman and NMR spectroscopy on peralkaline and metaluminous silicate glasses. The complexes found include: (1) Na-F (-O) complexes (NF), (2) mixed F-O Na-Al-F complexes with $^{[4]}$Al (NAF), (3) Na-Al-F complexes with $^{[6]}$Al (CF), and (4) Al-F complexes with both $^{[4]}$Al and $^{[6]}$Al (TF). According to their study, the last three complexes are linked to the aluminosilicate network by bridging oxygens of Al-O-Si. The $^{[4]}$Al and $^{[6]}$Al mean that the Al is either in a 4-fold or 6-fold coordination with the rest of the melt structure. Precise structural details of these proposed complexes are not yet resolved.

Most of these complexes result in the depolymerization of the melt with the addition of fluorine. The Na/Al ratio of these complexes decreases as the Al/(Al+Si)

increases. The formation of these Na-Al bearing complexes may then lead to depolymerization of aluminosilicate melts because Al^{3+} reacts with fluorine to form Al-F bonds. The TF (referred to as the topaz-like structures) forms $Al_2(AlO_3)F_2$ when one Na^+ per Al^{3+} is released to become a network modifier for each Al^{3+}, again causing depolymerization. Lastly, the CF (referred to as the cryolite-like structures) can result in depolymerization because more Na^+ is released than Al, increasing the Na/Al ratio in the silicate framework. A special attribute of the CF complexes is that they can also result in melt polymerization. This can occur when some of the network modifying Na^+ is scavenged from the aluminosilicate to form these cryolite complexes (Mysen et al., 2004). Not much information has been gathered on Na-F complexes or if they cause depolymerization (Mysen and Richet, 2005). Changing bulk properties, such as viscosity, indicate fluorine overall acts mostly as a depolymerizer, weakening the melt structure (Giordano et al., 2004).

In order to truly understand the effects of fluorine, more studies need to be conducted, especially on more polymerized melts. This study will examine the effect of fluorine on both dacite and rhyodacite melt compositions. These compositions are slightly less polymerized then the various rhyolites and other melts previously studied and may contain fluorine in nature.

1.4 Geologic Setting

The field area chosen for this study was Santiaguito Dome Complex of Santa Maria Volcano in Guatemala. This area is unique due to the fact that it is the only volcano in the world to have active dacite lava flows. Santiaguito is a dome complex, composed of 4 main domes, located in the crater of Santa Maria Volcano (Figure 1.6). It

is located at 14.8°N latitude and 92.0°W longitude near Quetzaltenango, south west Guatemala (Figure 1.7). It is located in the Central American volcanic arc at the triple junction of the North American, Cocos and Caribbean plate boundaries where the Cocos plate is being subducted. The volcanic arc is a west to northwest trending belt of composite volcanoes stretching more than 100 km in length. Santa Maria was mostly constructed between 25,000 and 40,000 years ago, and now reaches an elevation of 3772 m above sea level (Rose, 1972b). The cone is composed mainly of basaltic andesite (Harris et. al., 2003).

Figure 1.6. A photo of the active dome Caliente of Santiaguito Dome Complex and Santa Maria Volcano (photo taken by Bridget Hellwig, 2005).

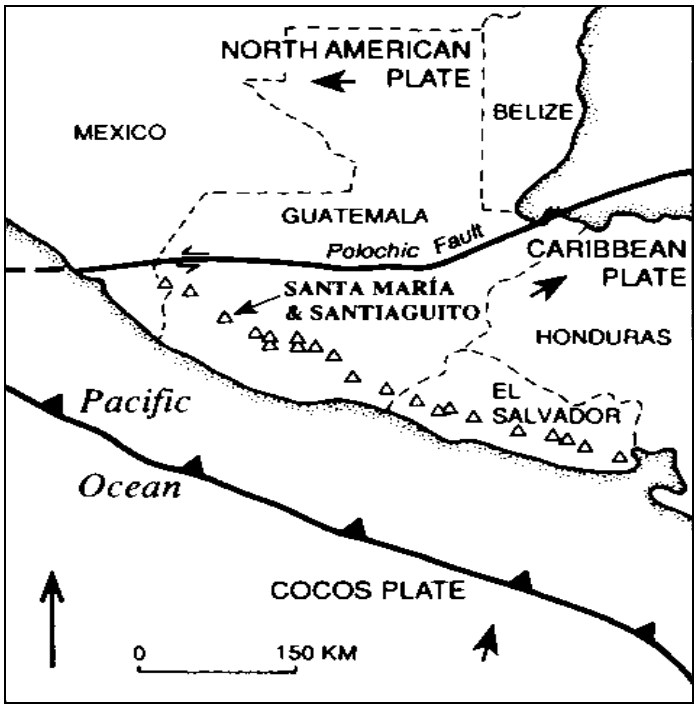

Figure 1.7. A location map of Santa Maria Volcano, Guatemala (Conway et al., 1994).

In 1902, Santa Maria experienced a Plinian eruption, ejecting primarily dacitic pumice and ash with a volume of 8.5 km^3, which left a crater of approximately 0.5 km^3 in size in the southwest flank of the volcano (Rose, 1972b). From 1902 on, Santa Maria continued to have minor volcanic activity until 1922 when lava extrusion began to occur in the crater, thus beginning the formation of Santiaguito dome complex. The dome complex grew between 1922 and 1984 by lava extrusion in a regular, cyclic pattern (Bluth and Rose, 2004). This regularity is one reason why Santiaguito is an ideal location to view active volcanic activity.

Santiaguito Dome Complex is characterized as a plug dome whose cyclic pattern produced the dome complex which grew in six spurts of extrusion (Rose, 1972b, 1978). These six episodes produced the four domes seen there today: Caliente, La Mitad, El Monje, and El Brujo (Figure 1.8). In 1922, Caliente Vent began with lava extrusion and pyroclastic eruptions and was considered the principal or central vent of the complex. It

also formed long block flows until 1939 when the activity shifted 700 m west of Caliente producing La Mitad. La Mitad also consisted of dome extrusion and lava flows. In 1949, El Monje dome began activity with initially high extrusion rates producing the new dome. Another westward shift occurred in 1958 forming El Brujo vent about 1.5 km west of Caliente vent, and included increased block flow activity. In 1972, extrusion continued at El Brujo, but also began again at Caliente. This combined activity lasted 3 years. After 3 years, activity ceased at El Brujo, but Caliente remained active with emplacement of block lava flows and vertical ash eruptions as the main style of volcanic activity. The activity continues today at Caliente, with numerous block lava flows and ash eruptions. Extrusion rate of the lavas at a time-averaged rate is approximately 0.45 m^3/s. Today, Santiaguito is approximately 1.1 km^3 in volume, composed of the dome and the block lava flow units (Harris et al, 2004).

Figure 1.8. A photo of the Santiaguito Dome Complex with (left to right) El Brujo, El Monje, La Mitad, and Caliente Domes (photo taken by Bridget Hellwig, 2005).

Explosive activity is a commonly observed at Caliente Dome (approximately 20 times per day). The activity seems to be more frequent in the morning. These explosive eruptions release pyroclastic material from ring fractures that are located around the plug dome with a radius of about 70 m (Bluth and Rose, 2004) (Figure 1.9). The explosive events occur in intervals ranging from 5-100 minutes. These events can be short bursts producing 1-3 km high ash-rich plumes or can last up to 20 minutes and have the potential to turn into pyroclastic flows (Johnson et. al., 2004).

Figure 1.9. Aerial photo of Caliente dome (photo taken by Bridget Hellwig, 2006).

Santiaguito Dome Complex is fascinating for a number or reasons, but is particularly interesting because it is producing block lava flows. These flows are dacitic to rhyodacitic in composition and contain approximately 35% phenocrysts (Harris et. al.,

2002). It is unexpected to find such silicic magmas that are also crystal rich, but are still able to flow over long distances (around 4 km). The block flow surfaces are composed of angular to rounded blocks forming a rubbly surface that covers the complex. These active block flows are subject to gravitational collapse of the flow fronts and rock falls which can be very dangerous. Rock falls can produce explosions, while collapse can produce Merapi-style pyroclastic flows of block and ash which pose hazards to surrounding villages (Harris et al., 2003).

In addition to the 80 years of regular, episodic activity at Santiaguito dome complex, another notable feature is a decrease in the silica content of erupted material by approximately 2% since 1970. One possible result of this decrease is that individual block flows have lengthened their travel over time. Other reasons could be a change in temperature or the amount of water in the magma (Harris et. al., 2003).

Due to the uniqueness of Santiaguito Dome Complex, it was chosen as the locality for the basis of our dacite and rhyodacite samples. The compositions of synthesized glasses were based on the geochemistry of the actual dacites and rhyodacites found at the volcano. These compositions were then tested to determine the effect of temperature, water and fluorine content on their viscosity. One important question is the relative effects on magma viscosity of relatively small changes on temperature and water content. The physical effects of crystal content on magma viscosity can be accounted for using the Einstein-Roscoe equation (Marsh, 1981; Pinkerton and Stevenson, 1992), but the other variables must be measured.

1.5 Summary

- The purpose of the project is to determine the effects of water and fluorine content on the viscosity of dacite and rhyodacite melt compositions, which are important in explosive volcanism.
- Viscosity is one of the most important parameters affecting volcanic activity and is dominantly controlled by melt composition, temperature, and volatile content. Only a few weight percent of water can decrease the viscosity of a melt by several orders of magnitude. This effect is stronger on more silicic compositions.
- Although several models have been developed in order to predict magma viscosity, none of them are able to satisfactorily predict the viscosity of hydrous dacites.
- Fluorine is another volatile which can have an affect of the viscosity in a similar fashion to water. Very few studies have been conducted on the effects of fluorine on silicate melt viscosity, and these have mostly been on highly polymerized melts. A model needs to be developed in order to predict the effect fluorine has on viscosity.
- Several mechanisms of fluorine dissolution have been proposed, where some could lead to melt depolymerization and a viscosity decrease, while others would lead to melt polymerization and a viscosity increase.
- Santiaguito Dome Complex in Guatemala was chosen as the ideal locality on which to base our synthetic compositions due to the potential applications to understanding its unique dacite lava flows.

The next chapter will discuss the methods that were used in this study including making of the synthetic glasses including the addition of water and fluorine, density measurements, parallel plate and concentric cylinder viscometry. The results of viscosity measurements will be described in Chapter 3.

CHAPTER 2 – METHODS

2.1 Overview

This chapter will describe the various methods used in this study, including sample preparation, parallel plate viscometry and concentric cylinder viscometry. The sample preparation section will include a description of the choice of composition for the study and glass synthesis. The procedures for hydration and fluorination of the samples will also be described. The density of all samples was measured in order to determine the partial molar volume of water and fluorine in these glasses. The sections on both parallel plate and concentric cylinder viscometry will involve a description of the apparatus and significant parts, sample preparation, the experimental procedure and the theory/calculations used in data analysis, and the test run showing the accuracy of the viscometer. Parallel plate viscometry measures the high viscosity and low temperature range of melts while the concentric cylinder measures the low viscosity and high temperature range. Most magmas occur in nature at temperatures between these ranges, in fact between the solidus and liquidus.

2.2 Sample Preparation

2.2.1 Compositions

The compositions chosen for this study were a synthetic (iron-free) dacite and rhyodacite composition. These compositions were chosen because viscosity data on these is sparse, including the effect of water and fluorine on their viscosities. Dacite and rhyodacite compositions are important to understand because they are involved in explosive volcanism which can be very hazardous. Some active examples include Mt.

Unzen, Mt. St. Helens, Mt. Pelee and many others. The synthesized compositions were based on samples collected from the active Santiaguito Dome Complex in Guatemala.

The oxides that were used in the compositions were SiO_2, TiO_2, Al_2O_3, MgO, CaO, Na_2O, and K_2O. Calcium, sodium, and potassium were added in the form of carbonates because the oxides are either very refractory (CaO) or hygroscopic (Na_2O, K_2O). Iron was not used in the samples for two main reasons. First, Fe in a melt will promote crystallization. Iron can also lead to oxygen fugacity issues such as the uncertainty in Fe^{2+}/Fe^{3+} and the potential to change during the experiment.

Preparation of hydrous and fluorine-bearing samples is described in sections 2.2.3 and 2.2.4 below. A ternary diagram showing previously studied compositions in comparison with the dacite and rhyodacite from this study (Figure 2.1), illustrating the important gap between andesites and rhyolites that these compositions occupy.

2.2.2 Glass Synthesis

Once the compositions were chosen, glasses were synthesized from the oxide and carbonate powders listed above. The precision of weighing for each component was within a milligram, and the total weight of powder used for each glass was approximately 70 grams. In order to guarantee enough sample for both parallel plate and concentric cylinder analysis, double batches were made of each composition. After weighing out one batch of powder, the sample was mixed in a shatterbox for five minutes to homogenize it. After mixing, the samples were put in platinum crucibles and placed in a Thermolyne high temperature muffle furnace (46200) to undergo decarbonation.

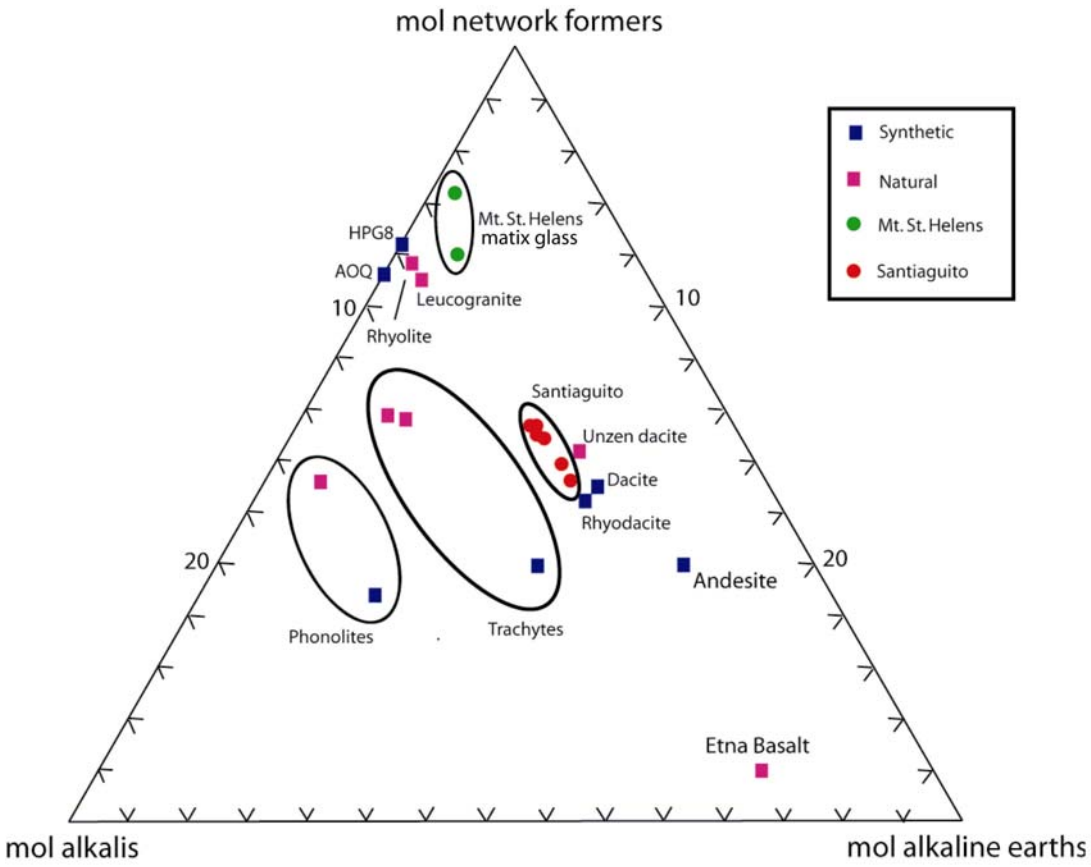

Figure 2.1 A ternary diagram showing various silicate melt compositions. The samples include haplogranite (Dingwell et al., 1996), AOQ (Schulze et al., 1996), leucogranite (Whittington et al, 2004), Mt. St. Helens, Santiaguito, rhyolite (Zhang et al., 2003), trachytes (Whittington et al., 2001; Giordano et al., 2005), phonolites (Whittington et al., 2001, Giordano et al., 2000), Unzen dacite (Giordano etal., 2005), andesite (Richet et al., 1996), and Etna Basalt (Giordano et al., 2003).

Decarbonation removes the CO_2 component from $CaCO_3$, Na_2CO_3, and K_2CO_3 and is achieved by slowly heating the sample in increments up to 1050°C. Slow heating is required to avoid foaming as CO_2 gas is released.

After decarbonation of each individual batch, the samples were taken up to 1600/1650°C, well above their liquidus temperature. After being held at 1600°C for at least an hour, they were taken out of the furnace and quenched by placing the bottom of the platinum crucible in water, while ensuring that no water came in contact with the sample. After each individual batch was fused for the first time, the batches were

combined. This double batch (~140 grams) was then crushed in the shatter box again for 10 minutes and remelted at 1650°C for an hour. After the second melt, the samples were again quenched to glass, crushed in the shatterbox and then melted overnight to get all of the air bubbles out of the sample. The reason that the samples underwent two fusion and grinding cycles was to ensure that the sample was homogeneous in composition. The final step involved pouring the sample into a graphite crucible to allow the glass to cool slowly, producing glass plugs approximately 6.5 cm long and 2.5(bottom) to 3(top) cm in diameter, which are easy to drill cores from.

Finally, the samples were annealed by putting them back in the platinum crucible and placing them in the furnace, then heating them 3ºC/min to 700°C, around the glass transition temperature. After reaching 700ºC, the sample was cooled back down to room temperature at 2ºC/min. This allowed the sample to relax, releasing internal stresses. This avoids shattering during core drilling for parallel plate viscometry and relaxes the density of the sample.

2.2.3 Hydrous Sample Synthesis

The hydrous samples for this study were made in collaboration with Professor Harald Behrens at the Institut fur Mineralogie in Hannover, Germany. Bastian Joachim and Andre Stechern made the samples using an internally heated high pressure vessel (IHPV, Figure 2.2). Descriptions of the procedure for making hydrous samples can be found in Behrens et. al. (1996), Behrens (1995), and Holtz et al (1995). The anhydrous glass was first ground with a ball mill to get it into a fine powder. The powder was placed into platinum capsules with a length of 3 cm. In order to get a cylindrical sample, ideal for the parallel plate, one side of the capsule had to have a flat surface. To achieve

Figure 2.2. The internally heated pressure chamber used in this study in the Institut fur Mineralogie in Hannover, Germany (Photo by Bastian Joachim).

this, one side of the capsule was closed by a cap. The final amount of powder and water needed to be calculated before filling the capsule because it is necessary to fill the capsules in layers to guarantee a homogeneous glass. To make these glasses, 4 layers of powder were used alternating with 3 layers of distilled water. After each powder layer was emplaced, the content of the capsule was compressed using a steel rod. Finally, the upper side of the capsule was closed and welded shut.

The platinum capsules containing glass and water were placed in the IHPV and heated to high temperatures at carefully controlled pressures (Table 2.1). All capsules with more than 1 wt.% water used a vessel which has places for 3 capsules, but can only go up to 1250ºC. Samples with lower water contents require higher temperatures because crystals formed in the samples using the lower temperature. The vessel used for these is typically used for rapid quench experiments to allow rapid cooling from 1300°C or more.

During an experimental run, three thermocouples are used to monitor temperature and ensure a minimal thermal gradient across the sample. The first step in running an experiment is verifying that the whole system is sealed, allowing the pressure to be increased using an intensifier, with argon as the pressuring medium. When the desired pressure is achieved (2 or 3 kbars, Table 2.1), heating can begin. These pressures were used because if the pressures are too high the samples are in danger of forming crystals, but if the pressures are too low, then the samples can form bubbles due to volatile saturation. The heating program started with 10ºC/min until 100ºC is reached, then 20ºC/min until 1200-1250ºC. Once the peak temperature is attained, it needs about 15-20 minutes to stabilize, which causes no problems for the actual synthesis.

Table 2.1
Hydration conditions, water contents, and densities of hydrated glasses

Sample name	P (kbar)	T (°C)	t (hr)	KFT analyses[a] (wt.% H_2O)	KFT analyses[a] (mol% H_2O)	ρ^b (g/cm^3)	ρ^c (g/cm^3)
Rhyodacite							
Anhydrous						2.476	
RD0.5	2.0	1350	7	0.38	1.41	2.475	
RD1.0	2.0	1350	7	0.97	3.55	2.471	
RD3.0	3.0	1250	18	2.84	9.90	2.446	
RD4.0	2.0	1250	18	3.61	12.34	2.420	
RD5.0	3.0	1250	18	5.09	16.77	2.415	
Dacite							
Anhydrous						2.459	
D1.0	2.0	1350	7	0.97	3.60	2.450	
D2.0	3.0	1250	18	2.27	8.14	2.445	2.428
D3.0	3.0	1250	18	2.79	9.87	2.437	2.403
D4.0	2.0	1250	18	3.73	12.88	2.400	
D5.0	3.0	1250	18	4.94	16.55	2.396	

[a]Water content measured by Karl-Fischer titration at the IMH, Hannover. These values include a +0.1 wt.% correction due to water retained in the melt after heating.
[b]Densities of glasses measured by the Archimedean method using distilled water. Errors are typically better than 0.001 g/cm3 based on repeat measurements on three chips of each sample.
[c]Relaxed glass densities measured after viscosity determinations of T_g.

After about 12 hours, power to the heater is switched off, quenching the sample. In the first few minutes, cooling occurs rapidly (around 200ºC/min). When the sample finally reaches room temperature, then the pressure can be decreased, and the sample can be recovered for use in viscosity experiments.

The exact water contents of the sample were then measured using Karl Fisher Titration (KFT). KFT is an analytical method for quantifying water content within a sample. The principle behind it is based on the Bunsen Reaction between iodine and sulfur dioxide in an aqueous medium. This process can then be modified for the determination of water with a system containing excess sulfur dioxide (Behrens, 1995). The samples made included nominal water contents of 1, 2, 3, 4, and 5 wt. % for the dacite and 0.5, 1, 3, 4, and 5 wt. % for the rhyodacite. The measured values are listed in Table 2.1, and show good agreement with the nominal values.

2.2.4 Fluorine Sample Synthesis

The fluorine-bearing samples were made following the methods of Giordano et al. (2004) by substituting AlF_3 for Al_2O_3 in the initial synthesis in powder form. When adding AlF_3 into the sample, the exchange which occurs is F_2O_{-1}. The fluorine samples that were made for this study included the nominal values of 0.3, 0.6, 1.0, and 2.0 wt.% F. The AlF_3 was measured into the sample during the initial weighing process and then the glass was made following the same method as described above.

One difference between the original compositions and the fluorine samples is that during melting, the fluorine samples produced a lot more bubbles within the melt. The samples were left at high temperature in the furnace over longer periods of time to get rid

of the bubbles (up to a day and a half). When the fluorine samples were meausured using an electron microprobe in conjunction with Washington University – St. Louis, it was determined that none of the samples contained any significant fluorine. The bubbles in the samples were probably caused by fluorine loss from the melt during sample preparation. This absence of fluorine in the samples was not expected.

2.2.5 Density Measurements

After the glass samples were made and annealed, their densities were measured. This was based on Archimedes principle using a Mettler Toledo balance and the difference in weights of the samples in air and in a liquid. The liquid that was used to measure our densities was distilled water. The equation used to calculate density was

$$\rho = \left(\frac{A}{(A-B)} (\rho_o - \rho_L) \right) + \rho_L \qquad (2.1)$$

where ρ is the density of the sample, A is the weight of the sample in air, B is the weight of the sample in liquid (distilled water in our measurements), ρ_o is the density of the liquid, and ρ_L is the air density (equal to 0.0012 g/cm^3). Temperature of the distilled water was measured to ±0.1ºC which could lead to about a 4% error with small samples. Three different samples of each glass were measured for their density. Each of the three samples was then measured twice to ensure that the values were consistent. The samples were measured within 0.001 g/cm^3. The density was calculated for each and the average of these is reported in Table 2.1.

2.3 Parallel Plate Viscometry

2.3.1 Description of Viscometer

Parallel plate viscometry can be used to measure viscosities near the glass transition, in the range of $10^{8.5}$ to 10^{13} Pa.s. Viscosity is determined by measuring the change in height versus the time, for a fixed temperature, and then calculating strain rate ($d\varepsilon/dt$) under a known stress (σ). The viscosity is measured in Pa.s.

The viscometer used in this study is a Rheotronic III 1000ºC parallel plate viscometer, designed by Theta Industries, Inc. The apparatus is mounted on a stand and

Figure 2.3. The parallel plate viscometer in Room 2, Geological Sciences Building.

includes the mounting headplate, the furnace, the measuring head, the specimen holder assembly, the temperature control, the signal conditioner and the computer (Figure 2.3).

The stand at the base of the viscometer needs to be level to ensure that stress is applied perpendicular to the sample. The mounting head-plate is connected to the back of the stand and holds the important parts of the viscometer including the measuring head and specimen holder assembly, which can be lowered into the stationary furnace.

The furnace is located at the base of the head-plate and is cylindrical in shape (Figure 2.4). The furnace can go up to 1000°C in temperature. When running an experiment, the sample is lowered into the small circular opening at the top of the furnace. The furnace is connected to the temperature control box which controls either automatic or manual heating of the furnace (Figure 2.5). The temperature control also shows the furnace temperature as read by the built-in (control) furnace thermocouple, located within the furnace, but outside the sample holder.

The measuring head is located at the top of the head-plate (Figure 2.6). On top is the load plate where weights are placed to put stress on the sample. The plate is connected to the LVDT (linear variable displacement transducer), which is used to measure the exact length change of the sample during deformation. Located to the right of the LVDT is the micrometer, used for calibration of the LVDT before each experimental run. Also on the measuring head are two balancing weights, which are used to counteract the weight of the load rod of the specimen holder assembly and the plate which holds the load.

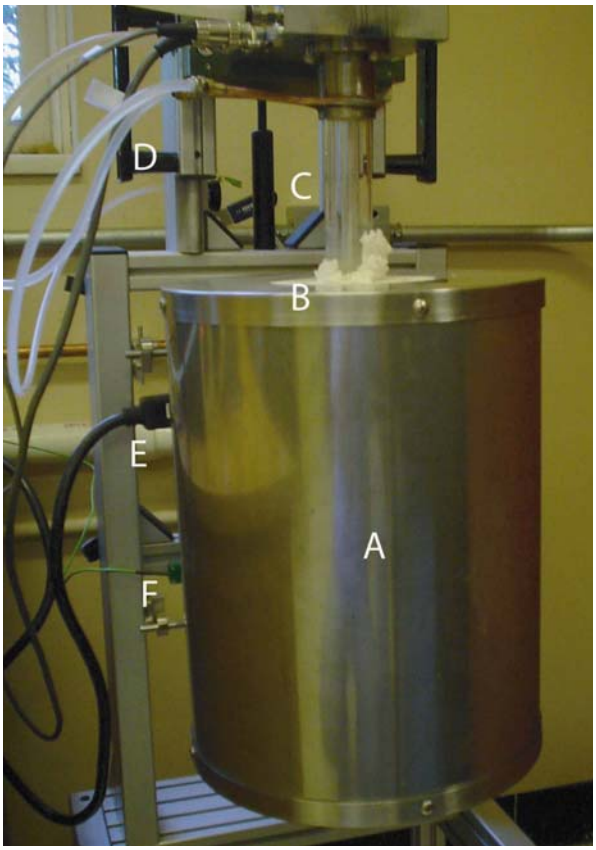

Figure 2.4. (A) Parallel plate furnace, (B) Kaowool, (C) Specimen holder assembly, (D) Cooling pipes, (E) Power Supply, and (F) Thermocouple connection

Figure 2.5. The signal conditioner (A), temperature control (B), and computer (C).

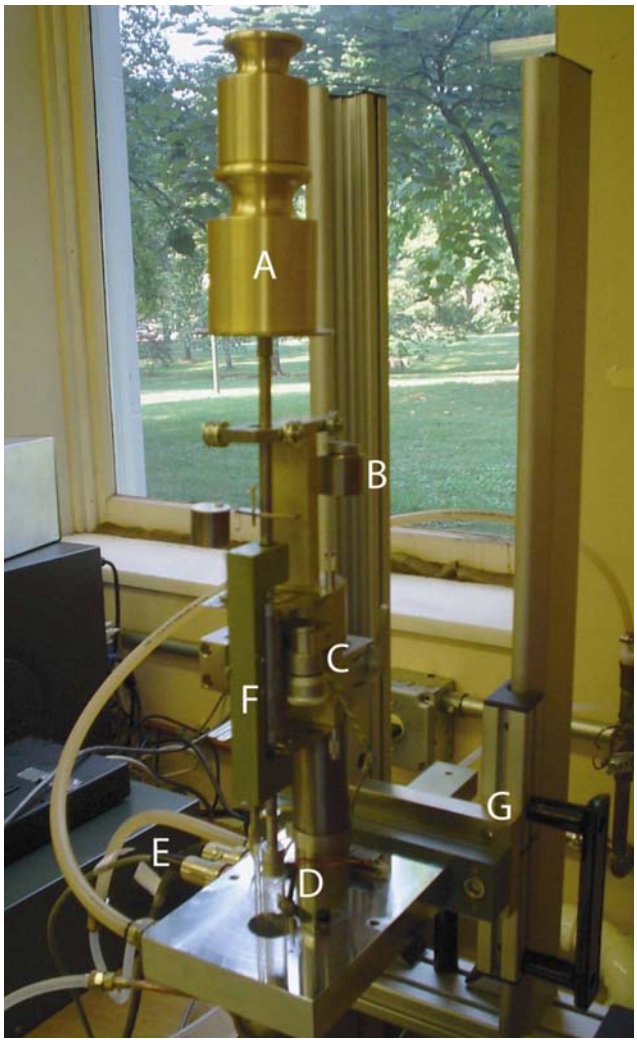

Figure 2.6. The measuring head including the (a) load plate and wieghts, (b) balancing weights, (c) the micrometer, (d) load rod, (e) cooling pipes, (f) LVDT (behind green rod), (g) head-plate.

At the base of the measuring head is a metal plate which covers all wires and allows water to pass though acting as a cooling device for the measuring head. The cooling prevents any damage to the important wires and various parts, especially the LVDT which needs to be kept at room temperature. Connected to the bottom of the plate is the specimen holder assembly, which includes the surrounding specimen holder, the load rod, the push rod, and the thermocouple (Figure 2.7 and 2.8). Figure 2.9 is a close

up sketch of the set up. The specimen holder is a cylindrical silica glass tube, which surrounds the load rod, push rod, thermocouple, and sample. The top of the specimen holder tube has a second cooling pipe which allows water to pass through it to prevent overheating of the specimen holder. The load rod is a hollow, cylindrical tube which is connected to the LVDT and the load plate in the measuring head. The load rod is placed on the top of the silica plate, directly above the sample. Weights are placed on top of the load plate, which then apply stress to the sample via the load rod, causing deformation during an experiment. The push rod, located to the left of the load rod, is used as a non-deforming reference to measure the change of height of the sample during deformation. It is made of silica glass which has a T_g of 1470 K (Mysen and Richet, 2005). It is set at a specific height at the start of the experiment and then the value is compared to how much the load rod changes position during deformation. This difference is measured within the LVDT. Both the load and push rods are silica glass because it has extremely small expansivity. Being made out of the same material also makes the measurements more accurate. This apparatus is basically a modified dilatometer. Sample temperature is measured with a K-type thermocouple which is placed in contact with the sample.

The signal conditioner is connected to the measuring head and receives voltage from the LDVT and passes it to the computer (Figure 2.5). The computer, which is connected to both the signal conditioner and the temperature control, records and saves the data collected from the experiment using a program called Dilasoft. The whole viscometer can be automatically run just using the computer which records the time, temperature, and specimen height or it can be run manually.

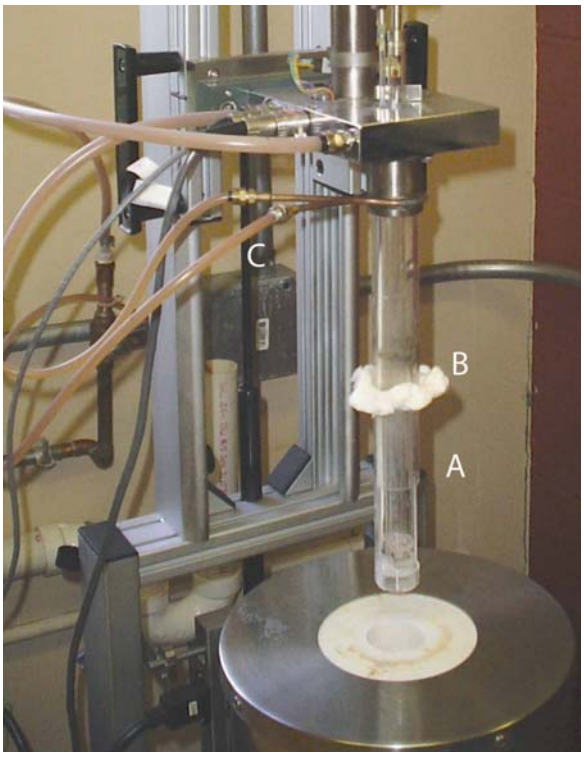

Figure 2.7. The specimen holder assembly including the (a) specimen holder, (b) the kaowool, and (c) the cooling pipes.

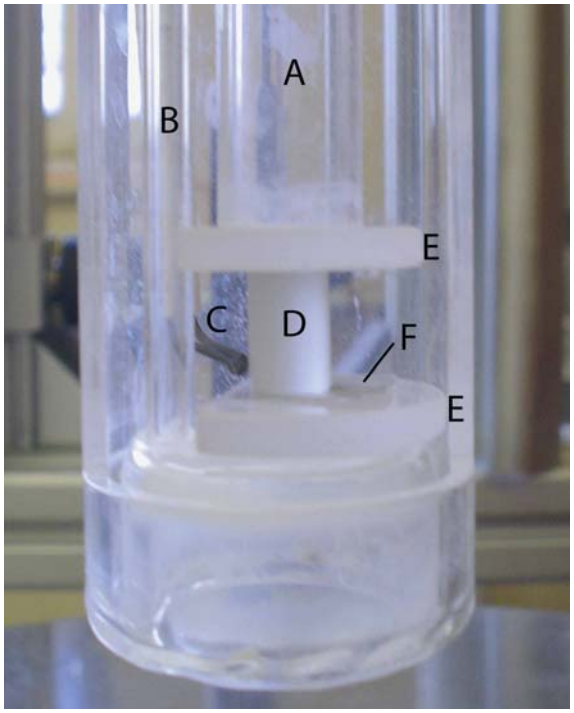

Figure 2.8. The specimen holder assembly including the (a) load rod, (b) the push rod, (c) the thermocouple, (d) sample, (e) silica plates, and (f) Platinum foil.

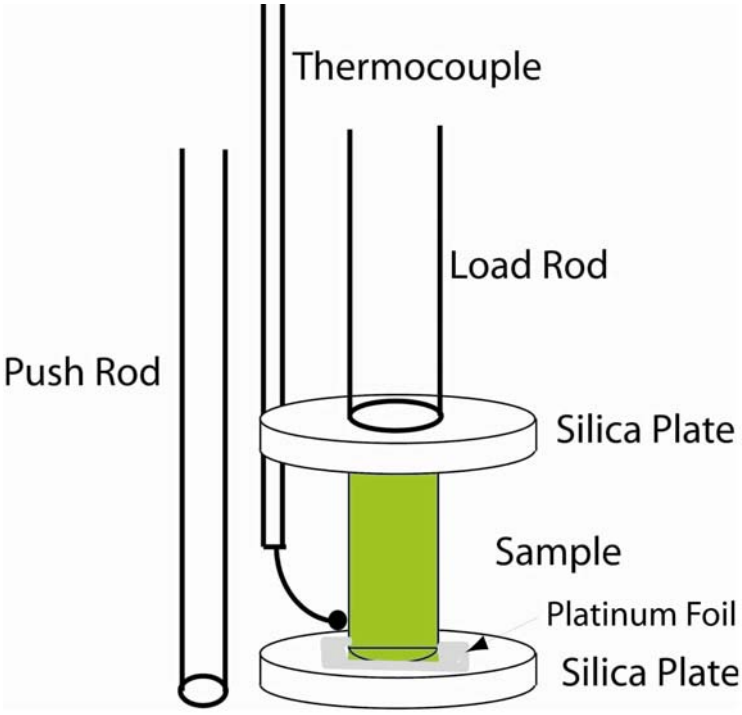

Figure 2.9. A sketch of the sample set up in the specimen holder assembly.

2.3.2 Sample Preparation

In order to run an experiment, certain steps are required when preparing the sample. First, the glass samples used must be annealed. The annealed samples are then drilled using a water cooled diamond core drill mounted on a drill press to obtain cylindrical glass cores. An ideal sample will typically have a height between 8 and 10.5 mm because a taller sample can allow for more deformation to occur, although samples as small as 3.5 mm can be run. The ideal width of a sample is between 6.5 and 7 mm. If the samples are thinner than this, they tend to deform too rapidly, especially at low viscosities, and deformation may be inhomogeneous. If the sample is thicker, then it typically does not deform quickly enough in the high viscosity range. The deformation of the sample depends on the applied load, but the dimensions given are optimal for a load of 1500 grams, which was used in all experiments on dacites and rhyodacites.

Once the samples have been cored, both ends need to be polished up to 600 grit size as a minimum. Both ends of the core also need to be parallel to each other (within 50 μm), to ensure parallel deformation during an experiment. After the sample has been made, the height, mass, width, volume, and density of the glass cylinder are measured and recorded. These measurements will be used in the experiment and during the calculations.

2.3.3 Experimental Procedure

Running an experiment on the parallel plate viscometer involves several steps. The first step is to position the sample on the base of the specimen holder assembly (Figure 2.8). The sample is set between two silica plates and two pieces of thin platinum foil (Figure 2.9). A silica plate is set on the base of the specimen holder with a piece of platinum foil (1 cm by 1 cm) on top of it, then the sample is placed in the center of the foil. A second piece of foil is then placed on the top of the sample with the second silica plate on top of that. To hold the sample in place, the load rod is lowered to rest on the top of the upper silica plate. Some special things to note when setting up the sample include making sure the thermocouple is touching the sample to ensure proper reading of the sample temperature, having the push rod parallel to the load rod to ensure the position is being read properly, and making sure the glass sample is directly below the center of the load rod to ensure even deformation.

After the sample has been correctly placed, the program needs to be set up within the software, Dilasoft, on the computer. A typical program involves running segments which measure viscosity every 10ºC with various length holds depending on the viscosity being attained. The holds vary, ranging from approximately 5 minute holds for

viscosities around 10^9 Pa.s to 10 hour holds for a viscosity of $10^{12.5}$ Pa.s. Programs can be changed during an experiment if necessary.

Next, various sample parameters need to be entered into the menu including height, width, volume of the sample and the applied load. The typical load used in this study was 1500 grams because it gave the best results found when testing the standards. The computer can only calculate viscosity based on loads up to 1000 grams. For this reason we calculate viscosity ourselves, which will be described in the next section. A changeover height and minimum height are also required. The changeover height used with our samples is when the sample deforms 40% of its original height, and if this is reached the program will jump to the next segment. There is no specific height value that the changeover height requires, though. The minimum height we used in this study is 0.01 cm less then the changeover height. If this height is reached, the program jumps to the last segment which is the cool down, ending the experiment. Both the changeover and minimum heights are useful when the viscometer is run automatically.

The last step before running an experiment is calibration of the LVDT. Calibration depends on the height of the sample being run. To check calibration, look at the present position when the sample is set up in the specimen holder assembly. If the position reads between 0 and -3 mm, the viscometer does not need to be recalibrated. If it lies outside this range, then the LDVT needs to be recalibrated, by moving the measuring head up or down until the position falls between these values.

2.3.4 Theory and Calculations

The viscosity of a melt is calculated by dividing the shear stress by the strain rate. The parallel plate viscometer does this by applying a specific load to a sample (known

stress) and then measuring the strain rate due to this stress at a specific temperature. The computer program can calculate viscosity, but not with using more than 1000 grams for load. Even when 1000 grams or less is used, the computer calculation is not as accurate as can be achieved by importing the raw data into Excel and processing it offline. This was discovered during the initial runs on the NIST standards, and is due to the software design being optimized for viscosity measurement during heating or cooling.

To calculate the viscosity from the raw data that is provided by the viscometer, we used the following equation (Dingwell, 1995):

$$\eta\,(Pa.s) = \frac{mgh^2}{3V\,\delta h / \delta t} \qquad (2.2)$$

where m is the applied mass (kg), g is the gravity (m^2/s), V is the volume, h is the height of the material, and t is the time (s). This equation is known as the "perfect slip" condition where the surface area between the cylinder and the plate increases with deformation and the cylinder does not bulge. This means that the cylinder remains parallel during deformation and that the deformation is uniform. The equation works well in calculating the viscosity from the parallel plate viscometer.

During the experiment, the computer logged data including time, temperature, and specimen height. Two plots were made to analyze the data, one being temperature as a function of time and the other being specimen height as a function of time. Examples of these graphs can be seen in Figures 2.10 and 2.11. Temperature versus time showed the length of the holds at a specific temperature, while the specimen height versus time showed the amount of deformation over time. The first step was to analyze each individual segment's hold to determine the viscosity for that specific temperature. One requirement in determining the viscosity is that the specimen needed to deform a

minimum of 5 micrometers during the segment to ensure an accurate viscosity reading, but more deformation is better. This is because the micrometer on the viscometer is believed to be no better than ±0.1 μm. With only 5 microns of deformation, this would give us an error of 2%.

The typical viscosity range which can be measured using the parallel plate is 10^{9} to $10^{12.5}$ Pa.s. This is the limit for the parallel plate because at viscosities much below 10^{9} Pa.s, the sample deforms much too quickly and the sample can become crooked during rapid deformation. For viscosities higher than $10^{12.5}$ Pa.s it takes an extremely long time for the sample to even deform 1 micron (>10 hours). Based on the NIST standards, the accuracy of the viscometer is within 0.05 log units while the precision is around 0.04 log units, based on repeat measurements.

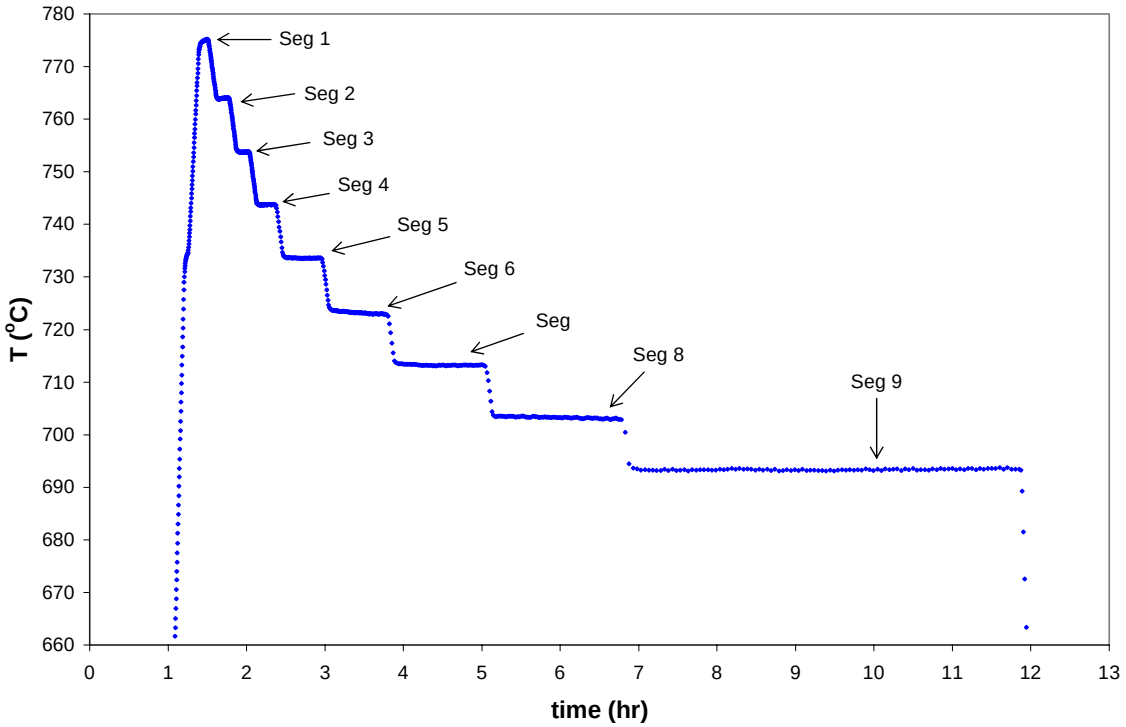

Figure 2.10. A plot of temperature as a function of time used during data analysis.

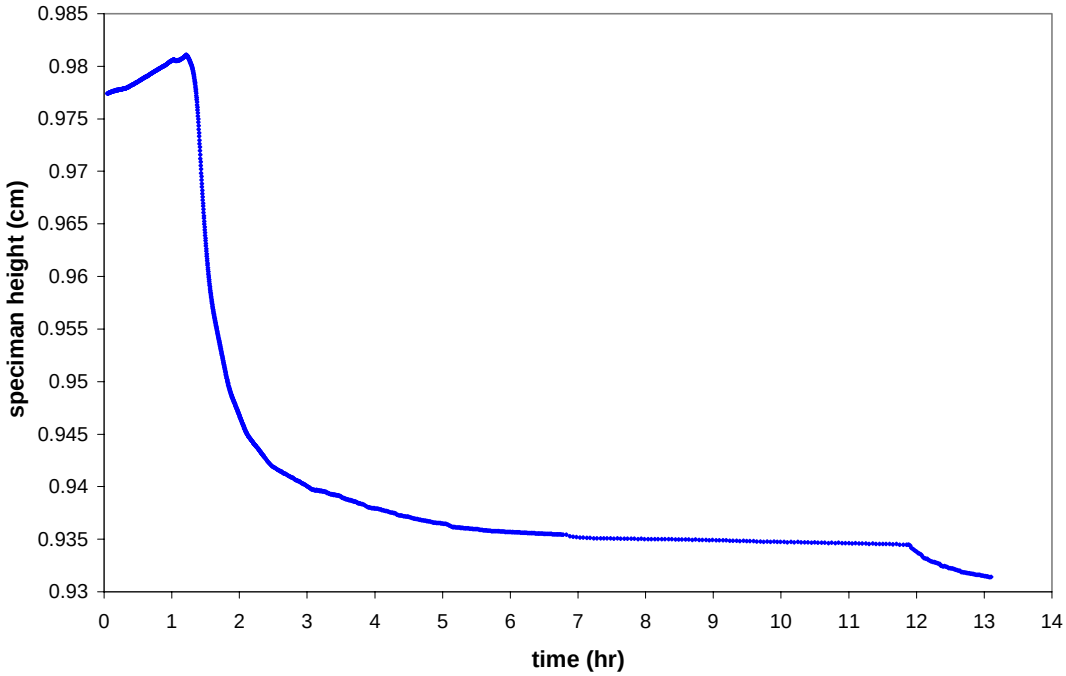

Figure 2.11. An example of the plot time vs. specimen height used in data analysis.

2.3.5 Accuracy and Precision

Before the viscometer was sent to us, the machine was set up and tested by the manufacturer using NIST standard glasses. After setting it up in the lab, it was first tested again before any unknown samples were measured. There is no empirical calibration required for the parallel plate viscometer: the required data are simply temperature, sample height and time. The samples used to test the viscometer were NIST standard reference materials which included 717a, a borosilicate glass, and 710a, a soda-lime silicate glass. The equation used to calculate and predict the viscosity of 717a is expressed as a TVF equation (NIST certificate – Appendix A):

$$\log_{10}\eta\ (poise) = -2.5602 + \frac{4852.2}{(T - 192.462)} \qquad (2.3)$$

where η is the viscosity in poises and T is the temperature in °C (1 poise (cgs) is equal to 0.1 Pa.s (SI)). The soda lime silicate glass, 710a, was also used to verify the accuracy of

the viscometer. Certified values are described by a consensus fit to the TVF equation (NIST Certificate – Appendix A):

$$\log_{10}\eta\ (poise) = -1.729 + \frac{4560}{(T - 240.8)} \qquad (2.4)$$

where η is the viscosity in poses and T is the temperature in °C.

The results of the duplicate experiments on the standard glasses are shown in Figure 2.12. The borosilicate glass was within 0.05 log units of the predicted viscosity which makes the viscometer very accurate. This run showed the machine was in good condition to run actual experiments for this study. The back up run on the soda lime silicate also showed fairly good results with accuracy being slightly more than 0.10 log units from the predicted viscosity. The official uncertainties for the NIST standards are within 0.1 log units and reproducibility of the data is within 0.05 log units (Appendix A).

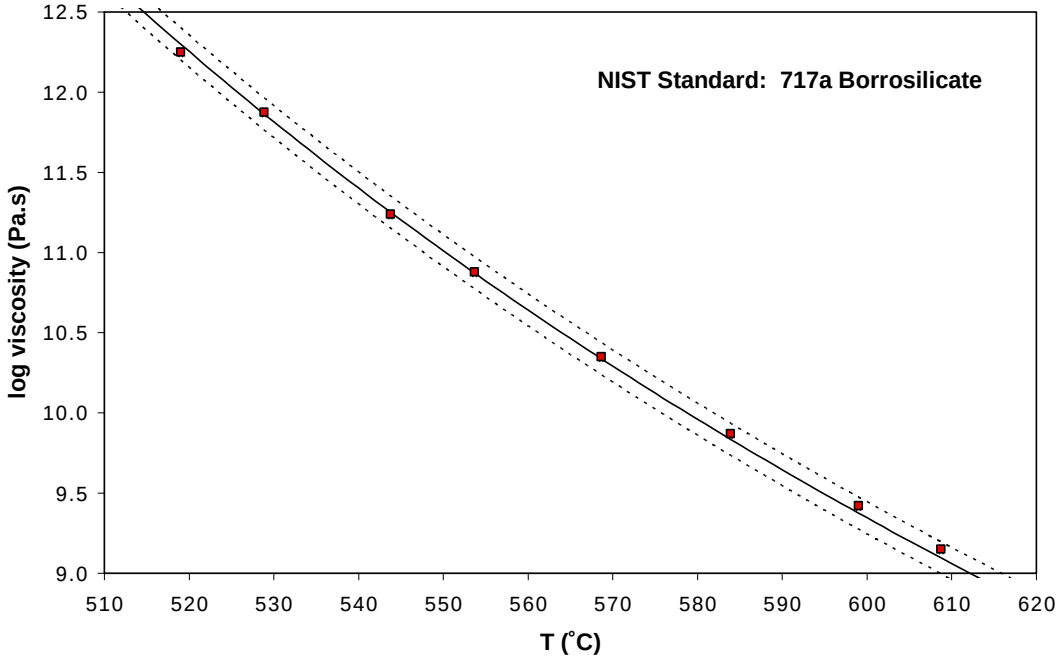

Figure 2.12. Test run results of the borosilicate glass. The solid line is the certified TVF equation and the dashed lines are ±0.1 log units. The points are the measured data points.

2.4 Concentric Cylinder Viscometry

2.4.1 Description of viscometer

Concentric cylinder viscometry can be used to measure liquid viscosity at super-liquidus temperatures, in the viscosity range ~10^{-2} to ~10^{7} Pa-s depending on the design and measuring head. Our apparatus will measure viscosity over the range ~10^{1} to ~10^{5} Pa-s. The concentric cylinder, also known as a rotational viscometer, used in this study was a Rheotronic II 1600ºC Rotating Viscometer designed by Theta Industries, Inc. A few modifications were made to the machine for better results on our samples. It is a Searle type viscometer where the outside cylinder contains the fluid and remains stationary while the inside cylinder (spindle) rotates, creating a torque. The important parts which make up the viscometer include the measuring head, the depth indicator, the cooling system, the sample holder rods, the furnace, the viscometer control, the furnace control, the power supply and the computer (Figure 2.13). Descriptions of these will be provided below.

Figure 2.13. The concentric cylinder showing all of its significant parts.

The viscometer is mounted on a stand which again needs to be carefully leveled. The mounting head-plate is connected to the back of the stand and holds the main parts of the viscometer including the measuring head, specimen holder assembly and the furnace.

The furnace is located at the base of the head-plate and is rectangular in shape (Figure 2.14). When running an experiment, the sample is lowered into the small circular opening at the top of the furnace, which can go up to 1600°C in temperature. The furnace control box controls either automatic or manual heating of the furnace (Figure 2.15). The temperature control also shows the actual furnace temperature as read by the built-in furnace thermocouple, which is used to control temperature.

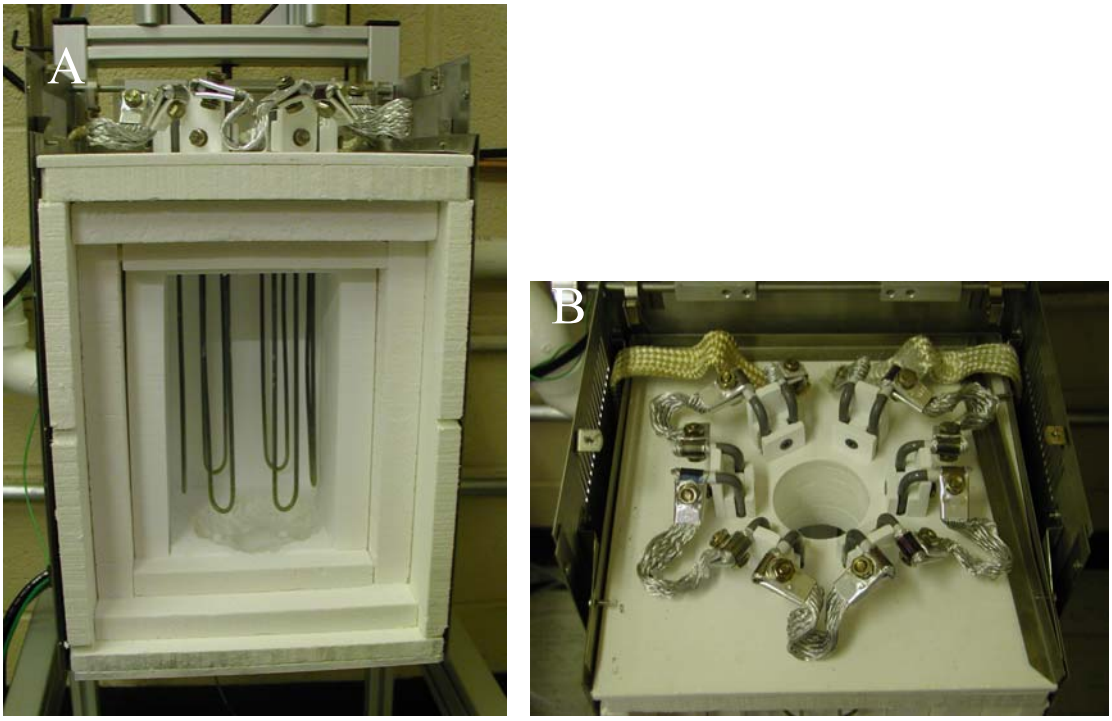

Figure 2.14 (a) Side view showing the heating elements within the furnace (b) top view showing the heating elements and the hole for the sample.

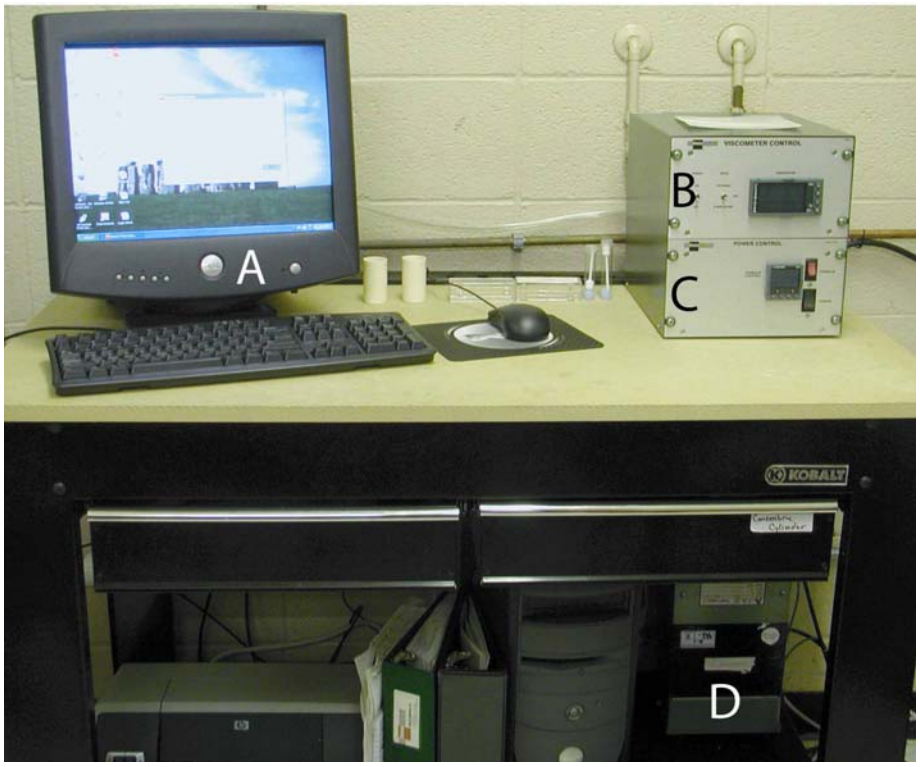

Figure 2.15. (A) Computer, (B) viscometer control, (C) furnace control, (D) the power supply which control the concentric cylinder viscometer.

The measuring head is a Brookfield HBDV-III Ultra, which is located at the top of the head plate (Figure 2.16). This can be used in "internal mode" allowing measurements to be made independent of the computer or "external mode," which is computer-controlled. In either mode, two calibration constants (SMC and SRC, see below) must be fed into the computer from the measuring head. The depth indicator is located to the right of the measuring head. It is used to measure the height of the spindle during an experiment. At the base of the measuring head is the cooling unit, which circulates water through the base of the measuring head during an experiment so that it does not overheat, and the spindle holder which controls the spindle rotation. The torque produced ranges from 0 to 100% and is in units of dyne-cm.

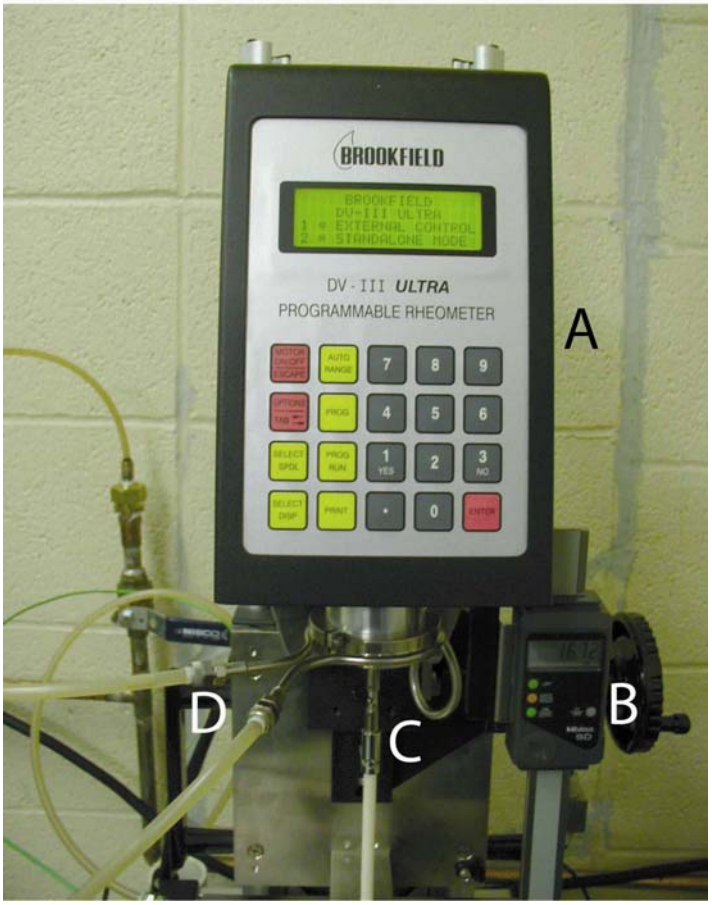

Figure 2.16. The measuring head including (A) measuring head, (B) depth indicator, (C) spindle holder, and (D) cooling pipes.

Below the measuring head is the sample rod assembly where the specimen is held during an experiment (Figure 2.17). The sample rod assembly is made up of three alumina rods which are held in place in a metal plate below the measuring head. Two of the rods are fixed, while the third rod, located on the right, can swivel out slightly so the sample can be placed in the rods. The sample is held at the base of these rods. An S-type thermocouple is located on the left side of the sample rods which is used to measure the sample temperature. A second cooling pipe runs through the metal plate to prevent overheating.

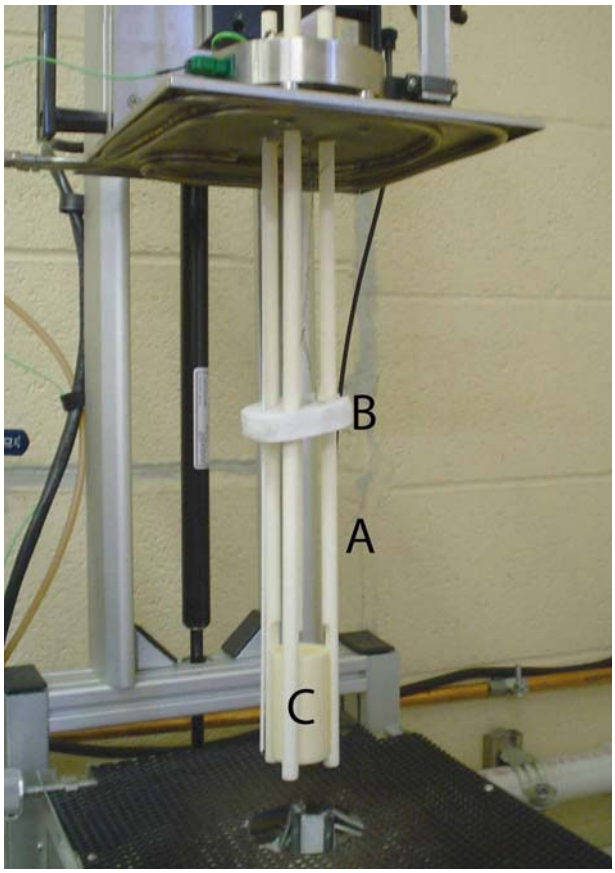

Figure 2.17. The sample rod assembly: (A) sample holder rods, (B) heat shield, and (C) crucible.

The other components making up the viscometer include the viscometer control, furnace control, the power supply and the computer (Figure 2.15). The viscometer control and the furnace control are within the same box. The viscometer control is located on top and controls the power to the measuring head and the choice of setting that will be run in the experiment. It also shows the temperature recorded by the sample thermocouple. The lower part of the box is the furnace control, which can be run either automatically by the computer, or manually. The power supply box (7205 hairpin 55V DR) plugs into the viscometer to provide power to both the measuring head and furnace. Lastly, the computer is connected to the viscometer and furnace control box and is typically used to run the experiment.

The original spindle and rotor apparatus that came with the viscometer consisted of two separate alumina pieces, where the rotor was inserted into the hollow spindle and held there with a thin piece of platinum wire. This set up did not work well with our samples because of their high viscosity requiring high temperatures where the platinum wire became hot and malleable and easily torn. The rotors themselves broke easily and had to be replaced frequently as well. We developed a new spindle/rotor made of a single, solid alumina tube. Using this new spindle required that the machine be recalibrated with new SRC and SMC numbers. This was done by trial and error, entering various numbers and running the spindle in the calibration oil (low viscosity oil with viscosity of $10^{4.1}$ Pa.s at 25ºC and $10^{0.27}$ Pa.s at 60ºC). These calibration constants depend only on viscosity and are independent of temperature. Once appropriate constants were found, they were saved in the measuring head to be used with the new spindle.

2.4.2 Sample Preparation

Preparation of a sample for the concentric cylinder is very straightforward. Approximately 60-70 grams of glass chunks are placed in an alumina crucible, giving a sample volume of approximately 25 cm^3. The mass of the crucible and sample are then recorded. The crucible has a 3.3 cm inner diameter and is 6.5 cm tall. The sample must not hang over the edge of the crucible before heating or it will drip in the furnace.

2.4.3 Experimental Procedure

Setting up the viscometer involves first attaching the spindle securely to the spindle holder. The spindle then needs to be zeroed, by placing an empty alumina

crucible in the holder rods and lowering the spindle into the crucible until it reaches the base. The depth indicator is zeroed at this point. The spindle is then raised until the depth indicator reads 10 mm and again is re-zeroed at this point. This is the closest the rotor is allowed to the bottom of the crucible in order to minimize the end effects. The spindle is then raised completely out of the crucible and the viscometer is now ready for the sample set-up.

The alumina crucible with sample is placed into the sample holder rods (Figure 2.18). The spindle can then be lowered until it is just above the sample, and needs to be aligned so that it is in the center of the crucible. Lastly, the thermocouple needs to be touching the bottom of the crucible to ensure that the sample temperature is being read accurately.

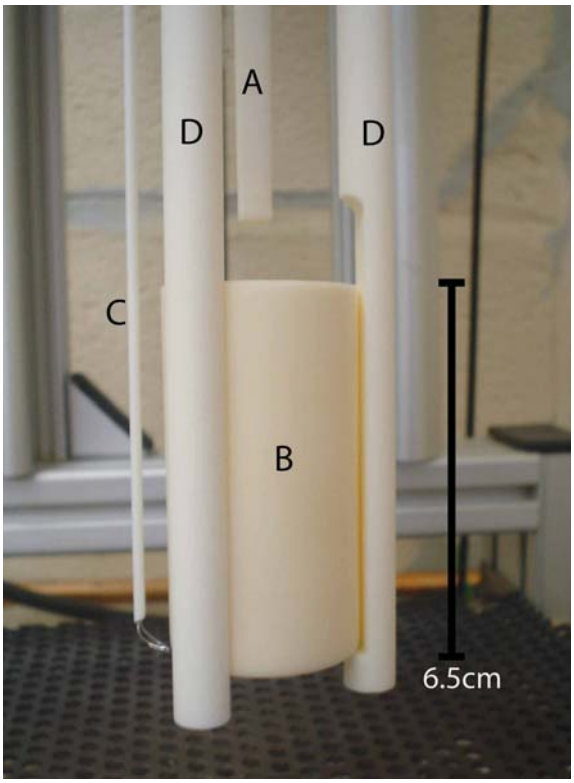

Figure 2.18. Sample set-up for the concentric cylinder. (A) Spindle, (B) crucible, (C) thermocouple, and (D) sample holder rods.

The third major step involves the computer which runs the experiment. The temperature program needs to be set up, where segments are typically programmed to decrease every 25ºC from high to low temperature. The program also includes determining the maximum temperature the furnace will heat up to find the "Top of Melt."

After all of the set up is complete, the actual experiment can be run. Unlike the parallel plate viscometer which can be set up and left to run, the concentric cylinder requires monitoring during the experiment, to adjust rotor speed and monitor the torque of the spindle. During segment 1, the machine heats up to the maximum temperature (typically 1590ºC). Segment 2 involves finding the "Top of Melt." This is done by lowering the spindle, rotating at 10 rpm, until it reaches the top of the melt, where initial contact of the spindle and melt will produce a torque reading. The third segment then requires the lowering of the rotor into the melt 18 mm because SMC and SRC are calibrated on the basis of exactly 18 mm (the viscometer could be recalibrated for different depths if desired). During this segment and each of the following segments, the speed (rpm) needs to be changed to get the appropriate torque values. The optimal range is between 70-85%, but values as low as 30% (17249 dyne-cm) give good results as determined by measurement on the NIST standard glasses. The maximum torque is 90% (51746 dyne-cm) for the HBDV III Ultra. The maximum speed of the rotor is 250 rpm and the minimum to still get good readings is 0.2 rpm. Segments are run every 25ºC until the rpm gets too small to get accurate readings. By doing this, the typical viscosity ranges achieved are between $10^{1.2}$ to 10^{5} Pa.s using the measuring head and rotor described here.

The third to last segment of the experiment is where the sample is heated back up to the maximum temperature and measured again to check the consistency of the data over the course of the experiment. This is a check for instrumental drift, volatilization of the sample, and for possible corrosion of the spindle for some melts. During the second to last segment, the rotor is raised out of the melt. The last segment is then the cool down of the viscometer and the end of the experiment.

2.4.4 Theory and Calculations

Concentric cylinder viscometry measures the low viscosity and high temperature range in melts with typical values ranging from $10^{1.2}$ to 10^{5} Pa.s in this study. In the food industry, viscosity is measured even lower, below 10^{0} Pa.s and lower (often measured in centipoise which equals 1/1000 Pa.s). Viscosity is defined as:

$$\eta = \frac{\tau}{\gamma} \tag{2.5}$$

where τ is the stress and γ is the strain rate. For the concentric cylinder apparatus, stress is a function of applied torque and spindle geometry, while the strain rate is a function of the angular velocity and cylinder geometry. These relationships can be expressed by the following equations:

$$\tau = \frac{M}{2\pi R_b^2 L} \tag{2.6}$$

$$\gamma = \left(\frac{2R_c^2}{R_c^2 - R_b^2} \right) \omega \tag{2.7}$$

where M is the torque, R_c is the radius of the crucible in cm, R_b is the radius of the rotor in cm, ω is the angular velocity of the rotor and L is the effective length (which includes the end effects). The angular velocity can be described as:

$$\omega = \frac{2\pi}{60} N \tag{2.8}$$

where N is the number of revolutions per minute of the spindle. Figure 2.19 shows the relationship between the spindle and the crucible geometry.

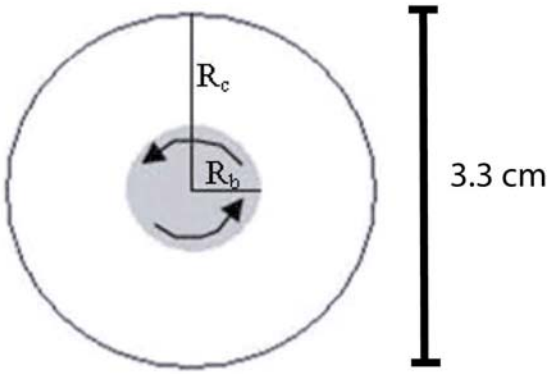

Figure 2.19. The relationship between the spindle and the crucible geometry.

During calibration of the viscometer, the use of the SMC (spindle multiplier constant) and the SRC (shear rate constant) come into play. The SMC is used during the calculation of viscosity and is found by trial and error in conjunction with the SRC. The SRC is used to calculate the shear rate and the shear stress based on the spindle dimensions. The shear rate can be calculated using the SRC and multiplying it by the speed (rpm). Once the SRC is determined, it can be entered into the measuring head as a constant. The SMC can then be found using the calculated SRC number while measuring the viscosity of the calibration oil.

Similar to the parallel plate viscometer, the program Dilasoft was provided to record the data collected from an experimental run, but the software is not useful when trying to interpret the data. Instead, the data is imported into Excel to be analyzed. Since the viscometer was tested with the NIST standards described earlier, it is known that the calculations performed by the measuring head itself are very accurate in calculating the viscosity, so these values are used directly. The data provided by the viscometer includes time, temperature, speed, torque, and calculated viscosity. When calculating viscosity only the last five minutes of each temperature segment are used to ensure that the temperature has equilibrated and the speed and torque have reached a steady state. The average speed and torque are used to calculate the viscosity using equations 2.6 and 2.7.

2.4.5 Accuracy and Precision

The rotating viscometer was tested at the manufacturer using NIST standards before shipping. After setting it back up in the lab we ran tests using the same NIST standard reference materials as before including 717a, a borosilicate glass, and 710a, a soda-lime silicate glass. The borosilicate glass was used as the primary reference material. The equations used to calculate and predict the viscosity of both the borosilicate glass and the soda lime silicate glass can be seen in section 2.3.5.

The results of experiments using both standards are shown in Figures 2.20 and 2.21. These standards cannot be heated above about 1400ºC, because 710a can lose Na and 717a can lose B through volatilization. We could still measure the viscosities of both materials from $10^{1.0}$ to $10^{4.4}$ Pa.s. The borosilicate glass gave results within 0.01 log units of the certified viscosity. The soda lime silicate gave results within 0.04 log units of the

certified viscosity. The precision of both of these was within 0.02 log units, based on replicate measurements at high temperature at the end of the experiment.

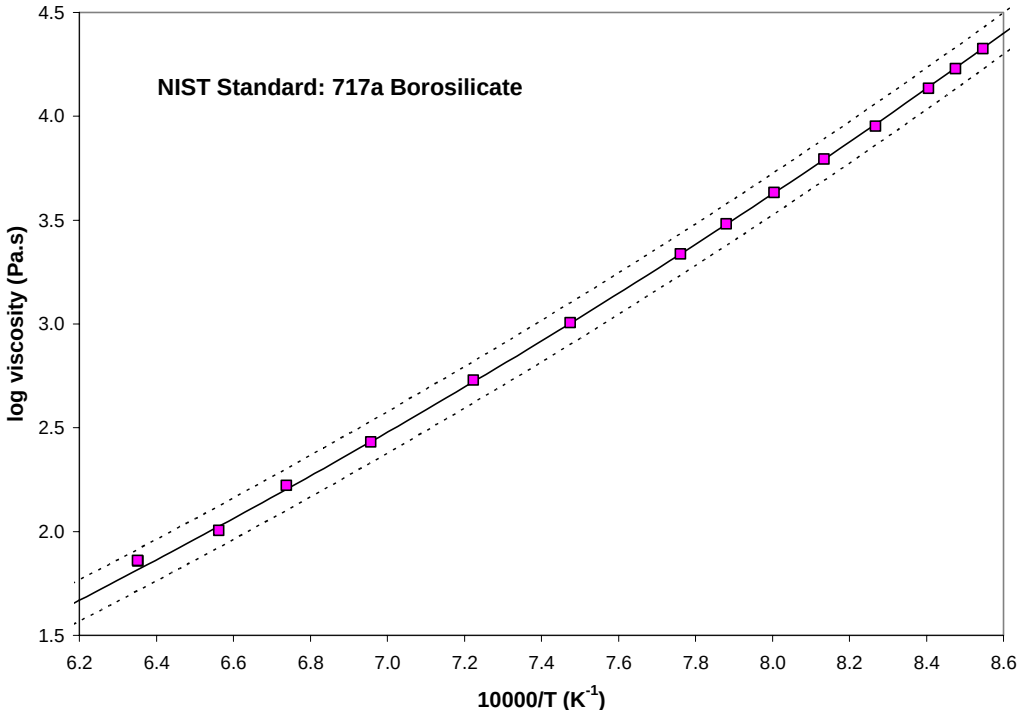

Figure 2.20. The test run results of the borosilicate glass.

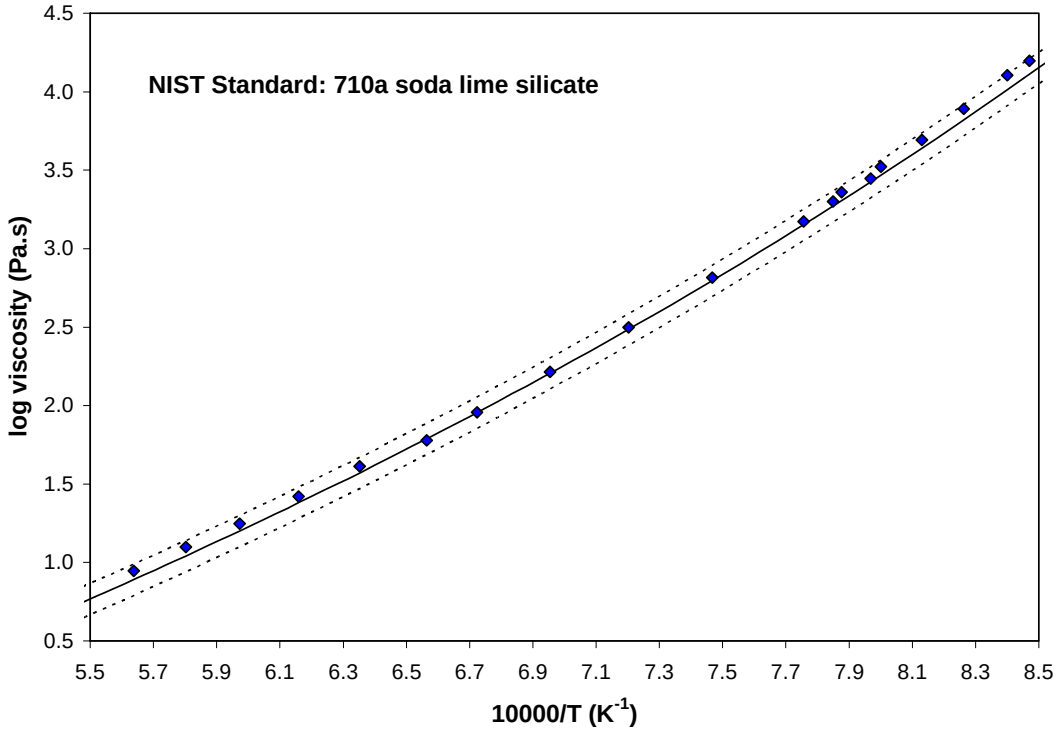

Figure 2.21. The test run results of the soda lime silicate glass.

2.5 Summary

- Synthetic dacite and rhyodacite glasses were made based on compositions from Santiaguito Dome complex, which are typical of arc volcano compositions. These compositions are vital to understand because they are involved in explosive volcanism.
- Hydrous samples were synthesized using an IHPV at the Institüt für Mineralogie in Hannover, Germany. Water contents ranged from 0.4 to 5.0 wt.%. Attempts to synthesized fluorine-bearing samples failed due to fluorine volatilization during synthesis.
- The densities were measured based on the Archimedes principle for each sample.
- The parallel plate viscometer was used to measure both anhydrous and volatile bearing samples in the glass transition range, between 10^{9} and $10^{12.5}$ Pa.s. The viscometer has an accuracy of 0.05 log units and precision of 0.04 log units based on the measurements of the NIST certified reference materials..
- The concentric cylinder viscometer was used to measure viscosity of anhydrous liquids at superliquidus temperatures in the range of $10^{1.5}$ to 10^{5} Pa.s. The accuracy of the viscometer is 0.04 log units and the precision of 0.02 log units based on the measurements of the NIST certified reference materials.

Having discussed the techniques that were used in this study, the next chapter will show the results of the viscosity data that was measured. It will include interpolation of viscosity at magmatic temperatures, measured between the data found by the parallel plate and concentric cylinder viscometers.

CHAPTER 3 – RESULTS

3.1 Overview

This chapter will present the results measured on the parallel plate and concentric cylinder viscometers of the viscosity of synthetic dacite and rhyodacite liquids as a function of temperature, water content, and NBO/T ratio. First, the viscosity of the two nominally anhydrous base compositions is described, and compared with data from previous studies on related compositions. Next, the results on hydrous samples are presented and the effect of water on decreasing liquid viscosity is discussed. The effects of fluorine are briefly described. Finally, the viscosity of different anhydrous samples with varying polymerization states is investigated.

In addition to presenting the raw data, TVF equations are fitted to each composition investigated. This allows (1) interpolation to magmatic temperatures for each sample and (2) parameterization which may be used to predict viscosities at high temperatures and volatile contents simultaneously.

3.2 Results

3.2.1 Anhydrous Samples

The anhydrous compositions were determined by electron microprobe analysis and are shown in Table 3.1. The sample compositions were chosen to be very slightly depolymerized, as determined by their NBO/T ratios (0.10 for the rhyodacite 0.06 for the dacite). The NBO/T represents the average number of non-bridging oxygens (NBO) per tetrahedrally coordinated cation. The NBO/T is calculated by taking $(2*(K_2O + Na_2O + CaO + MgO + FeO - Al_2O_3)/(SiO_2 + 2Al_2O_3)$ (Mysen and Richet, 2005). The Al^{3+} charge balances with the network modifying cations in order to achieve a tetrahedral state, thus it

is subtracted from them in the calculations to remove potential network modifiers that are actually charge balancing tetrahedral Al^{3+}. A fully polymerized melt will have a value of 0 for NBO/T, such as many rhyolites, while a depolymerized melt will have a high value of NBO/T, such as basalt with a value of 0.8.

Table 3.1
Compositions of anhydrous starting materials

	Rhyodacite	Std. Dev.[d]	Dacite	Std. Dev.[d]
wt.% oxides				
SiO_2	63.12	0.22	61.05	0.34
TiO_2	0.52	0.03	0.71	0.05
Al_2O_3	19.53	0.20	22.19	0.12
MgO	2.28	0.03	1.46	0.01
CaO	6.44	0.10	7.82	0.08
Na_2O	4.63	0.08	4.33	0.07
K_2O	1.62	0.02	1.48	0.02
Total	98.15	0.69	99.05	0.68
mol % oxides				
SiO_2	69.49		67.56	
TiO_2	0.43		0.59	
Al_2O_3	12.67		14.47	
MgO	3.74		2.41	
CaO	7.59		9.27	
Na_2O	4.94		4.64	
K_2O	1.14		1.04	
molar mass (g)	64.91		65.85	
NBO/T[a]	0.10		0.06	
Al/(Al+Si)	0.27		0.30	
SM[b]	17.41		17.38	
NK/NKMC[c]	0.35		0.33	

[a]NBO/T = $(2*(K_2O + Na_2O + CaO + MgO + FeO - Al_2O_3)/(SiO_2 + Al_2O_3 + Al_2O_3))$ Calculation based on Mysen and Richet (2005).
[b]SM parameter = $(Na_2O + K_2O + MgO + CaO)$ Calculation based on Giordano and Dingwell (2003).
[c]NK/NKMC = $(Na_2O + K_2O)/(Na_2O + K_2O + MgO + CaO)$
[d]Values are the average of 6 spots taken by the JEOL 733 Superprobe at Washington University-St. Louis.

Low and high temperature viscosities of the anhydrous rhyodacite and dacite melts are reported in Tables 3.2 to 3.4. When investigating the viscosities of silicate liquids, it is important to measure both the high and low viscosity/temperature range because non-Arrhenian behavior can be observed. If viscosity is only examined over a restricted range of temperatures, the viscosity may appear to be Arrhenian, though this obviously is not the case (Figure 3.1). By measuring both the high and low temperature range of viscosities, values of the intermediate temperature range relevant to magmatic processes can be interpolated instead of extrapolated, giving much more accurate predictions.

Table 3.2
High temperature viscosities of anhydrous rhyodacite and dacite

Rhyodacite		Dacite	
T (K)	log η (Pa s)	T (K)	log η (Pa s)
1865.8	1.48	1868.2	1.48
1848.5	1.56	1848.6	1.57
1824.3	1.67	1829.2	1.66
1799.9	1.79	1809.8	1.76
1775.7	1.91	1790.3	1.86
1751.5	2.03	1770.8	1.96
1727.2	2.16	1751.5	2.06
1703.1	2.31	1732.3	2.17
1678.9	2.45	1712.8	2.28
1654.6	2.60	1693.4	2.39
1630.3	2.76	1674.1	2.51
1605.9	2.92	1654.7	2.63
1581.7	3.10	1630.4	2.79
1556.9	3.28	1605.9	2.95
1532.5	3.47	1581.4	3.12
1507.5	3.67	1562.1	3.26
1483.1	3.88	1537.4	3.45
1458.4	4.11	1512.6	3.64
1438.5	4.30	1488.3	3.84
1418.3	4.50	1463.4	4.06
		1438.8	4.28
		1414.4	4.53

Table 3.3
Low temperature viscosities of rhyodacite samples

Anhydrous		0.38 wt.%		0.97 wt.%		2.84 wt.%		3.61 wt.%		5.09 wt.%	
T (K)	log η (Pa s)	T (K)	log η (Pa s)	T (K)	log η (Pa s)	T (K)	log η (Pa s)	T (K)	log η (Pa s)	T (K)	log η (Pa s)
1017.3	12.54[b]	912.4	11.91[6]	846.0	11.77[3]	745.1	11.38[3b]	702.8	12.07[5]	672.8	11.48[2b]
1022.1	12.35[a]	917.6	11.75[7]	857.7	11.23[1]	745.2	11.36[2b]	707.0	11.82[3]	681.1	10.93[1b]
1027.0	12.22[b]	922.0	11.51[4]	864.5	11.00[2]	753.3	10.94[2a]	712.7	11.53[4]	691.6	10.20[1a]
1032.4	12.03[a]	925.2	11.41[5]			753.5	10.88[3a]	719.3	11.22[2]		
1037.2	11.89[b]	929.5	11.16[2]			758.8	10.70[1b]	725.6	10.90[1]		
1042.0	11.71[a]	934.9	11.04[3]			766.8	10.52[1a]				
1047.7	11.58[b]	939.1	10.80[1]								
1052.5	11.42[a]										
1057.1	11.29[b]										
1063.0	11.11[a]										
1067.2	10.97[b]										
1074.3	10.75[b]										
1077.4	10.67[b]										
1082.1	10.50[a]										
1087.5	10.39[b]										
1092.2	10.22[a]										
1097.4	10.12[b]										
1102.4	9.95[a]										
1107.5	9.86[b]										
1112.5	9.69[a]										
1117.4	9.60[b]										
1122.6	9.46[a]										
1127.5	9.36[b]										
1132.7	9.21[a]										
1137.8	9.12[b]										
1143.1	8.97[a]										
1146.2	8.93[b]										

[a,b]For the anhydrous sample, superscripts indicate measurements on 2 different cylinders RD0a and RD0b.
[1,2,3....]Numbers on the hydrous samples indicate the order in which the measurements were taken. Letters indicate which cylinder.

Table 3.4
Low temperature viscosities for the dacite samples

Anhydrous		0.97 wt.%		2.27 wt.%		2.79 wt.%		3.73 wt.%		4.94 wt.%	
T (K)	log η (Pa s)	T (K)	log η (Pa s)	T (K)	log η (Pa s)	T (K)	log η (Pa s)	T (K)	log η (Pa s)	T (K)	log η (Pa s)
997.3	12.76[b]	835.4	12.05[5]	775.9	12.28[5]	740.3	11.61[3]	677.5	12.07[4b]	661.5	11.46[4]
1002.5	12.57[c]	842.8	11.73[4]	785.9	11.84[4]	751.1	11.15[2]	679.7	11.98[3a]	668.8	11.11[2]
1012.5	12.16[a]	848.9	11.38[2]	795.5	11.35[2]	759.8	10.69[1]	682.3	11.76[4a]	671.9	11.05[3]
1017.6	12.06[b]	855.0	11.28[3]	804.8	11.12[3]			688.8	11.49[3b]	681.7	10.53[1]
1022.4	11.84[c]	861.5	10.83[1]	809.6	10.79[1]			691.9	11.27[2a]		
1027.3	11.73[b]							696.0	11.08[2b]		
1032.3	11.56[a]							697.8	10.93[1b]		
1037.5	11.40[b]							698.8	10.91[1a]		
1042.4	11.25[a]										
1047.5	11.03[b]										
1052.7	10.94[a]										
1057.5	10.77[b]										
1062.3	10.62[a]										
1067.2	10.49[b]										
1072.4	10.34[a]										
1074.7	10.25[c]										
1077.5	10.22[b]										
1082.5	10.07[a]										
1087.2	9.97[b]										
1092.8	9.80[a]										
1102.6	9.55[a]										
1112.5	9.31[a]										
1122.8	9.07[a]										
1126.3	9.02[a]										

[a,b,c]For the anhydrous sample, superscripts indicate measurements on 3 different cylinders.
[1,2,3,...]Numbers on the hydrous samples indicate the order in which the measurements were taken. Letters indicate which cylinder.

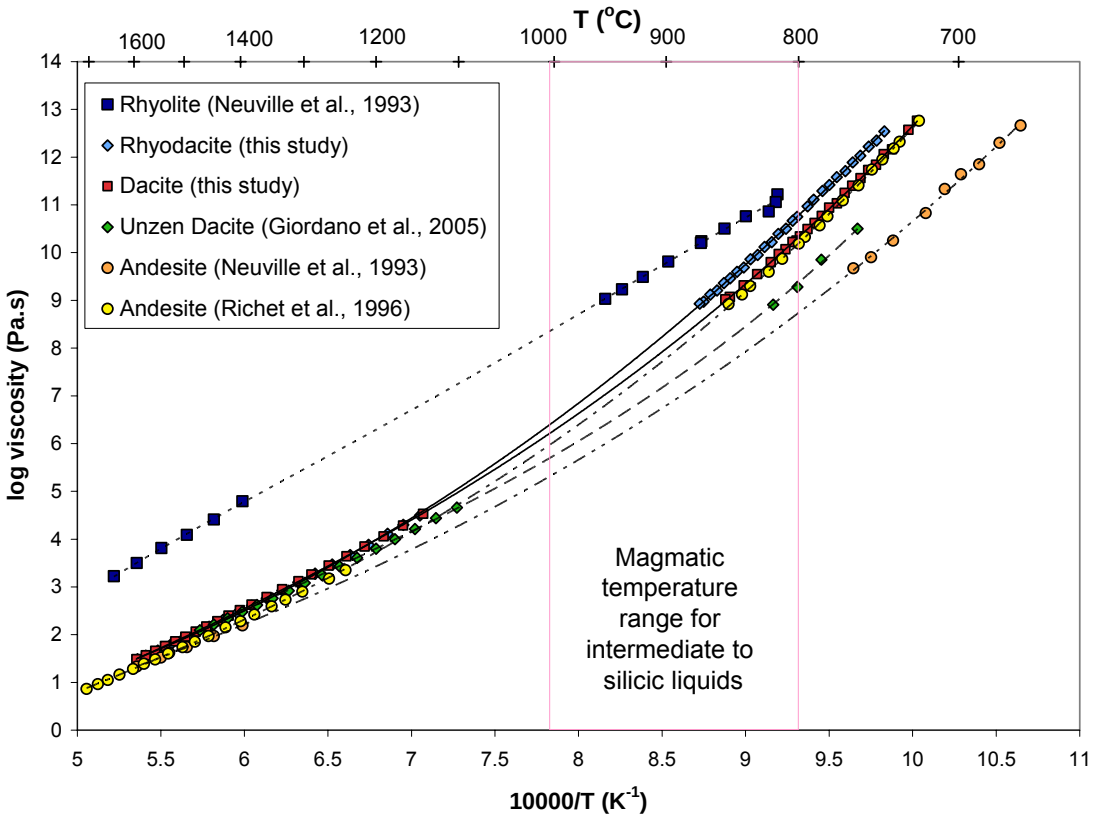

Figure 3.1. Viscosities of the anhydrous melt compositions versus reciprocal temperature. For comparison are two synthetic andesite (Richet et al., 1996; Neuville et al., 1993), Unzen dacite (Giordano et al., 2005), and Little Glass Butte Rhyolite (Neuville et al., 1993). The lines are TVF curves fit to the measured data.

Results from previous studies of various anhydrous melts are also shown in Figure 3.1 including a dacite from Mt. Unzen (Giordano et al., 2005), two synthetic andesites (Richet et al., 1996; Neuville et al., 1993), and rhyolite from Little Glass Butte, California (Neuville et al., 1993) in comparison with the rhyodacite and dacite of this study. At high temperatures, the viscosities of all these compositions are very similar, except for the rhyolite. The spread between all the data, excluding the rhyolite, is about 0.6 log units at 1200ºC. This is not the case at lower temperatures, where the compositions are more spread out, with the Neuville et al. (1993) andesite being the least viscous and the synthetic rhyodacite being the most viscous. At 1000ºC, the spread is

about 1.3 log units, increasing to 2 log units at 800ºC. The range between 800 and 1000ºC is very important since this is the typical magmatic temperature range of silicic to intermediate liquids. The rhyolite, being the most highly polymerized, is more viscous than the other liquids, and also behaves in a more Arrhenian fashion.

3.2.2 Hydrous Samples

The low temperature viscosities of the hydrous rhyodacite and dacite melts are reported in Tables 3.3 and 3.4, and plotted against inverse temperature in Figure 3.2, respectively. As mentioned in Chapter 1, the higher the water content of the sample, the more restricted the accessible viscosity range becomes. With lower water contents, higher temperatures and lower viscosities can be measured. Water loss is always a concern when measuring hydrous samples, but it is immediately evident when it occurs. Due to the very strong dependence of viscosity on water content, as soon as even a small amount of water is exsolved, the viscosity being measured will drastically increase. Several of the water samples were run using two separate cylinders prepared from the same sample (Tables 3.3 and 3.4), and their viscosities matched up well, showing the precision and accuracy of our measurements. In addition, measurements were typically made at successively higher and lower temperatures to check for consistency during measurements on individual cylinders. The order in which measurements were taken is also listed in Tables 3.3 and 3.4. In the majority of experiments, some water loss and/or crystallization was observed at the highest temperatures. These data are not shown.

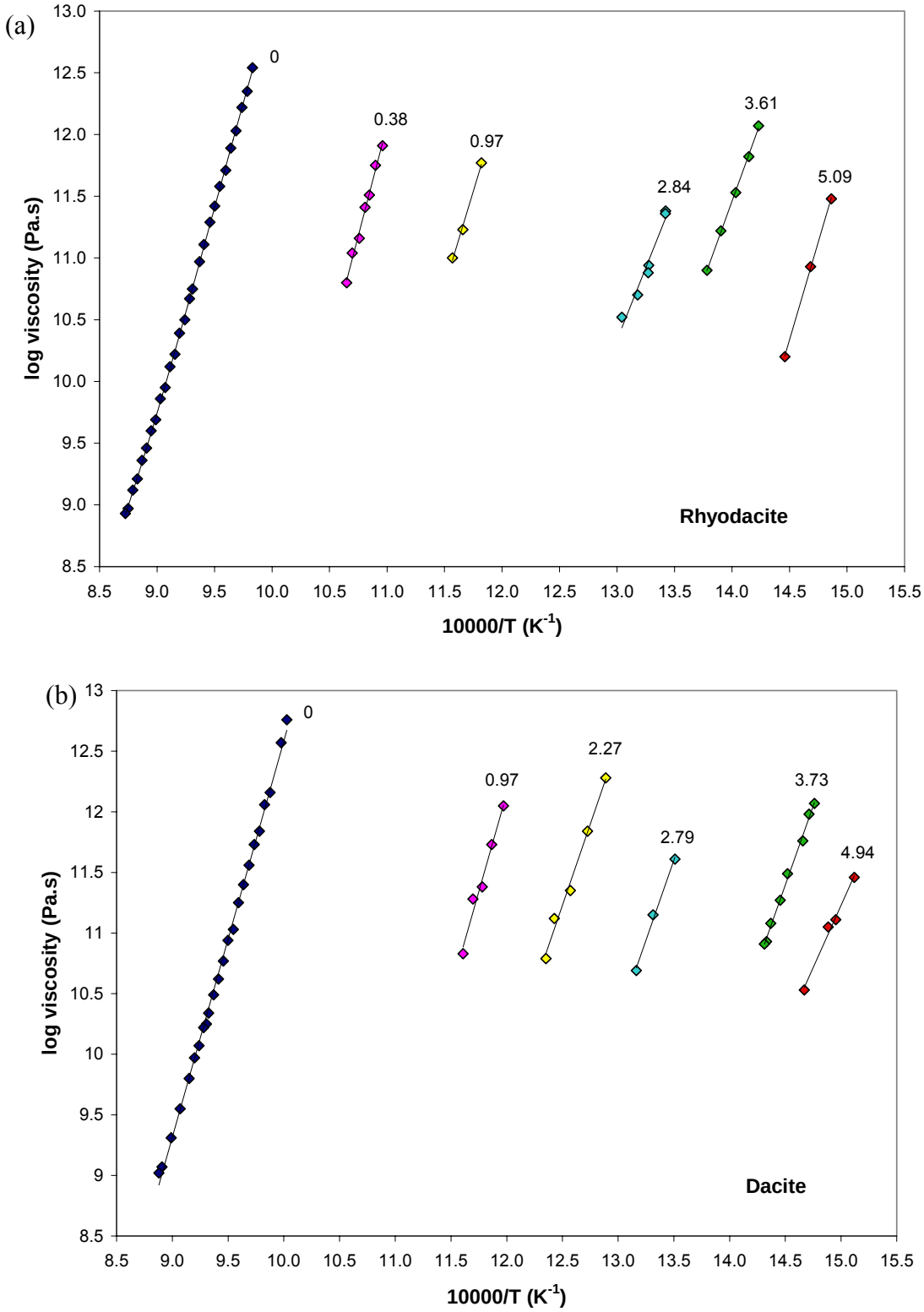

Figure 3.2. (a) Rhyodacite and (b) dacite viscosities versus reciprocal temperature near the glass transition range. Measurement errors are smaller than symbol size, numbers refer to water content in weight percent. The lines are the constrained TVF equations from Table 3.5.

The low temperature data was fitted using the Tammann-Vogel-Fulcher (TVF) equation, an empirical equation which allows for the non-Arrhenian behavior as observed in these samples:

$$\log\eta = A + \frac{B}{(T - C)} \qquad (3.1)$$

The TVF equation has three adjustable parameters, A, B and C, which were determined for each of the hydrous samples. First, the TVF equation was fitted to the anhydrous data for dacite and rhyodacite, using both the high and low temperature data. The value for parameter A of the anhydrous sample, the log η intercept at infinite temperature, was then assumed to be the same for the hydrous samples within that series. This was done because the hydrous samples cannot be measured at high temperatures due to exsolution of the water, and the limited amount of low temperature data is insufficient to well constrain an equation with three unknowns. A set of equations was then fitted for the hydrous samples with only B and C as adjustable parameters. The process used here is described by Richet et al. (1996) and Russell et al. (2003). The values of A, B and C found using the TVF equation are listed in Table 3.5.

The effect of water content is very strong in decreasing the viscosity of both the dacite and rhyodacite compositions (Figure 3.2). For example, at 1100 K, the viscosities of the rhyodacite are calculated to be $10^{10.01}$, $10^{5.07}$, and $10^{2.59}$ Pa.s for water contents of 0, 0.97, and 3.61 wt.%, while the viscosities of the dacite are calculated to be $10^{9.61}$, $10^{4.86}$, and $10^{2.2}$ Pa.s for water contents of 0, 0.97, and 3.73 wt.%. For both the rhyodacite and dacite, the addition of about 1 wt.% H_2O causes a decrease in viscosity of almost 5 orders of magnitude at 1100 K, while the addition of nearly 4 wt.% water causes a decrease of more than 7 orders of magnitude. The rhyodacite is affected slightly more

Table 3.5
Parameters for TVF equations, log10 $\eta = A + B/(T - C)$

Sample (wt.% H_2O)	A (Pa s)[a]	B (Pa s K^{-1})[b]	C (K)[b]	T^{12}(K)[c]	F_D
Rhyodacite					
Anhydrous	-4.79	8187 (21)	546.8 (1.4)	1034	0.07
0.38	-4.79	6268 (269)	537.6 (16.6)	911	0.09
0.97	-4.79	6199 (395)	471.3 (24.4)	841	0.08
2.84	-4.79	5970 (591)	374.6 (37.5)	730	0.06
3.61	-4.79	5219 (75)	392.9 (4.6)	704	0.08
5.09	-4.79	3579 (131)	452.9 (8.3)	666	0.13
Dacite					
Anhydrous	-4.45	7885 (8)	539.3 (0.5)	1019	0.07
0.97	-4.45	5650 (502)	493.1 (31.5)	837	0.09
2.27	-4.45	5982 (353)	418.2 (22.1)	782	0.07
2.79	-4.45	5211 (434)	416.1 (27.8)	733	0.08
3.73	-4.45	4710 (113)	392.0 (7.0)	678	0.08
4.94	-4.45	5261 (400)	331.0 (25.8)	651	0.06

[a]Constrained fit; parameter A was fitted for the anhydrous samples and then constrained to be the same value for hydrous samples.
[b]Numbers in brackets are absolute uncertainties.
[c]T_{12} indicates the temperature at which the viscosity is 10^{12} Pa s, taken to be the effective glass transition temperature.
[d]The fragility, F_D, is calculated where $F_D = C/B$. See text for details.

than the dacite. In both cases, the initial addition of water has the largest effects in decreasing the viscosity. The addition of more water into the sample continues to decrease the viscosity, but the resulting decrease is progressively smaller.

The effect of water on both the dacite and the rhyodacite is greater than on the synthetic andesite of Richet et al. (1996), but less than on the synthetic haplogranite of Dingwell et al. (1996). The andesite viscosity is decreased by 4 orders of magnitude with the addition of 1 wt.% H_2O, while the viscosity of the haplogranite decreases by more than 5 orders of magnitude for the same water content, at 1100 K. This is consistent with the order of polymerization of these melts, and will be discussed more in Chapter 4.

It can also be seen that water causes a larger decrease at lower temperatures than at higher temperatures (Figure 3.3), which is consistent with larger viscosity differences

between different anhydrous compositions shown in Figure 3.1. The calculated dacite viscosities show more scatter than for the rhyodacite sample, although a similar trend is clearly apparent. There could be several reasons for this. First, the calculations require extrapolation from the temperature range of the measurements for hydrous samples. Secondly, dissolved water within the samples could have been slightly inhomogeneous. This is unlikely because the thermal gradient across the sample during hydration was very small and water solubility is only very slightly dependent on temperature at the synthetic conditions (Behrens, 1995). A third explanation, that some water was lost at the beginning of the viscometry experiment, is doubtful. Once water has begun to exsolve, it would continue to do so during the measurements, and the data would be less consistent than observed.

Analyzing the variation of the viscosity as a function of water content at a constant temperature, shown in Figure 3.3, requires extrapolation well outside the measured viscosity range. An alternative approach is to consider isokoms (lines of constant viscosity) because the viscosity range investigated is more restricted than the temperature range. The 10^{12} Pa.s isokom corresponds approximately to the glass transition temperature of the samples. There is a strong decrease in the temperatures of all isokoms with the addition of water, which is greatest at the smallest water contents (Figure 3.4). For example, the temperature at which the viscosity of both series is 10^{11} Pa.s decreases by about 200 K with the addition of about 1 wt.% water, but by only 200 K more with the addition of a further 4 wt. %. Rhyodacite viscosities appear to continue to decrease at water contents higher than was investigated here, while the dacite series appears to be little affected by further added water in excess of about 3.5 wt.%.

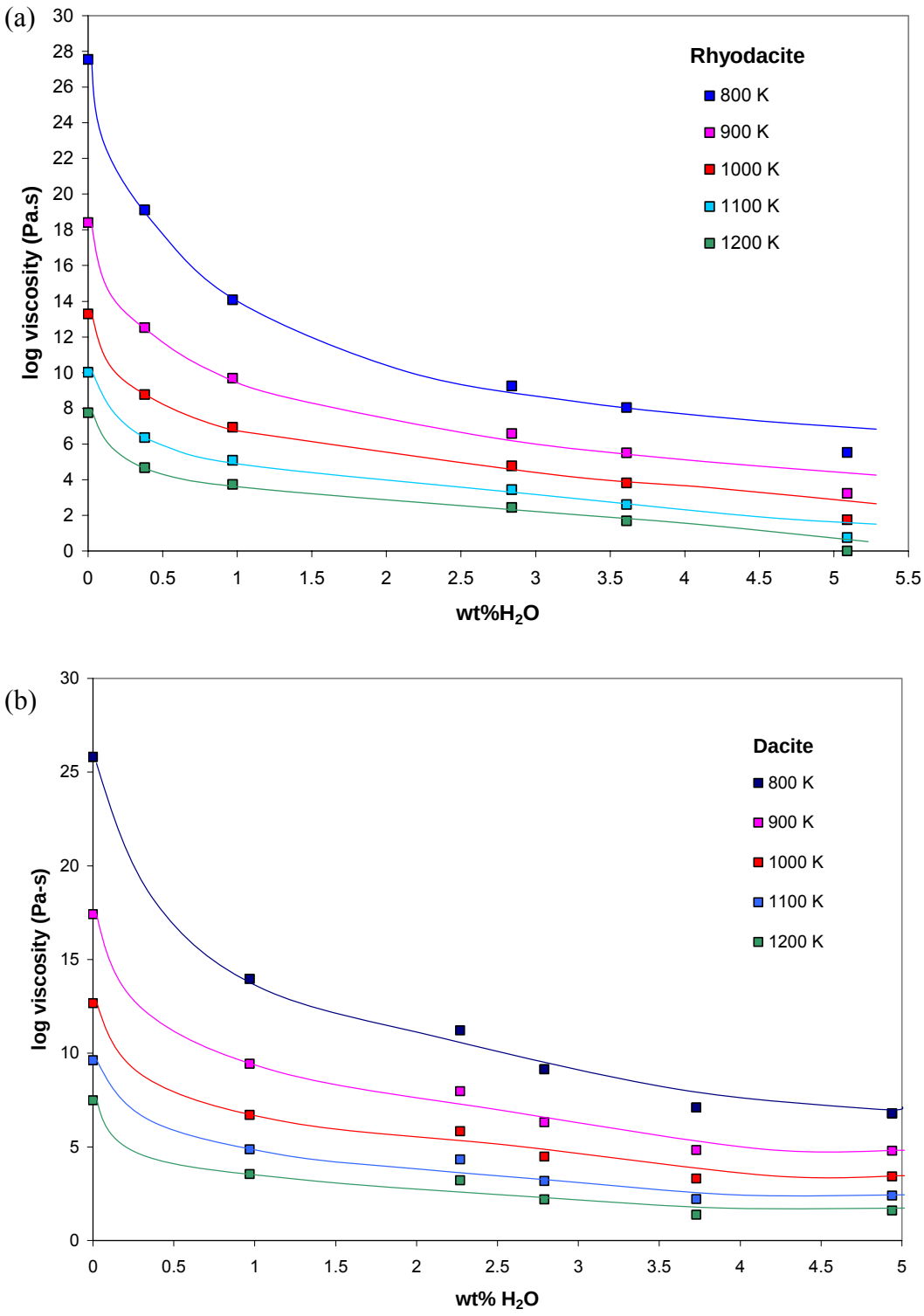

Figure 3.3 a and b. Viscosity of the (a) rhyodacite and (b) dacite hydrous melts as a function of temperature and water content. Symbols indicate points calculated from the constrained TVF equations of Table 3.5. The lines are intended to guide the eye.

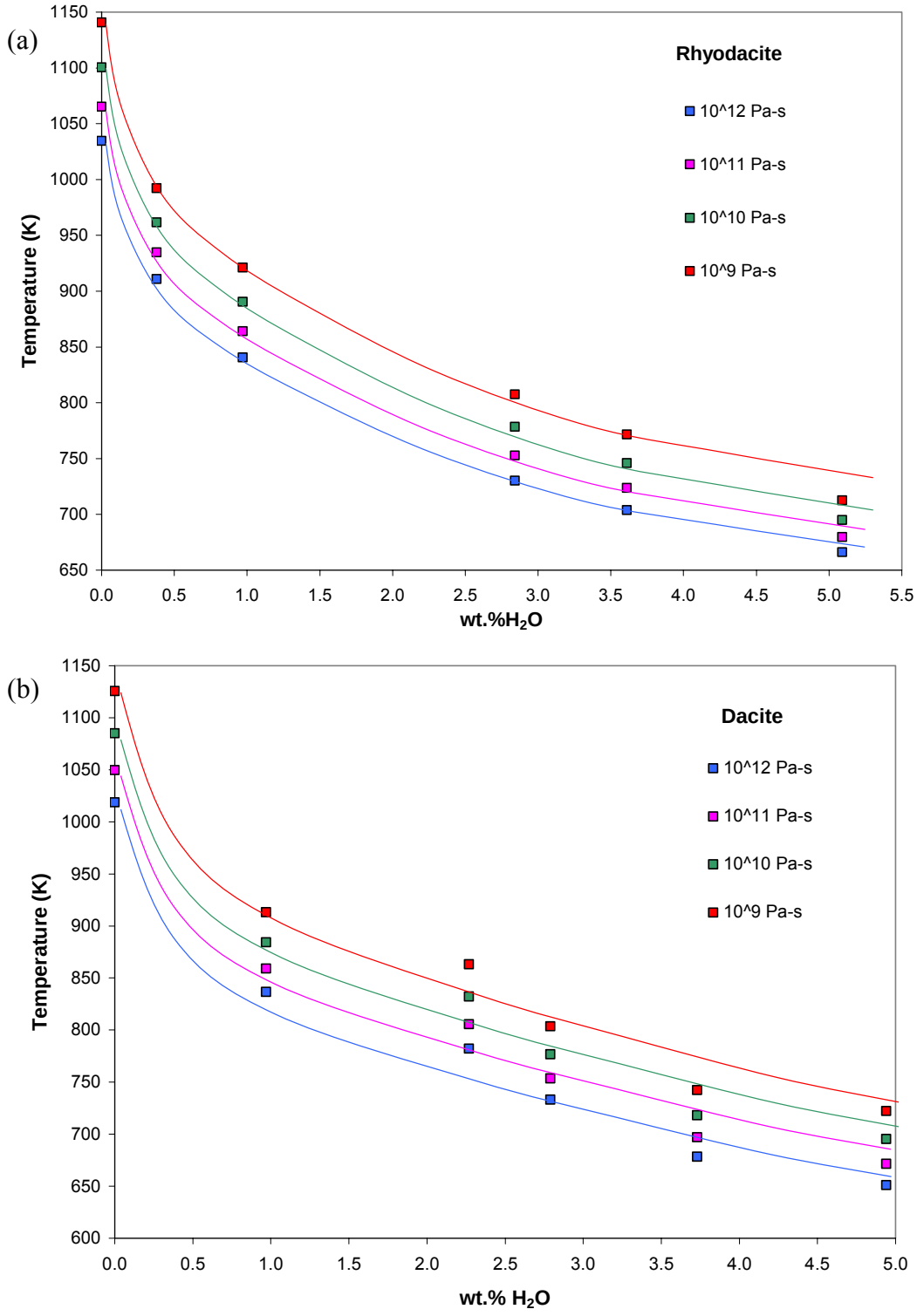

Figure 3.4 a and b. Temperatures of the 10^9, 10^{10}, 10^{11}, and 10^{12} Pa-s isokoms (lines of equal viscosity) against water content for (a) rhyodacite and (b) dacite. Symbols indicate points calculated from the constrained TVF equations of Table 3.5. The lines are intended to guide the eye.

There has been one previous study of hydrous dacite liquid viscosities, on a sample from Unzen Volcano in Japan (Giordano et al., 2005). Their dataset is rather limited, measuring a restricted range of water contents ranging from 1.31, 1.64, and 1.98 wt.% (Figure 3.5). The nominally anhydrous Unzen dacite is slightly less viscous when compared to the nominally anhydrous dacite and rhyodacite from this study, but the viscosities of hydrous samples are similar for all three compositions (Figure 3.6).

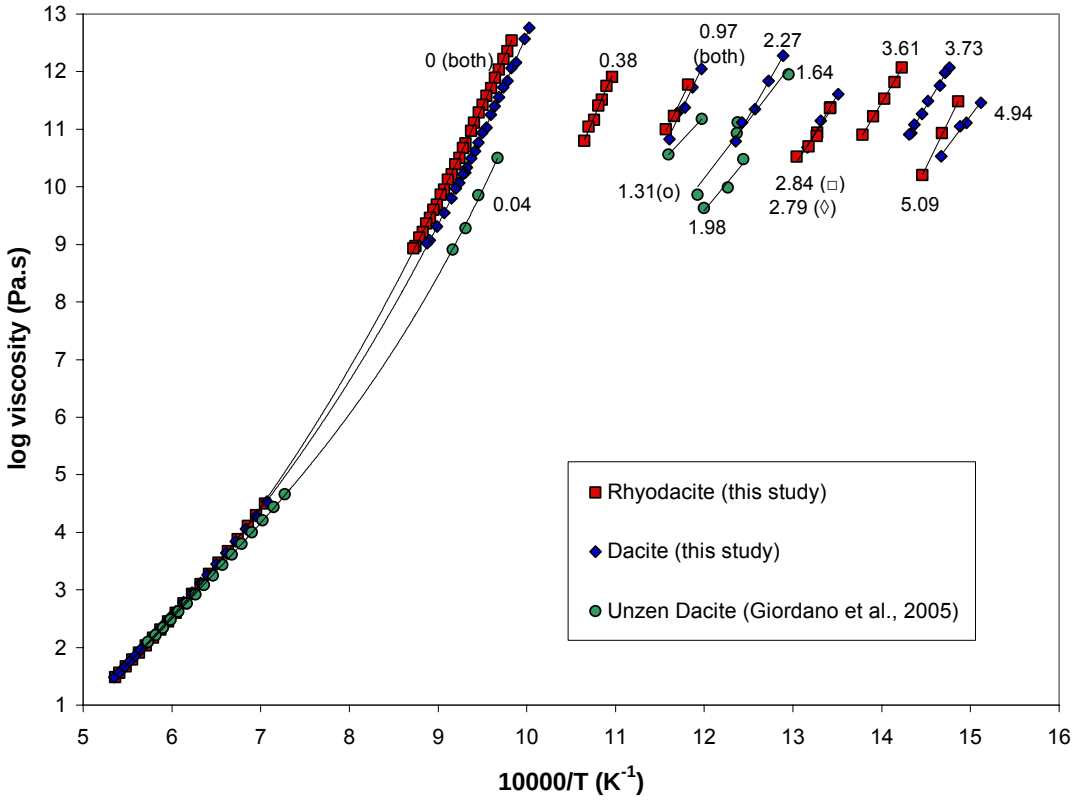

Figure 3.5. A comparison of the viscosities of the Unzen dacite (Giordano et al., 2005) and the dacite and rhyodacite from this study. Points are actual measured data, lines are fitted curves and the number indicated the water content within each sample.

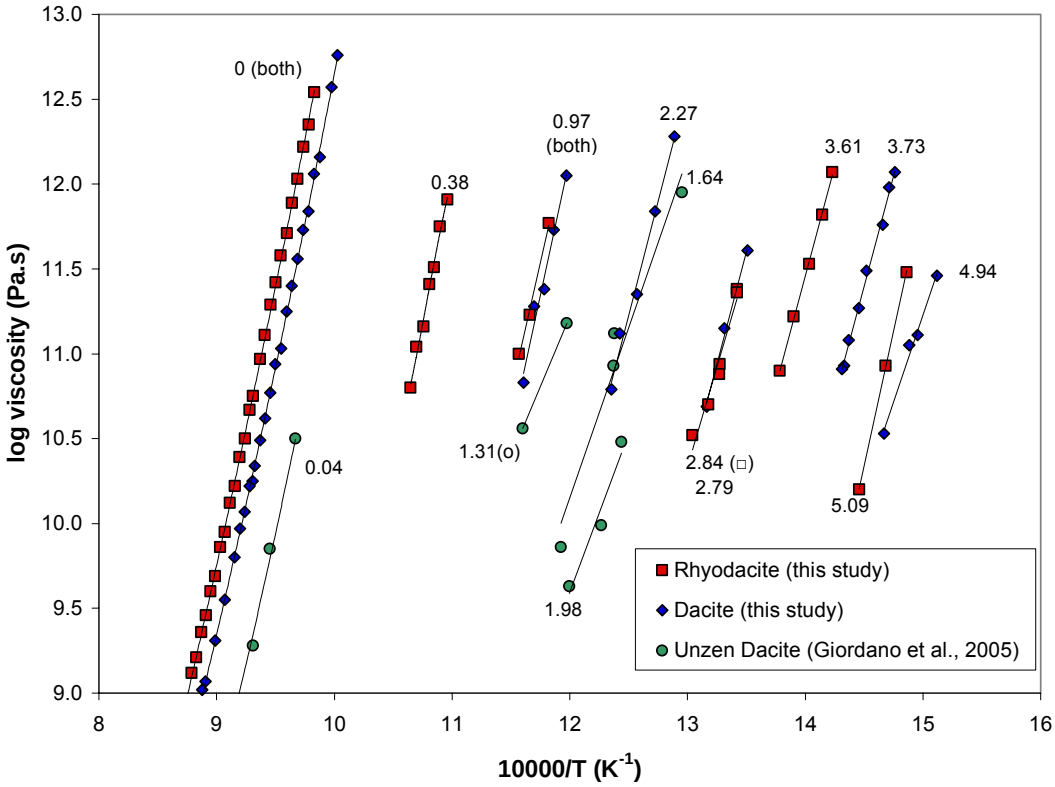

Figure 3.6. A comparision of the Unzen dacite and the dacite and rhyodacite from this study at the high viscosity range. Points are actual measured data, lines are fitted curves and the number indicates the water content in wt.%.

Water content not only reduces the viscosity of silicate melt compositions, but also causes the viscosities to depart more strongly from Arrhenian laws. This agrees with previous observations for andesites (Richet et al., 1996), phonolites and trachytes (Whittington et al., 2001) and haplogranite (Dingwell et al., 1996). Melt "fragility" (F) is a concept that provides a quantitative indicator of the degree of non-Arrhenian behavior of the melt (Angell, 1985). Fragility is used to distinguish between the two extreme behaviors of glass forming liquids: strong (Arrhenian) and fragile (non-Arrhenian). Fragile liquids show rapid viscosity decreases upon heating above the glass transition because they have large configurational heat capactities. The fragility can be quantified using the B and C parameters of the TVF equation:

$$F_D = C/B \qquad (3.2)$$

(Angell, 1985; Angel, 1991). The calculated values of fragility are listed in Table 3.5 and plotted as a function of water content in Figure 3.7. While hydrous samples typically have a higher fragility than anhydrous samples, there is no clear trend.

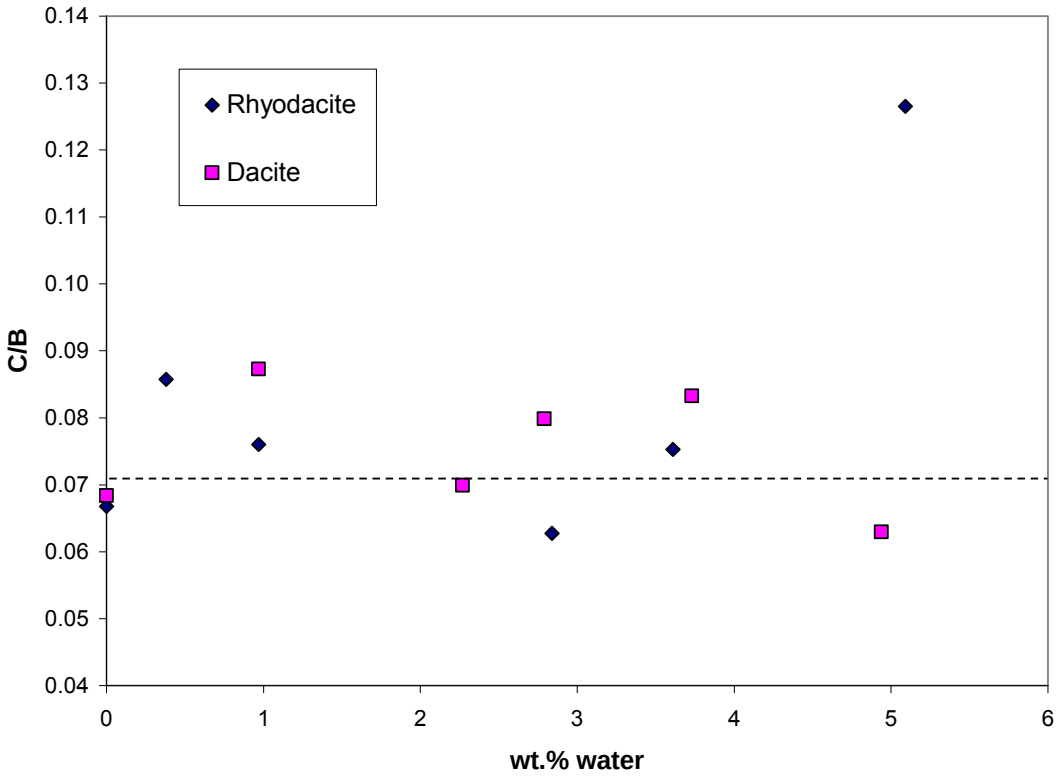

Figure 3.7. The fragility (C/B) as a function of mol% water of the rhyodacite and dacite liquids.

The molar volumes of the samples were calculated from density measurements (Table 2.1). As the molar fraction of dissolved water increases, the molar volumes of hydrous glasses decrease (Figures 3.8 and 3.9). The points show some scatter due to the different fictive temperatures of different glasses underwent during synthesis. The fictive temperature of the glass is the temperature at which the supercooled liquid would have the same configuration as the glass (Mysen and Richet, 2005). Both the rhyodacite and

dacite show linear trends in their molar volume, with a partial molar volume of water of 11.54±0.005 cm^3/mol for rhyodacite and 12.15±0.005 cm^3/mol for dacite. There is no discernible difference between the hydrous samples synthesized at 2 and 3 kbars, although the anhydrous glasses (synthesized at 1 atm) predictably lie slightly above the best fit line to the hydrous glasses for both series. The main conclusion that can be made is that given a constant partial molar volume of water for all water contents, the volume change for the speciation reaction (equation 1.6) is zero. This is consistent with data on many other hydrous glass compositions from granite to basalt (Richet et al., 2000)

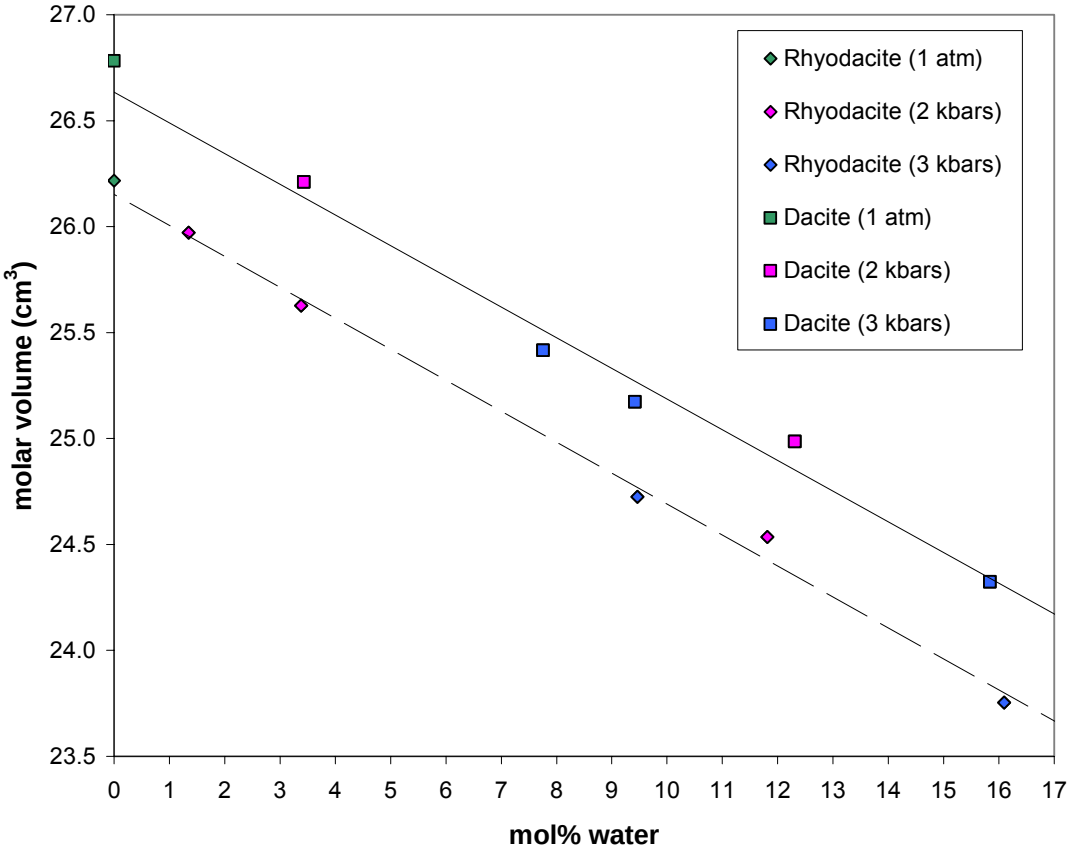

Figure 3.8. Molar volume as a function of mol% water for the dacite and rhyodacite. The lines are best fit to the compacted hydrous glasses. Error bars are smaller than the symbols.

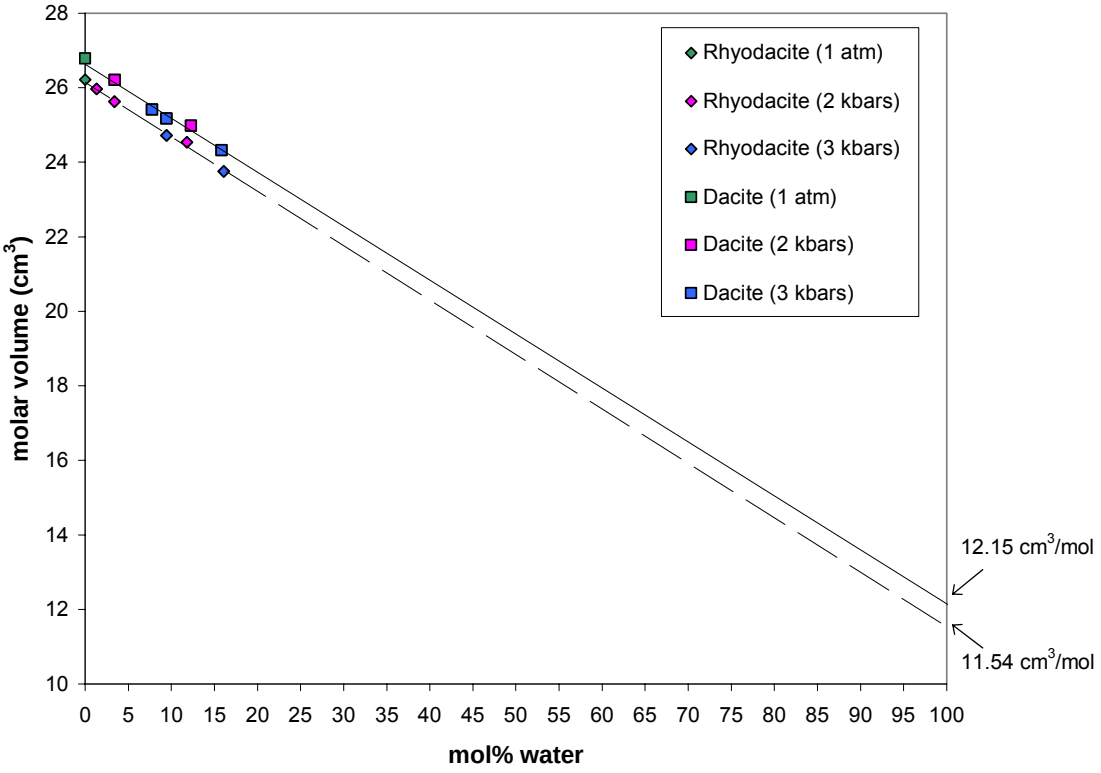

Figure 3.9. Molar volume as a function of mol% water for the dacite and rhyodacite. The lines are best fit to the compacted hydrous glasses. Error bars are smaller than the symbols.

3.2.3 Fluorine-bearing Samples

The fluorine-bearing samples which were made for this study were analyzed with an electron microprobe to determine the actual amount of fluorine remaining within the sample after synthesis. The nominal values of fluorine within both the dacite and rhyodacite samples were 0.3, 0.6, 1 and 2 wt.% F. When the samples were analyzed, almost no fluorine was detected in any of the samples (Table 3.6). The bubbles that formed during the synthesis of these samples probably allowed for the fluorine to leave the sample. The samples nominally containing 1 and 2 wt.% F showed trace amounts of fluorine remaining within them, but the others were fluorine free.

Table 3.6
Compositions of the rhyodacite F-samples measured by electron microprobe

	RD0	RD1	RD2	RD0.3	RD0.6	Std. Dev. [k]
wt.% oxides						
SiO_2	63.12	63.38	62.13	61.66	60.11	0.35
TiO_2	0.52	0.58	0.53	0.55	0.53	0.06
Al_2O_3	19.53	19.72	19.02	18.35	18.37	0.31
MgO	2.28	2.40	4.30	6.16	7.79	0.08
CaO	6.44	6.45	6.28	6.24	6.06	0.06
Na_2O	4.63	4.59	4.54	4.48	4.50	0.02
K_2O	1.62	1.52	1.51	1.58	1.56	0.08
F	0.00	0.16	0.38	0.07	0.10	0.38
Total	98.15	98.81	98.69	99.08	99.01	1.34
mol % oxides						
SiO_2	69.49	69.39	67.36	65.52	63.41	
TiO_2	0.43	0.48	0.43	0.44	0.42	
Al_2O_3	12.67	12.72	12.15	11.49	11.42	
MgO	3.74	3.91	6.95	9.77	12.26	
CaO	7.59	7.56	7.29	7.10	6.85	
Na_2O	4.94	4.87	4.77	4.61	4.60	
K_2O	1.14	1.06	1.05	1.07	1.05	
norm. min. (mol%)						
Quartz	15.21	15.64	11.98	8.81	4.67	
Plagioclase	66.05	66.33	63.65	60.24	59.98	
Orthoclase	9.17	8.56	8.42	8.64	8.47	
Diopside	4.05	3.14	3.87	5.25	4.36	
Hypersthene	5.51	6.33	12.08	17.06	22.53	
molar mass (g)	64.91	64.88	64.04	63.22	62.69	
density (g/cm^3)[a]	2.47	2.45	2.48	2.49	2.51	
NBO/T[b]	0.10	0.10	0.17	0.25	0.31	
Al/(Al+Si)	0.27	0.27	0.27	0.26	0.26	
SM[c]	17.41	17.41	20.06	22.55	24.75	
NK/NKMC[d]	0.35	0.34	0.29	0.25	0.23	
mol% NF[e]	82.47	82.59	79.94	77.45	75.25	
mol% alk[f]	6.39	5.94	5.82	5.68	5.65	
mol% alk earth[g]	11.14	11.47	14.24	16.87	19.11	
T norm[h]	94.35	91.04	85.35	80.08	76.46	
alk NBO[i]	1.85	3.06	4.25	5.02	5.37	
ae NBO[j]	3.80	5.90	10.40	14.90	18.17	

Table 3.6 continued
Compositions of the dacite F-samples measured by electron microprobe

	D0	D1	D2	D0.3	D0.6	Std. Dev. [k]
wt.% oxides						
SiO_2	61.05	60.31	58.89	58.36	57.19	0.31
TiO_2	0.71	0.66	0.64	0.60	0.60	0.06
Al_2O_3	22.19	21.26	20.84	20.21	19.76	0.21
MgO	1.46	3.34	5.10	6.98	8.63	0.11
CaO	7.82	7.42	7.24	7.19	7.05	0.06
Na_2O	4.33	4.16	4.08	4.03	3.95	0.02
K_2O	1.48	1.29	1.35	1.36	1.34	0.10
F	0.00	0.16	0.14	0.10	0.04	0.53
Total	99.05	98.60	98.28	98.83	98.56	1.40
mol % oxides						
SiO_2	67.56	66.19	64.13	62.35	60.59	
TiO_2	0.59	0.54	0.52	0.48	0.48	
Al_2O_3	14.47	13.75	13.37	12.73	12.34	
MgO	2.41	5.46	8.28	11.12	13.63	
CaO	9.27	8.73	8.45	8.23	8.01	
Na_2O	4.64	4.43	4.31	4.17	4.06	
K_2O	1.04	0.90	0.94	0.92	0.90	
norm. min. (mol%)						
Quartz	13.05	11.67	7.85	4.80	1.82	
Plagioclase	72.71	69.45	67.30	64.15	62.21	
Orthoclase	8.42	7.26	7.55	7.46	7.29	
Diopside	1.98	1.23	1.29	2.44	2.53	
Hypersthene	3.85	10.39	16.01	21.14	26.15	
molar mass (g)	65.85	64.91	64.21	63.37	62.71	
density (g/cm^3)[a]	2.46	2.49	2.50	2.52	2.55	
NBO/T[b]	0.06	0.12	0.19	0.27	0.33	
Al/(Al+Si)	0.30	0.29	0.29	0.29	0.29	
SM[c]	17.38	19.52	21.98	24.44	26.60	
NK/NKMC[d]	0.33	0.27	0.24	0.21	0.19	
mol% NF[e]	82.59	80.48	78.02	75.56	73.40	
mol% alk[f]	6.08	5.33	5.25	5.09	4.96	
mol% alk earth[g]	11.33	14.19	16.73	19.35	21.64	
T norm[h]	90.94	89.10	84.15	79.03	75.04	
alk NBO[i]	3.16	2.98	3.78	4.37	4.65	
ae NBO[j]	5.90	7.93	12.06	16.60	20.31	

Footnotes for Table 3.6

[a] Densities of glasses measured by the Archimedean method using distilled water. Errors are typically better than 0.001g/cm^3(or 1kg/m^3).

[b]NBO/T = (2(K_2O + Na_2O + CaO + MgO + FeO -Al_2O_3)/(SiO_2 +Al_2O_3 + Al_2O_3)) Calculation based on Mysen and Richet (2005).

[c]SM parameter is the total fraction of structural modifiers, irrespective of whether they are actually charge balancing and is equal to: (Na_2O + K_2O + MgO + CaO) Calculation based on Giordano and Dingwell (2003).

[d]NK/NKMC = (Na_2O + K_2O)/(Na_2O + K_2O + MgO + CaO)

[e]mol% NF = (SiO_2 +Al_2O_3 + Al_2O_3 + TiO2)

[f]mol% alk = (K_2O + Na_2O)

[g]mol% alk earth = (CaO + MgO)

[h]T norm = T/(NBO + T) = (SiO_2 +Al_2O_3 + Al_2O_3 + TiO2)/(2(K_2O + Na_2O + CaO + MgO + FeO -Al_2O_3) + (SiO_2 +Al_2O_3 + Al_2O_3 + TiO_2))

[i]alk NBO = (NBO/(T + NBO))*100*(mol% alk/(mol% alk + mol% alk earth))

[j]ae NBO = 100 – T norm – alk NBO

[k]The standard deviation is the average standard deviation of all rhyodacites and all dacites based on six analyses per chip.

The only sample which contained fluorine at or above the detection limit (~0.25 wt%) was RD2. Table 3.7 shows the electron microprobe analyses of the original synthesized sample (RD2), a glass core after a parallel plate experiment (RD2pp), and the quenched glass after a concentric cylinder experiment (RD2cc). The results show that RD2 and RD2pp samples probably still contain trace amounts of fluorine (somewhere between 0.15 to 0.35 wt.%), while the sample used in concentric cylinder viscometry probably lost the remaining fluorine during the high temperature experiment.

Wave scans were collected for several samples on the electron microprobe. The fluorine peak lies around a position of 200 nm (Figure 3.10). Two standards are shown representing what the peak would look like with 48.66 wt% F (Calcium fluoride) and 8.78 wt.% F (fluor-phlogopite). Sample peaks are not visible on this diagram in comparison to the standards, but there is a small peak that can be seen in RD2pp (Figure 3.11), indicating that trace amounts of fluorine are present. Because the peak is close to

the detection limit, it is more easily visible when the moving average is plotted (Figure 3.12). To determine the amount of fluorine within RD2pp, the standard wave scans can be used in comparison to the samples. After background subtraction, the fluor-phlogopite containing 8.78 wt.% F has about 58 counts, while sample RD2pp has approximately 2. Therefore, RD2pp contains about ±0.3 wt.% F.

Table 3.7
Compositions of RD2: original synthesis, after parallel plate, and after concentric cylinder

	RD2	RD2pp	RD2cc
wt.% oxides			
SiO_2	62.58	61.76	62.07
TiO_2	0.57	0.50	0.53
Al_2O_3	18.92	18.85	19.22
MgO	4.31	4.32	4.27
CaO	6.39	6.28	6.19
Na_2O	4.54	4.55	4.53
K_2O	1.52	1.50	1.52
F	0.37	0.38	0.12
Total	99.21	98.14	98.45

Determined by electron microprobe (RD2 coverage of 6 analyses, RD2pp abd RD2cc average if 3 analyses.

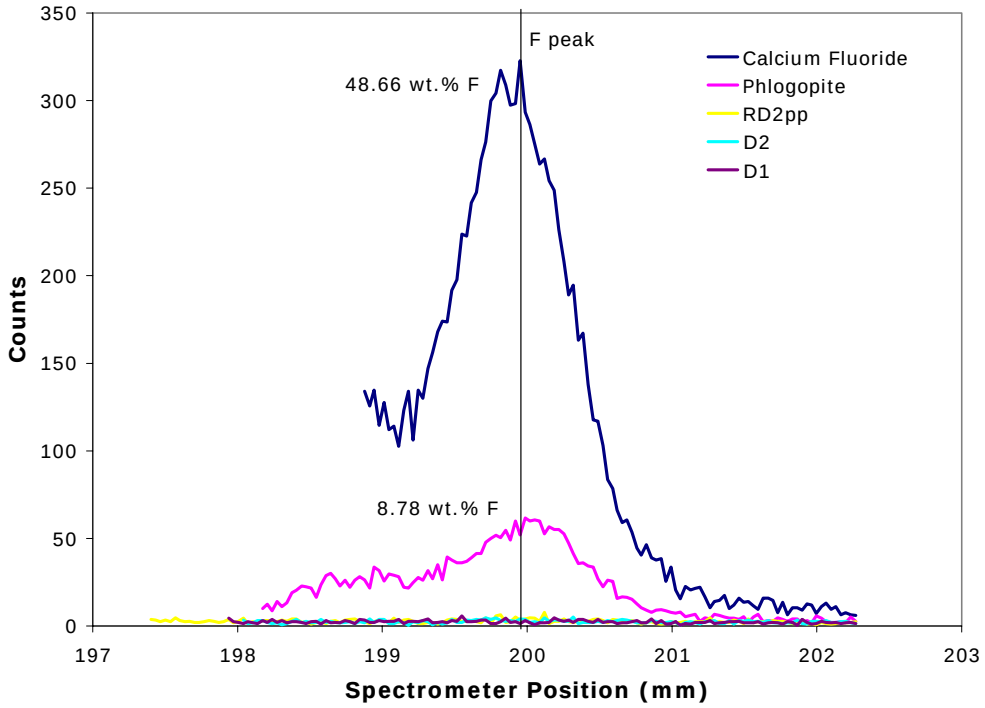

Figure 3.10. A wave scan showing the fluorine peak. The samples include 2 standards (phlogopite and CaF2), and 3 samples from this study (RD2pp, D1, and D2).

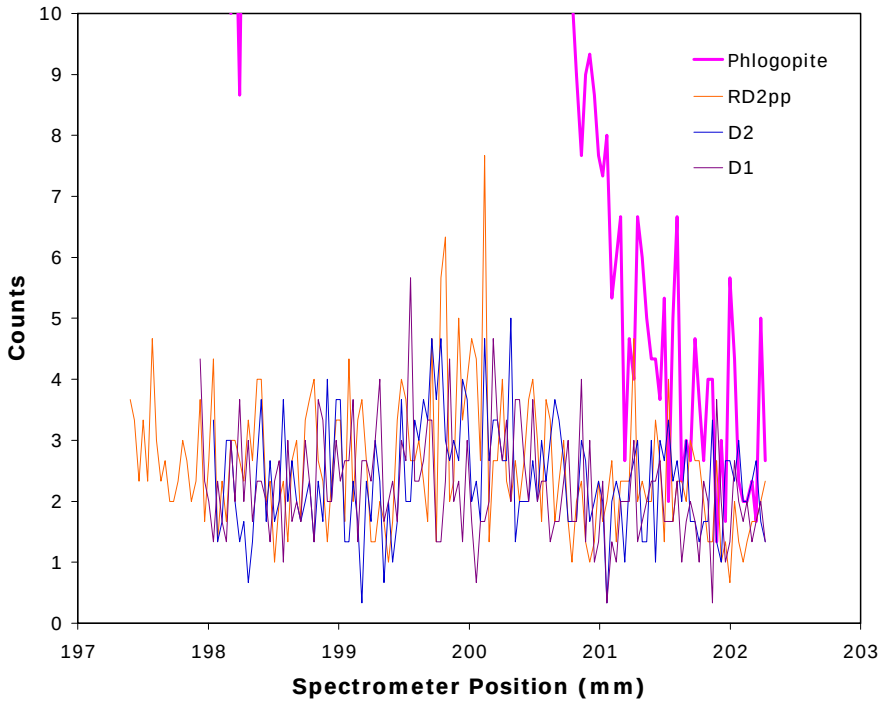

Figure 3.11. A smaller scale wave scan showing the data for the samples of this study (RD2pp, D1, and D2).

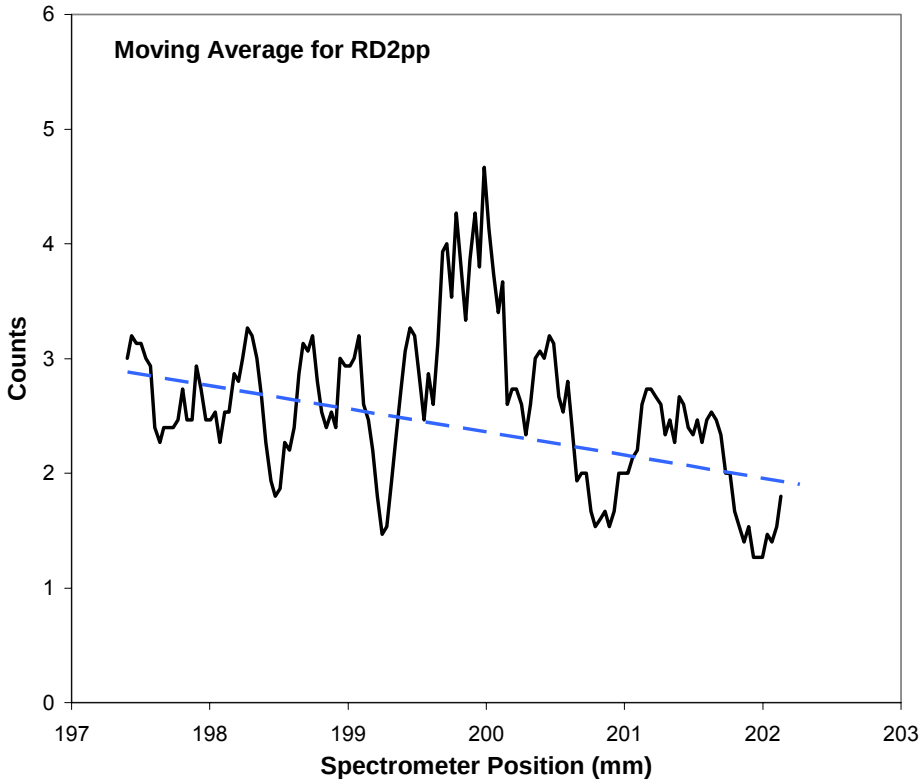

Figure 3.12. The moving average (every 5 points) of the wave scan for RD2 pp showing the fluorine peak. The dashed line is a linear baseline for the data.

Parallel plate viscometry measurements are sensitive to trace volatile contents. For example, this can be seen with the data for of RD0, RD1, RD2, and RD with 0.38 wt% water (Figure 3.13). Samples RD1 and RD0 have very similar compositions, yet the viscosities are different by 0.7 log units. The electron microprobe showed that sample RD1 potentially contained 0.1 to 0.2 wt.% F, thus its lower viscosity probably results from trace amounts of fluorine. Sample RD2 may also contain trace amounts of fluorine, but its relatively low viscosity is probably mainly due to its significantly higher MgO content compared to RD0 (see Table 3.6). The rhyodacite (RD0) containing 0.38 wt.% water plots at much lower viscosities than any of the others and about 4 to 5 log units lower than anhydrous RD0. The effects of water on dacites are greater than that of fluorine, about twice as great if the estimated F content for RD2 is correct. This is

consistent with previous studies which show a similar effect of water and fluorine on fully polymerized melts (Dingwell et al., 1985; Baker and Vaillancourt, 1995) but no effect of fluorine on highly deploymerized melts (Dingwell, 1989). The experiments presented here suggest that geologically reasonable fluorine contents will have a detectable affect on the viscosity of dacites and rhyodacites at magmatic temperatures, of the order of 1 log unit decrease for 0.35 wt.% F.

Even though fluorine was lost from the samples during synthesis, they can still be used to investigate the effect of variable anhydrous, volatile free compositions on the viscosity. The effects will be described in the next section.

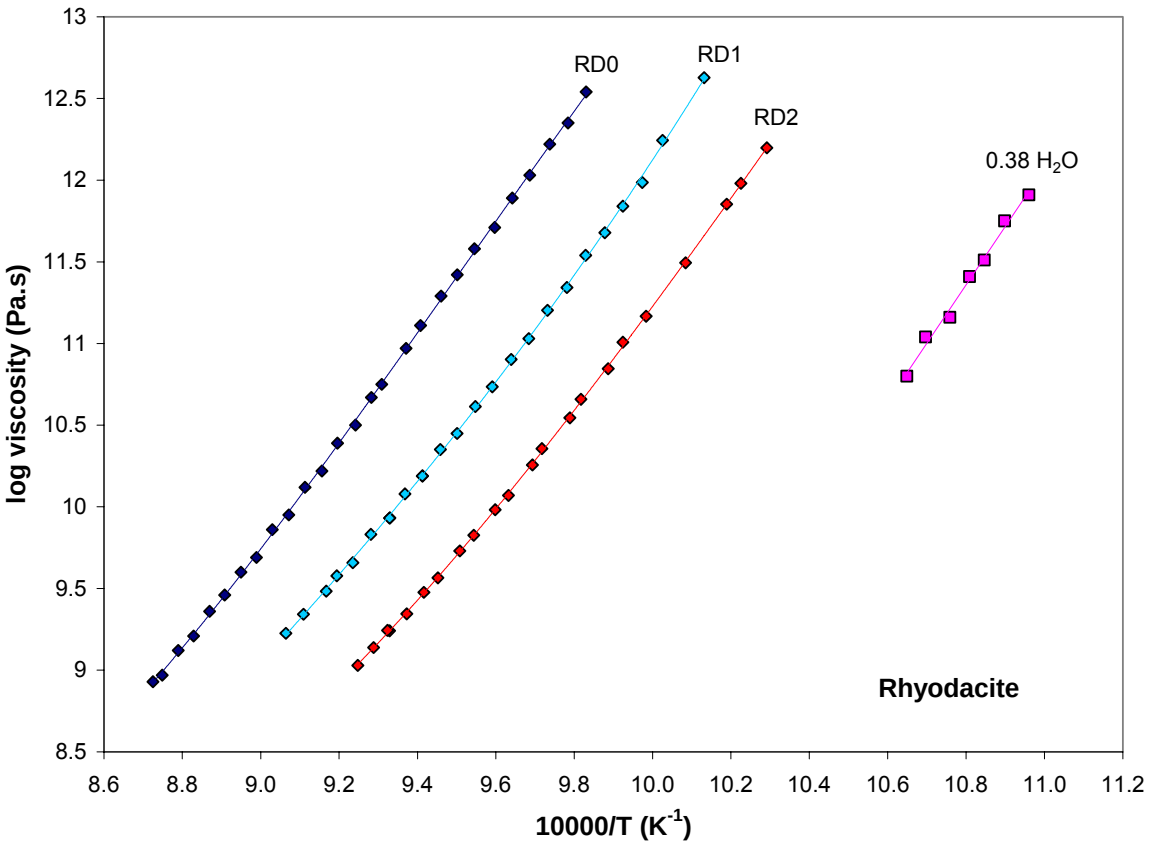

Figure 3.13. Log viscosity as a function of inverse temperature for RD0, RD1, RD2, and RD with 0.38 wt.% water showing the effect of fluorine on the samples in comparison to the effect of water.

3.2.4 Variable compositions

Within each series, the main difference is changing SiO_2 and MgO content, while other elements have near-constant concentrations (Table 3.6). The suite of ten compositions in total, including the RD0 and D0 base compositions, forms a systematic compositional array through the andesitic and dacitic liquid fields on a total alkali versus silica diagram (Figure 3.14). This diagram does not include the other major tetrahedral network forming cation (Al^{3+}) or network modifying elements other than Na and K. Therefore the compositions have also been plotted on a ternary diagram showing network formers (NF), alkalis (alk), and alkaline earths (alk earth) in mol% (Figure 3.15). For these compositions, network formers are Si, Al, and Ti, the alkalis are K and Na, and the alkaline earths are Ca and Mg. Both series lie on trends between dacites from Santiaguito and Unzen and basalts from Santa Maria (calc-alkaline) and Etna (alkali). This trend correlates with increasing NBO/T values as Mg content increases and the Si content decreases.

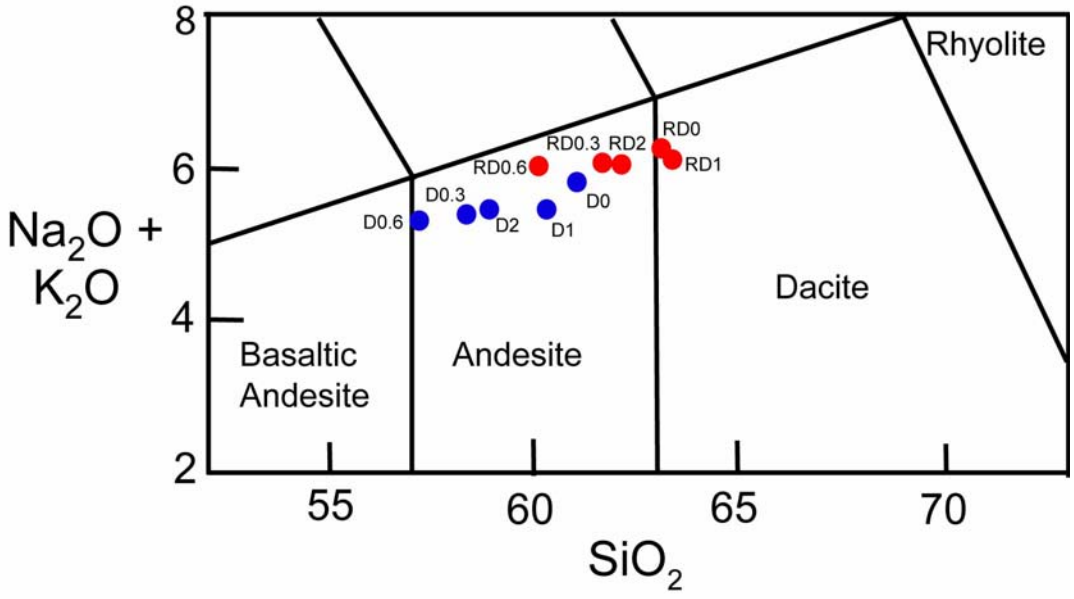

Figure 3.14. A total alkali silica diagram showing the compositional relationship of the samples of this study (i.e. 8 andesites and 2 dacites).

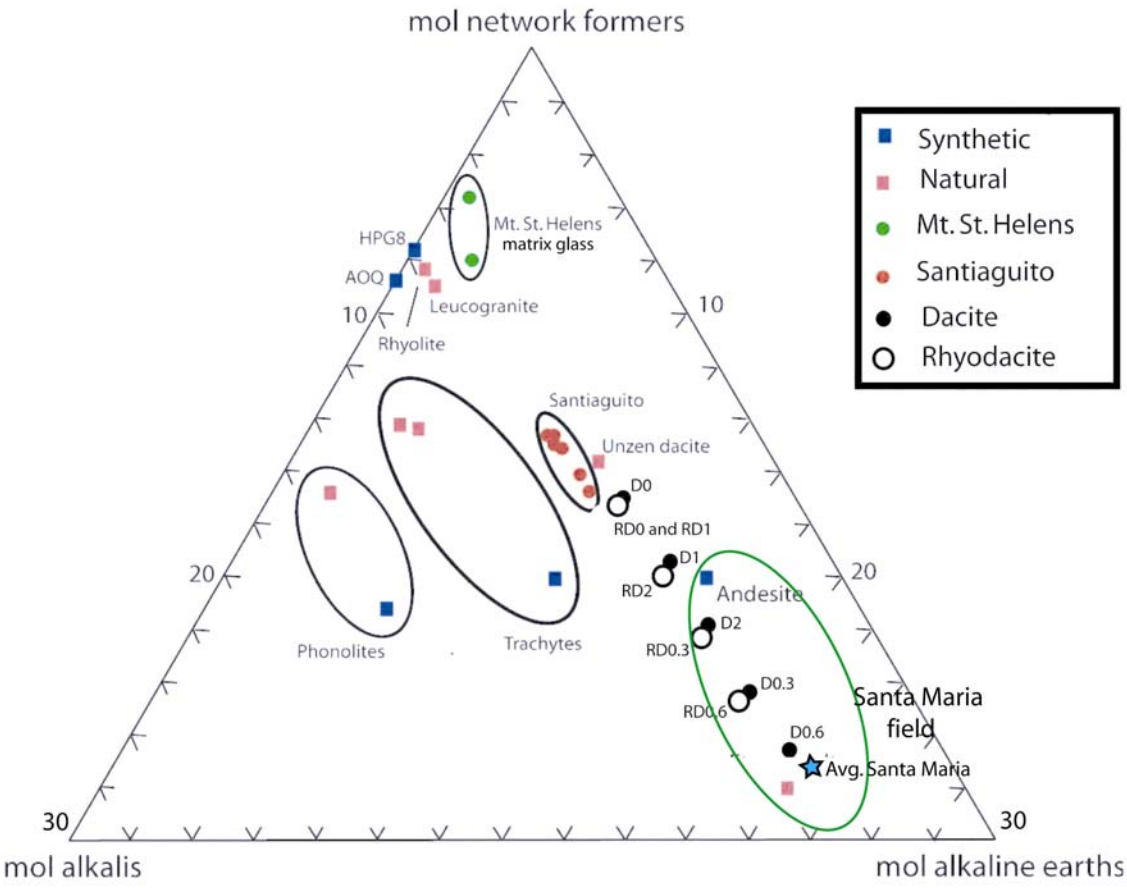

Figure 3.15. A ternary diagram showing the relationship of the dacite and rhyodacite samples from this study with other compositions.

Figure 3.15 does not indicate whether potential network modifying cations are in fact charge balancing tetrahedrally coordinated Al^{3+}. For example, both D0 and RD0 plot in nearly identical locations but D0 has a smaller NBO/T (0.06) than RD0 (0.10) because of its higher Al content. In order to illustrate melt chemistry and structure even better, another ternary diagram was plotted showing "T norm," "alkali NBOs," and "alkaline earth NBOs" (Figure 3.16). The "T norm" is the ratio of T/(T+NBO) where T represents the tetrahedral cations (Si+Al+Ti). The "alkali NBO" is equal to (NBO/(T+NBO))*100*(alkalis/(alkalis + alkaline earths)), on a molar basis and the "alkaline earth" is equal to (100 - T norm - alk NBO). Again, the lowest NBO/T value

for each series is closest to the tetrahedral cation apex, but now the more polymerized nature of D0 becomes evident. It should be noted that, because these compositions are dominated by alkaline earths, and because alkalis preferentially charge balance Al^{3+}, most of the non-bridging oxygens in all of these liquids will be coordinated by the alkaline earth cations (Mg and Ca).

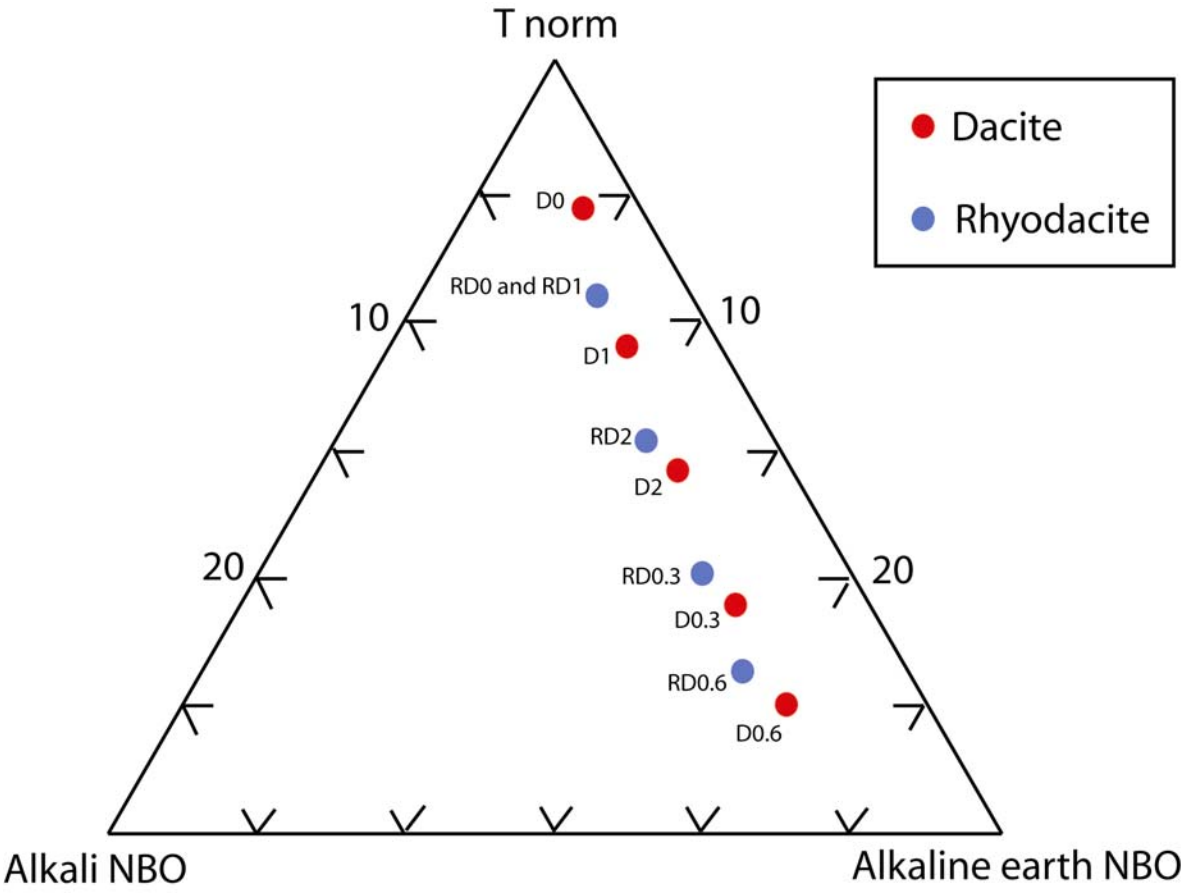

Figure 3.16. A ternary diagram of the dacite and rhyodacite compositions of this study in comparison of their T norm, Alkali NBO, and Alkaline earth NBO.

Though the trends of both compositional series look similar, there are specific differences (Table 3.6). First, the Al/(Al+Si) ratio of the rhyodacite is consistently between 0.26-0.27, while that of the dacite is higher, at 0.29-0.30. Secondly, values for

the NK/NKMC ratio (the ratio of alkalis to all network modifying cations) are consistently higher for the rhyodacite (0.29) than for the dacite (0.21). Viscosity measurements on the fluorine-free samples at high temperatures can be used to investigate the physical effects of varying NBO/T, Al/(Al+Si) ratio and alkali to alkaline earth ratio.

The high temperature data can be used because the microprobe showed that there is no trace of fluorine left in the samples, so their viscosity truly reflects their volatile-free composition and not the effects of fluorine. The parallel plate viscosity data was not included because some of the samples showed that they contained trace amounts of fluorine (Section 3.2.3).

The results demonstrate that even limited variations in bulk composition have significant effects on the viscosity of a melt (Tables 3.6, 3.9, and 3.10; Figure 3.17). Samples RD0 and RD1 have very similar compositions and their measured viscosities are consequently almost identical. Viscosity decreases systematically with increasing MgO and decreasing SiO_2 content, as represented by NBO/T values.

The data were fitted using the Tammann-Vogel-Fulcher (TVF) equation and the resulting A, B and C parameters are listed in Table 3.10. Despite moderate changes in composition, the "A" value found in all liquids are consistent within uncertainties (average value of -4.65) as suggested on theoretical grounds by Russell et al. (2003). Extrapolation of the TVF parameters again shows variable composition has a larger effect at lower temperatures (Figure 3.8).

Table. 3.8
High temperature viscosity data for the RD series

RD0		RD0.3		RD0.6		RD1		RD2	
T (K)	log η (Pa s)	T (K)	log η (Pa s)	T (K)	log η (Pa s)	T (K)	log η (Pa s)	T (K)	log η (Pa s)
1418.3	4.50	1315.6	4.92	1398.1	3.71	1379.9	4.79	1337.7	4.79
1438.5	4.30	1335.3	4.68	1423.0	3.50	1399.8	4.59	1357.5	4.57
1458.4	4.11	1355.1	4.47	1447.7	3.28	1419.4	4.39	1377.3	4.35
1483.1	3.88	1374.7	4.26	1472.5	3.08	1444.2	4.16	1397.1	4.16
1507.5	3.67	1394.5	4.06	1497.2	2.88	1468.9	3.95	1421.5	3.93
1532.5	3.47	1419.2	3.83	1521.7	2.70	1493.4	3.74	1446.7	3.70
1556.9	3.28	1443.8	3.61	1546.5	2.53	1518.2	3.54	1471.1	3.50
1581.7	3.10	1468.5	3.40	1570.9	2.37	1542.6	3.35	1495.8	3.30
1605.9	2.92	1493.4	3.20	1595.5	2.22	1567.1	3.18	1520.5	3.12
1630.3	2.76	1518.2	3.01	1620.0	2.07	1591.6	3.01	1545.2	2.94
1654.6	2.60	1542.5	2.84	1644.4	1.93	1616.2	2.84	1569.5	2.77
1678.9	2.45	1567.1	2.67	1668.9	1.79	1640.5	2.69	1594.2	2.61
1703.1	2.31	1591.6	2.50	1693.4	1.66	1664.8	2.54	1619.1	2.45
1727.2	2.16	1616.2	2.35	1705.1	1.60	1689.1	2.39	1643.1	2.30
1751.5	2.03	1640.4	2.20	1717.7	1.53	1713.4	2.25	1667.6	2.16
1775.7	1.91	1664.9	2.06	1742.1	1.41	1737.5	2.12	1691.8	2.03
1799.9	1.79	1689.5	1.92	1766.4	1.29	1761.6	1.99	1716.4	1.90
1824.3	1.67	1713.9	1.79	1790.4	1.19	1786.2	1.87	1740.8	1.77
1848.5	1.56	1738.1	1.66			1805.4	1.77	1765.0	1.65
1865.8	1.48	1762.5	1.54			1820.0	1.69	1789.6	1.51
		1786.8	1.42			1839.5	1.60	1808.8	1.42
		1815.7	1.29			1854.3	1.53	1823.6	1.37

Table 3.9
High temperature viscosity data for D series

D0		D0.3		D0.6		D1		D2	
T (K)	log η (Pa s)	T (K)	log η (Pa s)	T (K)	log η (Pa s)	T (K)	log η (Pa s)	T (K)	log η (Pa s)
1414.4	4.53	1333.1	4.74	1310.0	4.51	1340.5	4.69	1313.5	4.90
1438.8	4.28	1352.5	4.51	1329.8	4.27	1360.1	4.48	1330.0	4.74
1463.4	4.06	1372.6	4.28	1349.6	4.05	1379.8	4.27	1349.6	4.52
1488.3	3.84	1397.3	4.07	1369.3	3.84	1399.6	4.08	1374.0	4.24
1512.6	3.64	1422.3	3.81	1393.9	3.59	1419.1	3.85	1399.1	3.98
1537.4	3.45	1447.0	3.57	1418.6	3.35	1443.7	3.63	1423.0	3.74
1562.1	3.26	1471.6	3.34	1443.3	3.13	1468.5	3.43	1448.4	3.52
1581.4	3.12	1496.4	3.13	1467.6	2.92	1493.1	3.23	1471.4	3.31
1605.9	2.95	1521.1	2.93	1492.5	2.73	1517.7	3.04	1497.0	3.11
1630.4	2.79	1545.9	2.74	1517.1	2.54	1542.2	2.87	1521.7	2.92
1654.7	2.63	1570.3	2.56	1541.5	2.37	1566.8	2.70	1545.8	2.74
1674.1	2.51	1594.5	2.39	1566.0	2.20	1591.4	2.54	1570.5	2.57
1693.4	2.39	1619.1	2.23	1590.6	2.05	1615.6	2.39	1594.4	2.40
1712.8	2.28	1643.6	2.08	1614.9	1.90	1640.1	2.24	1619.2	2.25
1732.3	2.17	1668.0	1.93	1639.5	1.75	1664.4	2.10	1643.6	2.10
1751.5	2.06	1692.4	1.79	1663.8	1.62	1688.7	1.96	1668.2	1.96
1770.8	1.96	1716.9	1.65	1688.3	1.49	1713.1	1.84	1692.1	1.82
1790.3	1.86	1741.3	1.52	1712.7	1.37	1737.4	1.71	1716.5	1.69
1809.8	1.76	1765.5	1.40	1737.2	1.25	1761.6	1.59	1740.8	1.57
1829.2	1.66	1784.7	1.27	1761.3	1.14	1785.9	1.46	1760.0	1.47
1848.6	1.57					1810.4	1.34	1779.4	1.37
1868.2	1.48							1813.3	1.23

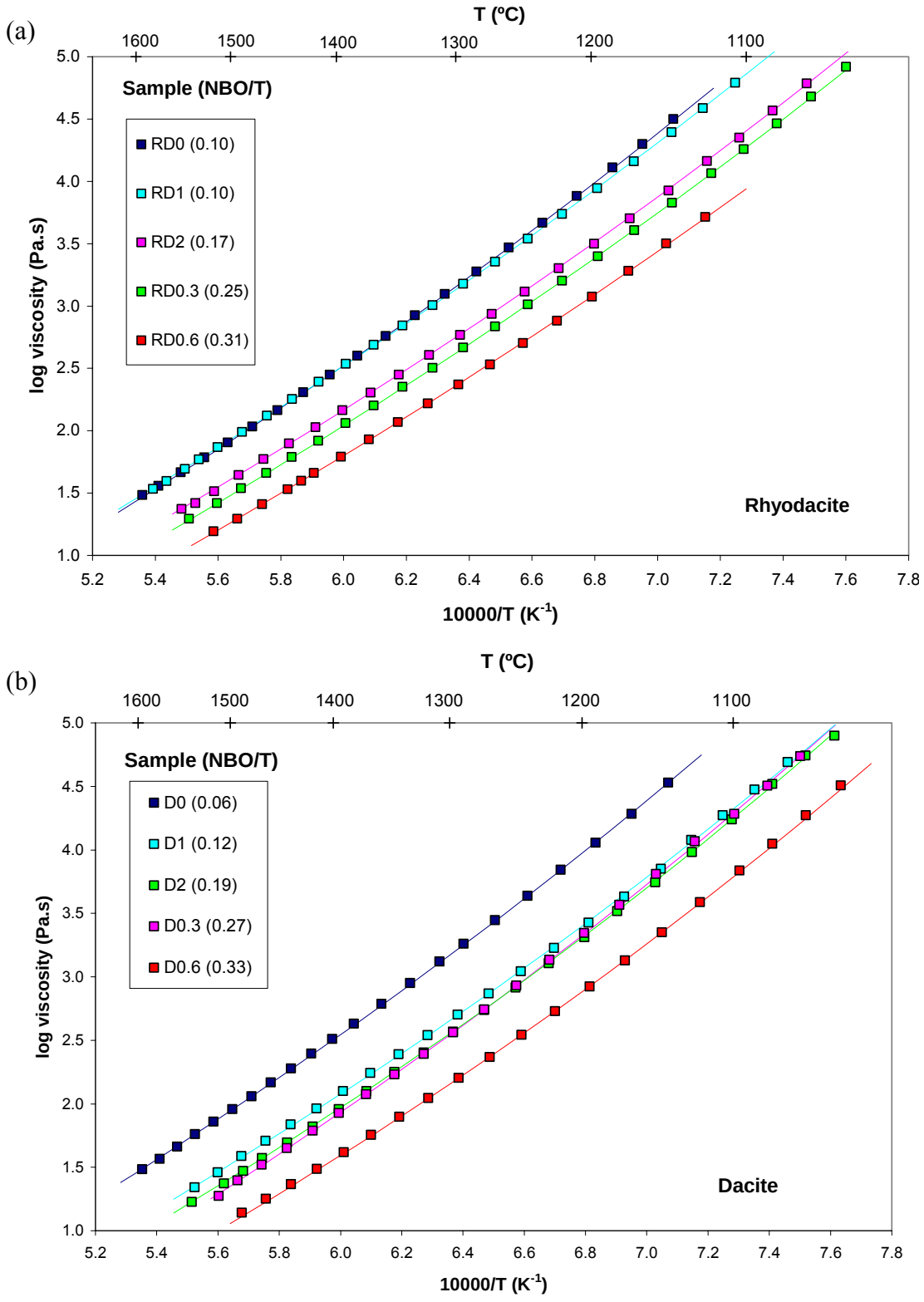

Figure 3.17 a and b. Viscosity as a function of inverse temperature for the (a) rhyodacite and (b) dacite. The points are the actual data points measured while the lines are calculated from the TVF parameters in Table 3.10.

Table 3.10
Parameters for TVF equations, $\log_{10} \eta = A + B/(T - C)$

Sample	NBO/T[a]	A (Pa s)[b]	B (Pa s K^{-1})[b]	C (K)[b]	T^{12}(K)[c]	F_D[d]
Rhyodacite						
RD0	0.10	-4.68 (0.08)	8349 (188)	507.5 (12.4)	1020	0.07
RD1	0.10	-4.73 (0.08)	8719 (173)	464.1 (11.0)	1035	0.09
RD2	0.17	-4.56 (0.10)	7908 (213)	490.9 (14.0)	1006	0.09
RD0.3	0.25	-4.76 (0.08)	8081 (174)	478.5 (11.1)	1002	0.09
RD0.6	0.31	-4.87 (0.16)	8062 (366)	458.1 (25.2)	997	0.11
Dacite						
D0	0.06	-4.56 (0.12)	8206 (269)	511.4 (17.9)	1057	0.10
D1	0.12	-4.42 (0.18)	7420 (366)	524.4 (24.8)	988	0.08
D2	0.19	-4.39 (0.09)	7071 (180)	554.7 (12.1)	986	0.08
D0.3	0.27	-4.96 (0.16)	7940 (330)	514.7 (20.8)	1024	0.10
D0.6	0.33	-4.58 (0.21)	6915 (405)	546.5 (27.6)	987	0.10

[a]NBO/T = $(2(K_2O + Na_2O + CaO + MgO + FeO - Al_2O_3)/(SiO_2 + Al_2O_3 + Al_2O_3)$ Calculation based on Mysen and Richet (2005).
[b]Numbers in brackets are absolute uncertainties.
[c]T_{12} indicates the temperature at which the viscosity is 10^{12} Pa s, taken to be the effective glass transition temperature.
[d]The fragility, F_D, is calculated where $F_D = C/B$ and described more in the text

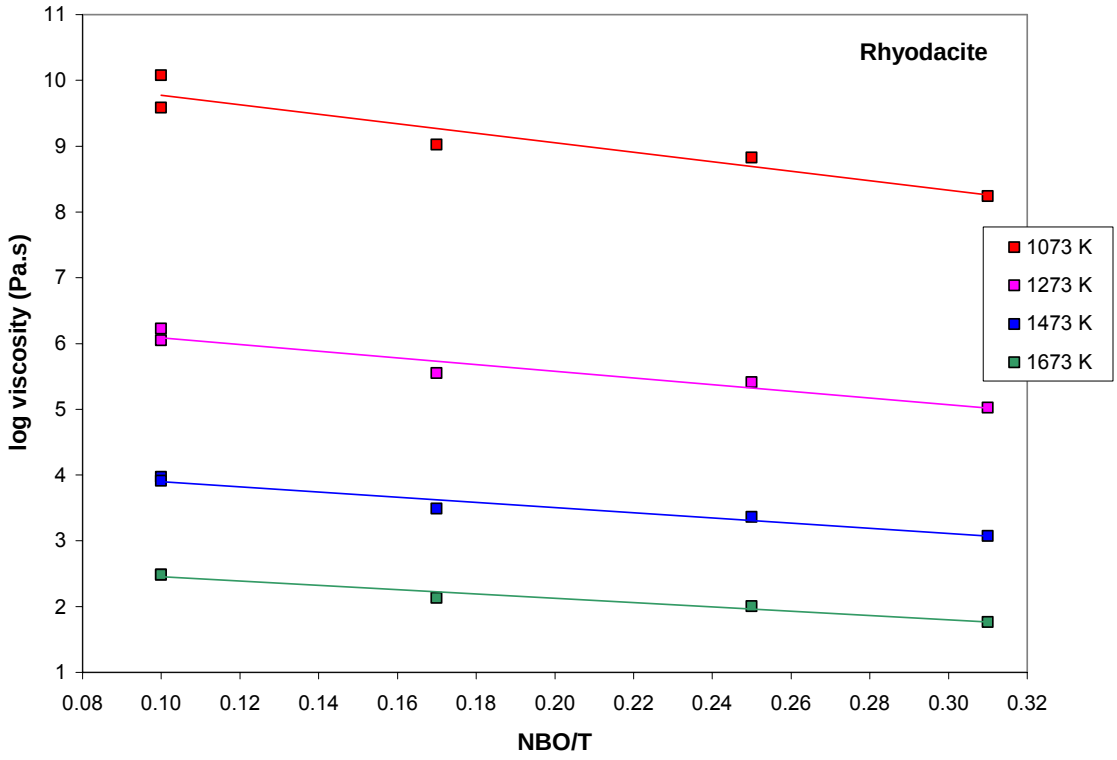

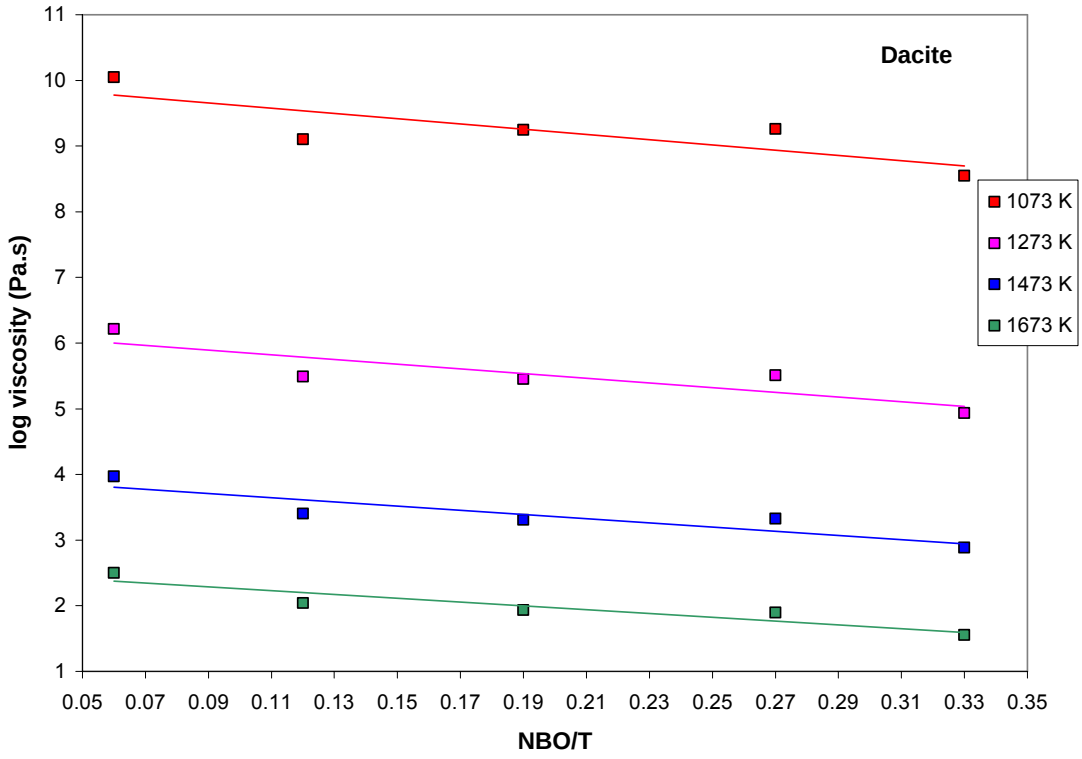

Figure 3.18 a and b. Log viscosity of the (a) rhyodacite and (b) dacite melts with variable composition as a function of NBO/T. Symbols indicate points calculated from constrained TVF equations of Table 3.10, while lines are to guide the eye.

For example, at temperatures of 800, 1000, and 1200ºC, RD0, with an NBO/T of 0.06, has viscosities of $10^{10.08}$, $10^{6.22}$, and $10^{3.97}$ Pa.s, respectively. When the NBO/T increases to 0.31 (RD0.6), the viscosities decrease to $10^{8.24}$, $10^{5.02}$, and $10^{3.07}$ Pa.s, respectively. At 800ºC, the viscosity decreased by almost 2 orders of magnitude, while at 1200ºC the viscosity decreased by much less than 1 order of magnitude. The dacite shows similar trends.

The effect of water is much greater than that of similar variations in molar MgO and SiO_2 content. With the addition of 4 wt% water, viscosity decreases by 7 orders of magnitude at 1100 K, while changing NBO/T from 0.10 (RD0) to 0.31 (RD0.6) only decreases the viscosity by less than 2 orders of magnitude. This emphasizes that knowledge of volatile content is more important than other compositional factors for dacite to andesite liquids.

3.3 Summary

- Dacitic liquids show non-Arrhenian behavior like the andesites, but unlike the near Arrhenian rhyolites.
- Anhydrous dacites are more viscous than andesites, but less viscous than rhyolites.
- Viscosity variations between different anhydrous melts are small at high temperatures and larger at lower temperatures.
- At 1100 K, the addition of about 1 wt.% water reduces the viscosity of both dacite liquids by almost 5 orders of magnitude, and the addition of about 4 wt.% water reduces the viscosity by more than 7 orders of magnitude.

- Water has a greater effect on the viscosity of dacites than on andesites, but a still greater effect on rhyolites.
- Variable MgO and SiO_2 contents, and consequently polymerization state of the melt, affect liquid viscosity to a much lesser degree than changing temperature and water content, at least over the NBO/T range 0.06 to 0.31, for liquids with similar ratios of alkalis to alkaline earths.

The next chapter will discuss petrological applications for the results presented in this chapter. First, it will examine the attempts to parameterize viscosity as a function of temperature and water content using the measured data from this study. The data will then be discussed in relation to water solubility and speciation and compared to previous studied compositions. Lastly, it will be applied to various magmatic processes such as magma degassing, vesiculation, crystal settling, magma ascent in dikes, and the flow of lava.

CHAPTER 4 – DISCUSSION

4.1 Overview

Chapter 4 will begin by attempting to parameterize viscosity as a function of temperature and water content. Next, it will explore water solubility and water speciation within silicic liquids, and comparisons will be made between the viscosity results of this study and previous data for related compositions. The chapter will finally consider some petrological implications of this study, including liquid viscosity versus magma viscosity, changing viscosity during ascent and degassing of magmas, and the rates of igneous processes such as crystal settling, magma ascent in dikes, and the flow of lava.

4.2 Viscosity Parameterization

For applications to petrology, it would be very useful to be able to predict the viscosity of hydrous liquids at any temperature and water content, especially at the intermediate temperature range, which is not experimentally accessible due to crystallization and/or degassing. In order to do this, some form of model needs to be developed, based on the available data collected from a limited number of samples. Several models have been developed for different compositions, but they are mostly empirical in nature and cannot be applied to other compositions. As described in Chapter 1, thermodynamic data required to apply the configurational entropy theory to dacites is not currently available. This section describes attempts to develop a model to predict dacite liquid viscosity based on data presented in Chapter 3.

As a starting point, the empirical parameterization scheme of Giordano et al. (2000) was adapted:

$$\log\eta = [a_1 + a_2 \ln(H_2O)] + \frac{[b_1 + b_2(H_2O)]}{[T - (c_1 + c_2 \ln(H_2O)]} \quad (4.1)$$

where a_1, a_2, b_1, b_2, c_1 and c_2 are all adjustable parameters, H_2O is the water content (wt.%), and T is the temperature (K). This equation is based on the original Tammann-Vogel-Fulcher (TVF) equation, modified to include water content. Giordano et al. (2000) applied this model to two trachytes, a phonolite, an Etna basalt, and a dacite from Unzen. Their average standard error for these samples (the difference between their measured values and the ones calculated with these equations) ranged from 0.10 to 0.23 for a trachyte and Etna basalt, respectively. This parameterization worked well for several of the compositions, but not for their dacite or basalt. This could be due to having a limited range in water content for the samples, e.g. the three dacite water contents ranged only from 1.37 to 1.98 wt.%. The lack of a suite of samples containing large variations in water content weakens the validity of these parameterizations in predicting the viscosity, due to poorly constrained extrapolations.

The same parameterization scheme was applied to the data from this study. First the calculated B and C parameters for each composition (Table 3.5) were plotted against water content (Figure 4.1). While both B and C decrease with water content, the graphs show considerable scatter.

In this study, the A parameter was assumed to be a constant for each series (determined using the anhydrous samples). A straight line was fitted to the B parameter values and the equation for the C parameter was modified slightly, with $C = [c_1 + c_2 \ln(1 + H_2O)]$, in order to fit the anhydrous samples. The values for b_1 and c_1 for both the dacite and rhyodacite were set equal to the B and C parameter values for the

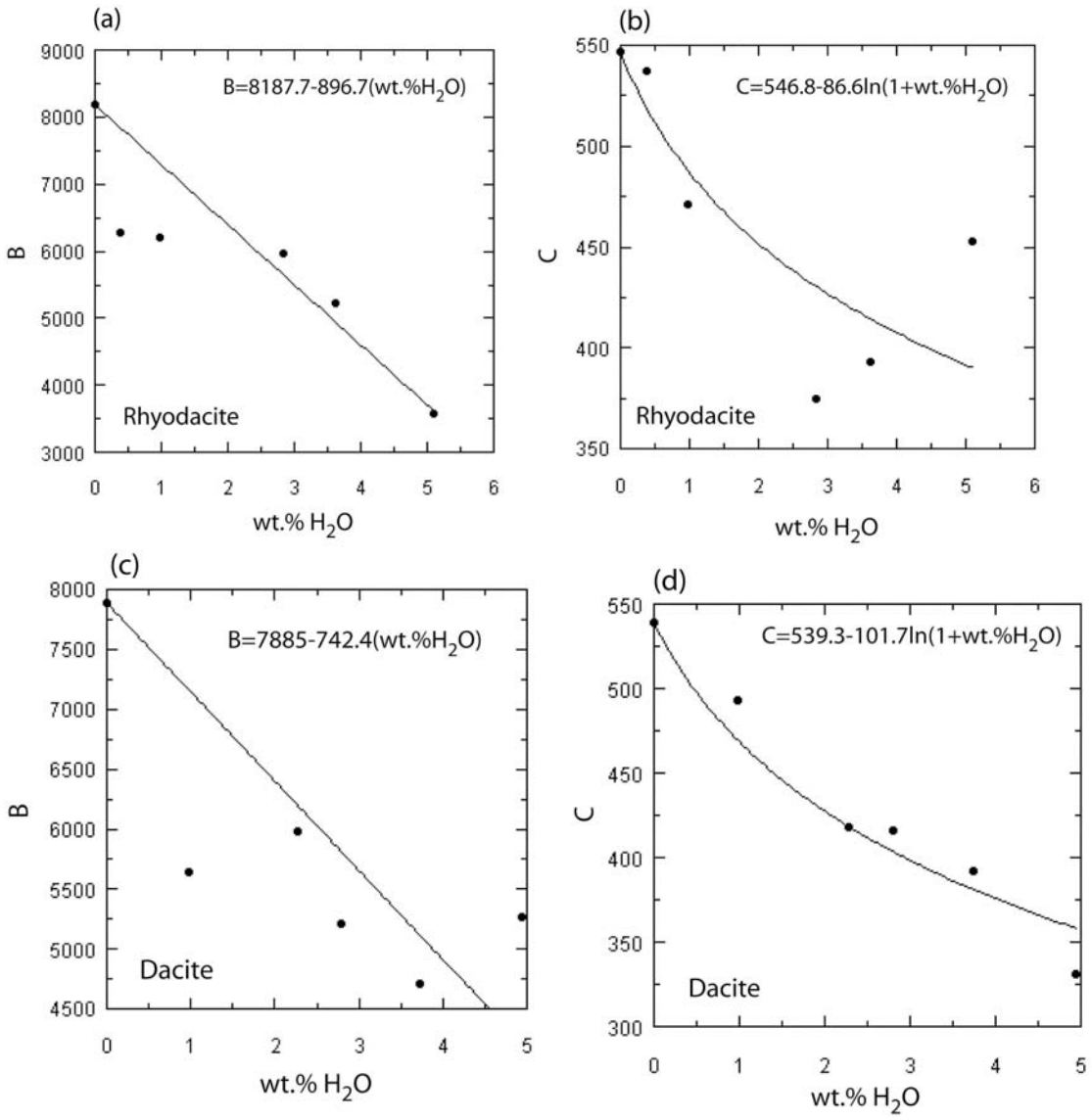

Figure 4.1a-d. Diagrams of B and C parameters as a function of water content (wt.%) and the fitted equations (lines) from above.

anhydrous samples, since those values are the most accurate due to the larger amount of data collected on them. Using these values and the fitted equations, values for b_2 and c_2 were determined.

The resulting equations are, for the rhyodacite:

$$\log \eta = -4.79 + \frac{[8187.7 - 896.7(H_2O)]}{[T - (546.8 - 86.6\ln(1 + H_2O))]} \qquad (4.2)$$

and for the dacite:

$$\log \eta = -4.45 + \frac{[7885 - 742.4(H_2O)]}{[T - (539.3 - 101.7\ln(1 + H_2O))]} \qquad (4.3)$$

The average absolute deviations (AAD) for the models were 0.04 and 0.01 for the anhydrous rhyodacite and dacite, respectively, but this excellent fit was expected since their TVF parameters were very well constrained by the large high and low temperature datasets. The AAD for the hydrous samples was 2.27 for the rhyodacite and 1.43 for the dacite. These values are unacceptably high and show that this parameterization scheme is not applicable for these samples. The deviation can be seen in Figures 4.2 and 4.3.

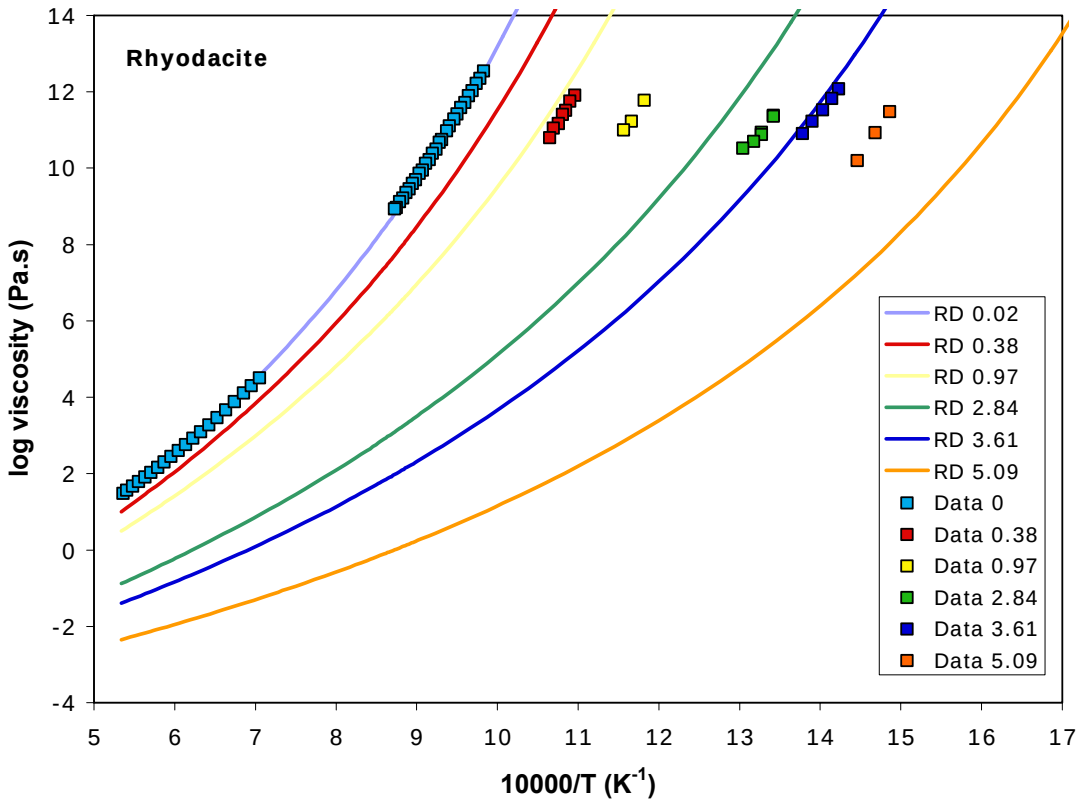

Figure 4.2. Log viscosity (Pa.s) versus inverse temperature. The lines represent the calculated values for each water content using Equation 4.2. The squares are measurements for rhyodacite.

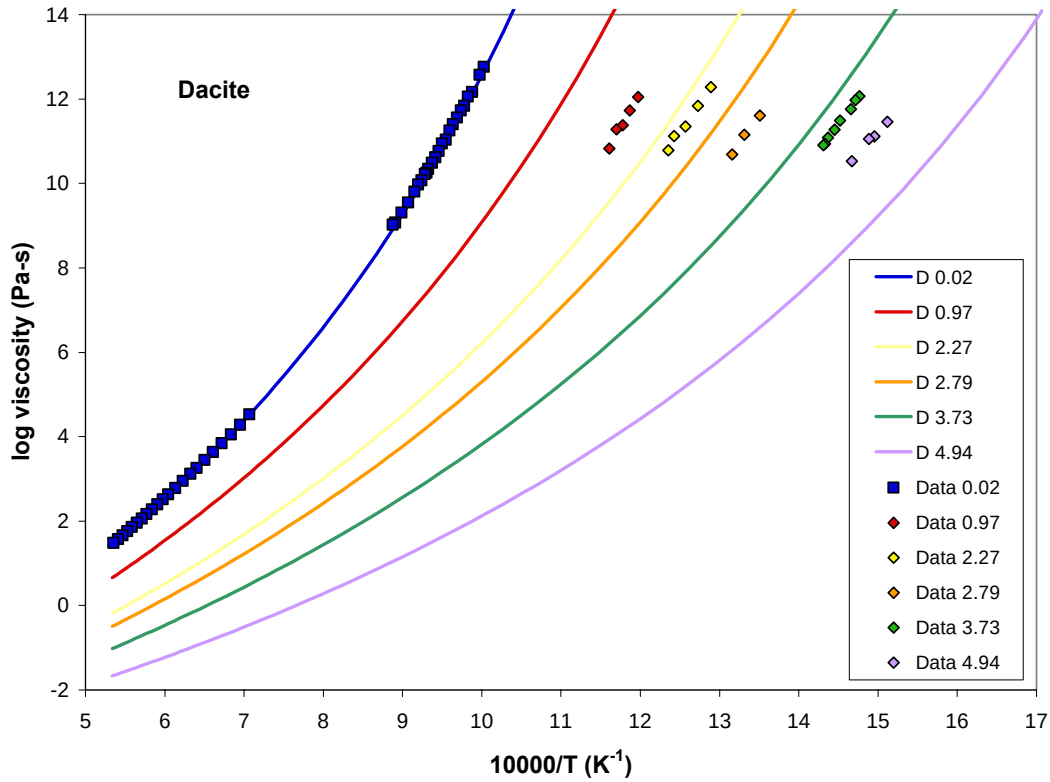

Figure 4.3. Log viscosity (Pa.s) versus inverse temperature. The lines represent the calculated values for each water content using equation 4.3. The squares are measurements for the dacite.

A number of other equations were used to fit the variations of B and C with water content, but none produced acceptable results. One variation used was an exponential fit to B and a linear fit to C, which actually reduced the AAD slightly, but not enough to be useful for extrapolation to high temperature and water content.

Parameterizations are very sensitive to the few measurements on the hydrous samples. There was a lot of scatter in the B and C parameters for the hydrous samples, due to the restricted temperature range over which they were measured. In order to develop a predictive model, more data needs to be collected. A few measurements using falling sphere viscometry (at high pressure, temperature and water content) would be another obvious target for future study.

4.3 Water Solubility and Speciation

As shown in Chapter 3, dissolved water greatly reduces the viscosity of silicate melts. The solubility of water is a function of temperature and pressure, and varies in a complex manner with the melt composition. Figure 4.4 displays the solubility of water at 1100 K in Kilauean basalt (Head and Wilson, 1987), dacite (this study), and Katmai rhyolite (Fierstein and Hildreth, 1992) compositions. Water solubility increases with increasing pressure for all compositions, and is always higher for more polymerized compositions. The rate of solubility increase is also greatest at low pressures, where the change in volume of the reaction between a free gas and the liquid is the largest and most susceptible to pressure changes. Holtz et al. (1995) found that between 300 and 800 MPa, there is an almost linear (positive) correlation between pressure and water solubility in haplogranite melt.

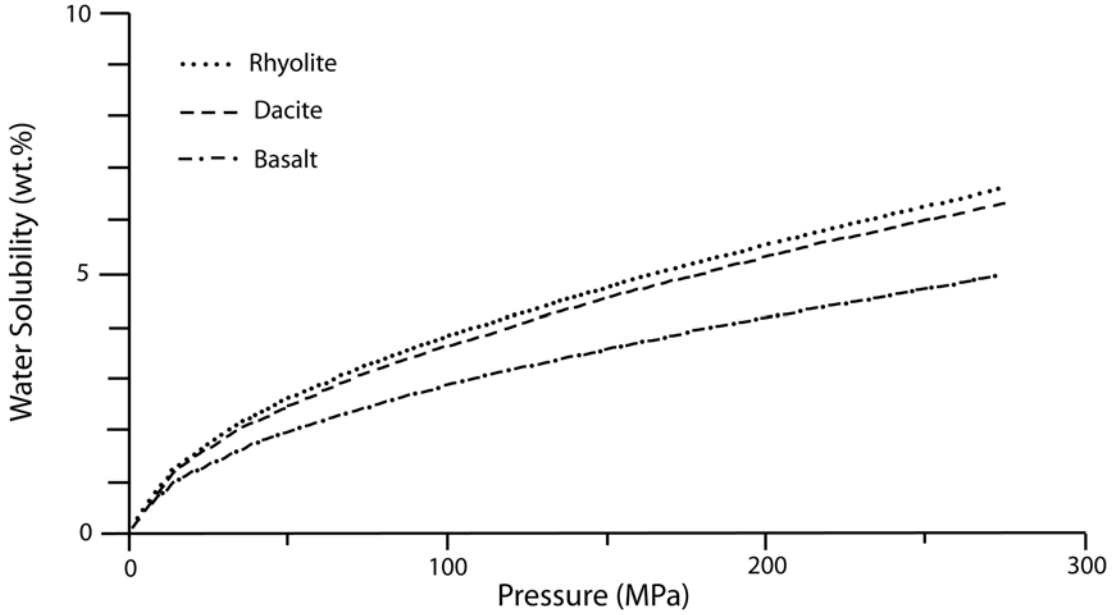

Figure 4.4. The solubility of water as a function of pressure at 1100 K for a Kilauean basalt (Head and Wilson, 1987), dacite (this study), and Katmai rhyolite (Fierstein and Hildreth, 1992). The haplogranite (Dingwell et al., 1996), andesite (Richet et al., 1996), and the rhyodacite from this study fall on the same trend as the dacite.

Water solubility is related to the mechanism by which the water dissolves in the melt. Water is known to be dissolved as both hydroxyl groups (OH^-) and molecular water in silicate melts (Stolper, 1982) as mentioned in more detail in Chapter 1. Water speciation can be measured using infrared spectroscopy and results are very similar for compositions ranging from basalt to granite (Silver et al., 1990). The concentration of the hydroxyl species increases rapidly when water is first added to the melt, but as the total amount of water increases, molecular water begins to appear and begins to dominate at water contents around 3 to 4 wt.%.

Stolper (1982) noted the correlation of viscosity to the concentration of hydroxyl ions, and interpreted the leveling off of the viscosity decrease at higher water contents as being due to the minor effect of molecular water on melt viscosity. While most studies have focused on granite or basaltic liquids, Ohlhorst et al. (2001) measured water speciation on Unzen dacite. Their results show that the OH^- and molecular water cross at approximately 3.8 wt.% total water, typical of most compositions (Figure 4.5).

If molecular water becomes the dominant species, around 3 to 4 wt% water for all aluminosilicate melts, then OH^- must have different effects on different bulk compositions, because polymerized silicic compositions are more strongly affected by water than depolymerized mafic compositions. At high temperatures, water speciation moves away from H_2O towards the OH^-, (Novak and Behrens,1995; Shen and Keppler, 1995) but the viscosity decreases are also smaller.

Several models have been developed for the structural role of hydroxyl groups. The first model is that water dissociates by reacting with bridging oxygens, resulting in

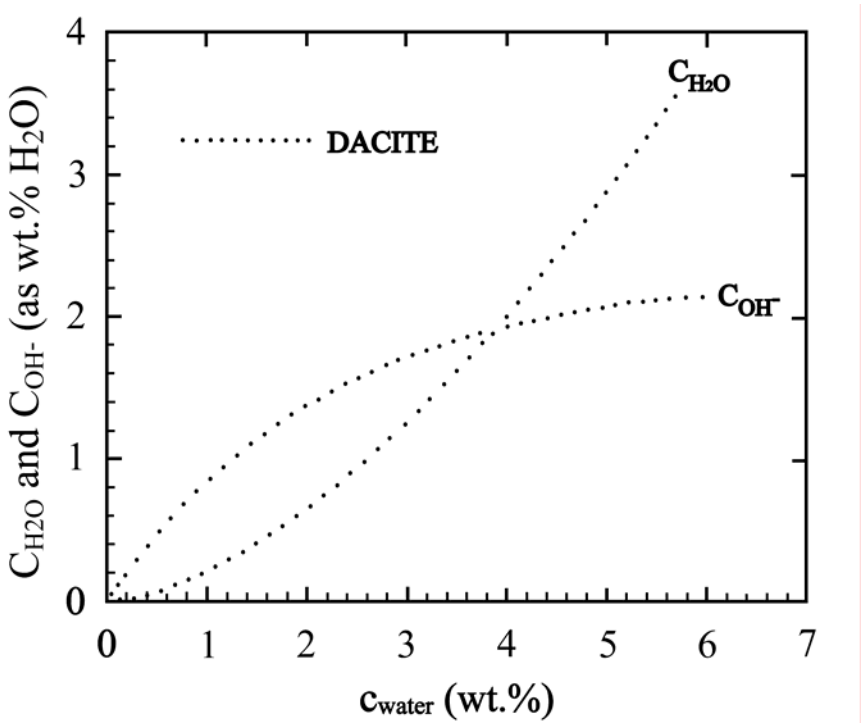

Figure 4.5. Measured concentrations of H_2O and OH (expressed as wt.% H_2O) versus total water content in a dacitic composition (modified from of Ohlhorst et al., 2001).

the depolymerization of the melt network (Burnham, 1975; Stolper, 1982; Sykes and Kubicki, 1993, 1994). The reaction can be expressed as:

$$\text{Si-O-Si} + H_2O = \text{Si-OH} \ldots . \text{OH-Si} \qquad (4.4)$$

An alternative mechanism for aluminosilicates is that on dissociation, a proton will substitute for an alkali or alkaline earth cation, involved in charge balancing tetrahedral aluminum in the anhydrous glass. The hydroxyl groups combine with the released alkali or alkaline earth cation to form metal hydroxide species (Kohn et al., 1989, 1992, 1998). This model can be expressed as:

$$NaAlSi_3O_8 + H_2O = HAlSi_3O_8 + NaOH \qquad (4.5)$$

Additional mechanisms involve possible interactions between water and non-bridging oxygens and/or network modifying cations. Robert et al. (2001) concluded on the basis

of Nuclear Magnetic Resonance (NMR) experiments on hydrous synthetic phonolite glass, that water probably dissolves by at least three different mechanisms. The relative importance of various dissolution mechanisms as a function of water content and anhydrous composition is still a matter of debate.

4.4 Water and the viscosity of silicate melts

There have been many previous studies on the viscosity of anhydrous silicate melts, and a growing number on hydrous melts (see Mysen and Richet, 2005 for a recent review). At high temperatures, the viscosities of different anhydrous compositions are almost indistinguishable, but at low temperatures, their viscosities diverge as a function of bulk composition. Examples of silicic liquids (andesite to rhyolite) were shown in Figure 3.1. At typical magmatic temperatures for these compositions, between 800 and 1000ºC, the spread between the viscosities is approximately 1.5 log units, with rhyolitic compositions being more viscous, the andesites being less viscous, and the rhyodacite and dacite in between.

Water can have a large decreasing effect on the viscosity of silicic liquids. The amount of the decrease depends on the melt composition, and is related to the degree of polymerization, which can be approximated by the ratio of non-bridging oxygens to tetrahedral cations (NBO/T), as described in Chapter 1. Figure 4.6 shows the temperature of the 10^{12} Pa.s isokom (approximately the glass transition temperature) for several different silicate compositions with NBO/T values between 0 and 0.86 as a function of water content.

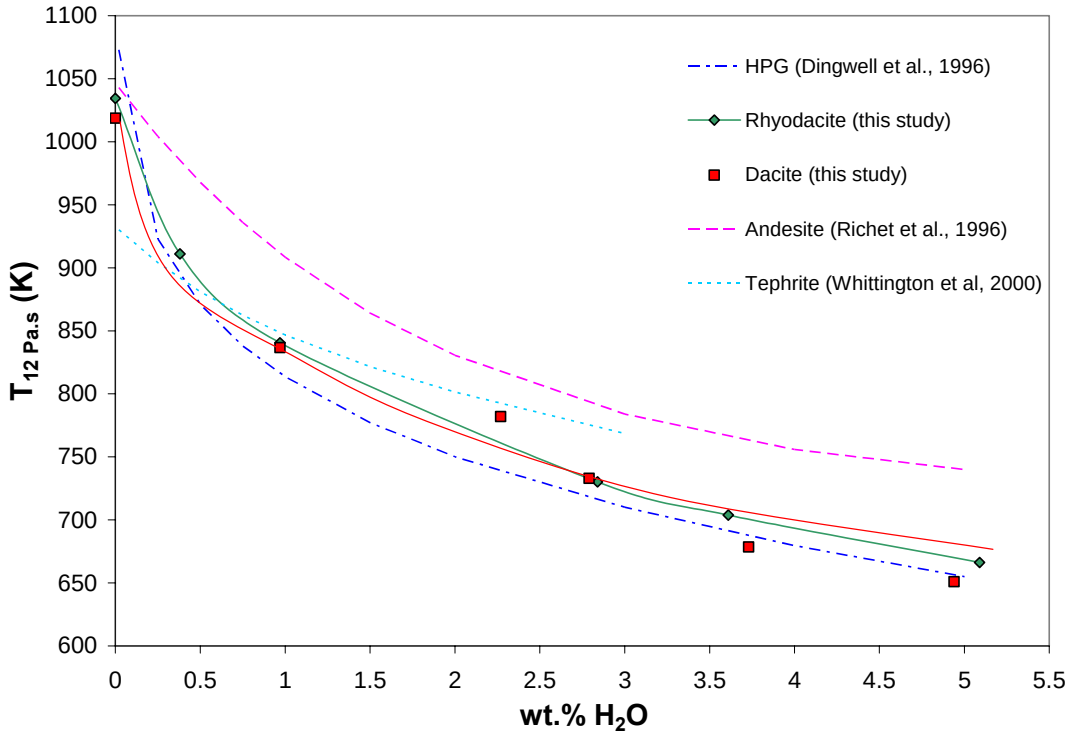

Figure 4.6. A comparison of various melt compositions at the 10^{12} Pa-s isokom as a function of water content. The compositions include haplogranite (Dingwell et al., 1996), andesite (Richet et al., 1996), tephrite (Whittington et al., 2000), and the dacite and rhyodacite from this study. The lines are calculated from models based on TVF equations from references cited and for the rhyodacite and dacite, the points are calculated.

At water contents in excess of about 0.5 wt.%, T_{12} for the nominally more polymerized melt (rhyolite, rhyodacite, dacite) are lower than for the more depolymerized melts (andesite and tephrite, an alkali basalt). This means that at low temperature and high water content, the more polymerized compositions are less viscous. This contradicts the common assumption that rhyolites and other highly polymerized melts are always more viscous then basalts and other depolymerized melts. In nature, magmatic temperatures for basalts are substantially higher than for rhyolites, so that basaltic lavas are in fact less viscous than rhyolites. However, the data shown in Figure

4.6 show that the high viscosity of erupted rhyolites is not a property inherent to the melt itself, but rather due to their low temperatures of formation.

Explanations for the anomalously powerful fluidizing effect of water on silicic magmas are still somewhat incomplete. One possibility that can be ruled out is different water speciation reactions for varying compositions. As shown in the previous section, water speciation for most compositions is remarkably similar. A full thermodynamic description awaits measurements of necessary data to apply configurational entropy theory. The first steps have been taken with recent measurements of the partial molar heat capacity of water in silicate melts (Bouhifd et al., 2006). Future calorimetery studies of rhyolites, dacites, etc. are an important goal.

The viscosity decrease caused by dissolved water was described in section 3.2. For both the dacite and rhyodacite, water contents of about 1 wt.% at 1100 K can cause a decrease on the order of almost 5 orders of magnitude, while the addition of nearly 4 wt.% water can decrease the viscosity by more than 7 orders of magnitude. Greater decreases are experienced by rhyolites, and smaller decreases are experienced by andesites and tephrites. At low water contents, more polymerized melts are much more affected by water content in the melt, but at higher water contents, the effect is not as great and the trends for all the samples level off and run nearly parallel.

The actual viscosity of dacitic liquids depends on temperature and water content. For likely magmatic values of 900ºC and between 0.5 and 5 wt.% water, liquid viscosity ranges between about 10^5 and 10 Pa.s (Figure 4.7a). Both the dacite and rhyodacite are substantially less viscous than either the haplogranite or andesite (figure 4.7b-d). The viscosity of haplogranite and andesite liquids is significantly higher, ranging from 10^4

Pa.s with 5 wt.% water to 10^7 Pa.s with 0.5 wt.% water at 900ºC (Figure 4.7c). The difference between dacite and haplogranite or andesite liquids is nearly constant at approximately 3 log units, at 800 to 1000ºC for water contents of 0.5 and 5 wt.% water. These differences in the viscosity of hydrous liquids of different compositions have important implications for the rates of magmatic processes.

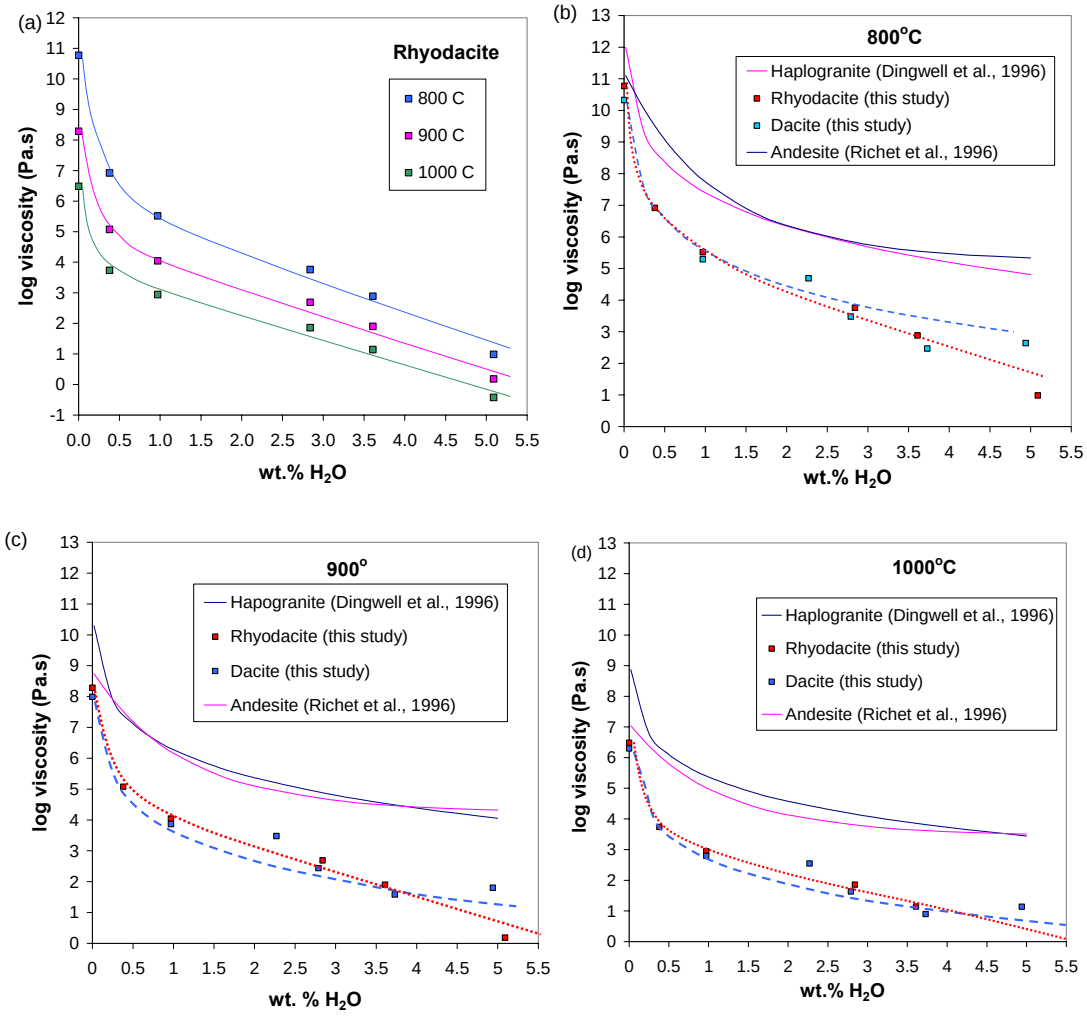

Figure 4.7a-d. Log viscosity as a function of water content at 800, 900 and 1000ºC for the rhyodacite (this study), dacite (this study), haplogranite (Dingwell et. al, 1996), and andesite (Richet et al., 1996). The lines for the haplogranite and andesite and the points for the dacite and rhyodacite are calculated from various TVF parameters. The lines for the dacite and rhyodacite are smooth curves intended solely to guide the eye.

The lower viscosity of the rhyodacite and dacite relative to the haplogranite (more polymerized) and andesite (less polymerized) seems odd, but can be explained by considering the details of their chemical compositions. Hydrous liquids that are dominated by alkalis are less viscous than those dominated by alkaline earths for the same degree of bulk composition (Whittington et al., 2001). The rhyodacite and dacite have a higher alkali to alkaline earth ratios than the andesite (Table 3.1), thus making them less viscous.

The difference in the glass transition is shown as a function of water content for haplogranite (Dingwell et al., 1996), rhyodacite (this study), dacite (this study), and the andesite (Richet et al., 1996). Initially, there is a large decrease in the glass transition with small amounts of dissolved water, but as the water content increases the effect becomes less dramatic. The trend of the glass transition of the dacite and the rhyodacite can also be seen to fall in between the haplogranite and andesite. Because the water speciation is similar for all three liquids (at the same water content), this cannot be what causes the different trends in the glass transition. Some other cause must be responsible, probably related to the configurational heat capacity of the different liquids.

4.5 Petrological applications 1: Liquid viscosity during degassing

This study measured the liquid viscosity of synthetic dacitic liquids which were based on dacitic lava flows from Santiaguito Dome Complex. The variation of liquid viscosity as a function of temperature and water content can be directly investigated, but magma viscosity in volcanic settings is also a function of other parameters such as bubble and crystal content and strain rate (Spera, 2000). The liquid viscosity cannot be

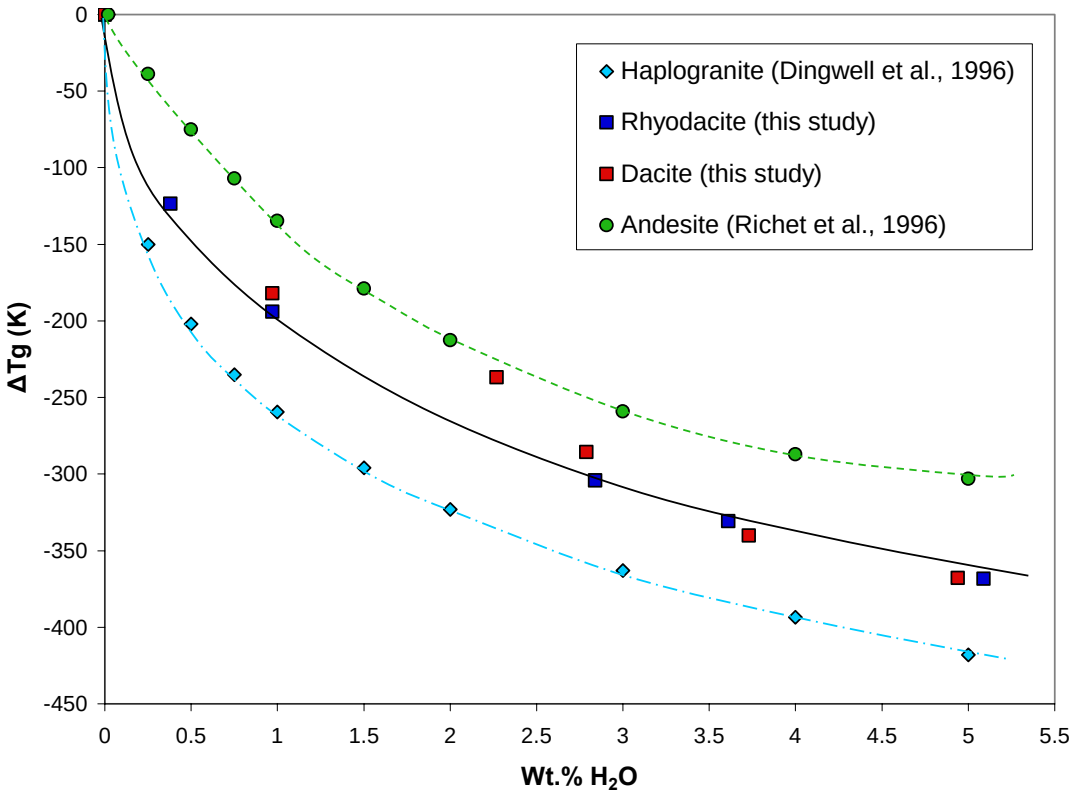

Figure 4.8. The different in the glass transition temperature as a function of water content comparing haplogranite (Dingwell et al., 1996), the dacite and rhyodacite (this study), and the andesite (Richet et al., 1996).

measured at natural magmatic temperatures due to crystallization or volatile loss, but it can be measured at higher and lower temperatures so that data on magmatic temperatures can be interpolated for anhydrous liquids. For hydrous liquids, it must still be extrapolated using parameterizations such as the TVF equation or measured at high pressure using falling sphere viscometry. Dacitic magmas from arc volcanoes can contain up to 5 wt.% water prior to an eruption, which has a large influence on the style of eruption.

Viscosity is also a major control on the rates of magma transport, crystallization, and degassing. While laboratory experiments typically determine liquid viscosity,

magma also contains bubbles and crystals. The physical effects of crystals can be calculated (assuming a homogeneous distribution of rigid spherical inclusions) using the Einstein-Roscoe equation (e.g. Marsh, 1981). Bubble content can decrease the viscosity by as much as 0.6 log units for bubble contents up to 70% by volume (Stein and Spera, 2002). The complex coupling of liquid viscosity, diffusivity, and degassing kinetics play a major role in bubble dynamics (Mourtada-Bonnefoi et al., 2004). The actual nucleation and growth of bubbles is impossible to observe in nature because they occur within the magma conduit.

Degassing is an important consequence of magma ascent at shallow levels, when the liquid becomes saturated with volatiles. Two important aspects of the dynamics of degassing are bubble nucleation and growth. These are influenced by the non-linear response of melt properties, including viscosity, in decreasing the water content during the degassing process (Sparks et al., 1994; Wilding et al., 1995). There can be a strong increase in viscosity during degassing of a melt, and this increase can then act as a brake on the efficiency of degassing by diffusive means. Hence, the functional form of the effect of water content on viscosity is a critical parameter to measure in experiments using synthetic samples (Sparks et al., 1994).

The style and intensity of volcanic eruptions depend on the behavior and rate of the vesiculation. Several studies have shown that very violent eruptions may be the result of extreme volatile super-saturation during magma ascent (e.g. Mangan and Sisson, 2000). The process of magma vesiculation can control the pressure-depth interval over which the initiation of explosive degassing occurs (Mangan and Sisson, 2004). When magma becomes supersaturated, it can lead to explosive vesiculation, governed by

decompression rate and the efficiency of the exsolution of the volatiles forming the gas bubbles.

Mangan and Sisson (2000, 2004, 2005) have conducted several studies to understand the degassing process and how it leads to explosive eruptions in rhyolites and dacites. Their studies and others show that bubbles can form by either homogeneous nucleation or heterogeneous nucleation, where the bubbles nucleate on a crystal or other inclusion (Bagdassarov and Dingwell, 1993). Homogeneous nucleation is more difficult because it occurs in a uniform melt, requiring more energy. Sparks et al. (1994, 1997) suggested that homogeneous nucleation is required to get extreme super-saturation pressure, allowing for explosive vesiculation. Mangan and Sisson (2000) measured vesiculation in rhyolite samples with 5.2 wt.% water at 900ºC and 200 MPa. They found that dissolved water concentrations required for vesiculation are much higher than predicted, and that vesiculation is a combination of both types of nucleation, which depends on the crystallinity of the magma as it enters the conduit.

Sparks et al. (1994) suggested the possibility of a viscous resistance influencing the rate of bubble growth. This means it is important to determine the viscosity and water content at which viscous forces begin to obstruct bubble expansion during magma ascent which can lead to an eruption. Thomas et al. (1994) termed this process a "viscosity quench," where brittle failure would occur at a critical viscosity, suggested to be 10^9 Pa.s for decompression rates and timescales of typical explosive eruptions. For the dacitic samples of this study, this would occur at 1100 K for samples containing 0.1 wt% water, at 1000 K for 0.25 wt.% water, and at 950 K for 0.5 wt.% water. These water

contents are typical for matrix glasses at Santiaguito Dome Complex and Mt. St. Helens, averaging about 0.25 to 0.35wt.% (Anderson et al., 1995).

Thomas et al. (1994) also proposed that there is a very sharp pressure gradient where fragmentation occurs within a magma conduit that is due to the substantial increase of melt viscosity associated with degassing, from between 4 and 5 wt% prior to vesiculation to about 1.5 to 1.8 wt.% after vesiculation and fragmentation as recorded in pumice. The sharp viscosity increase with loss of water could be a critical factor due to the bubble volume limit at which fragmentation must occur, leading to explosive eruptions.

In summary, fragmentation may occur when the water contents are low, after substantial vesiculation has already occurred, causing an increase in the viscosity. This prevents more degassing, building up pressure and possibly leading to an explosive eruption. The extreme influence of water on viscosity means that degassing rhyolitic magmas, the subject of most experimental studies, will experience relatively low viscosities to a late stage in the actual degassing process (Dingwell et al., 1996). Zhang et al. (2003) created a model that considered both viscosity and bubble growth within rhyolitic liquids and found that the physical effect of bubbles on the viscosity is small. In order to truly understand degassing and the effects of bubble content, studies need to be conducted that involve measuring the viscosity of both anhydrous and hydrous samples, especially at low water contents, and then measuring the effects bubbles have on the same compositions. This will allow for more reliable answers on what is actually occurring during vesiculation and degassing in a magma conduit.

The data from this study can be applied to degassing of dacitic liquids (Figure 4.9). Water solubility and pressure were determined using solubility data (Figure 4.4) in conjunction with the CONFLOW numerical model (Mastin and Ghiorso, 2000). At a constant temperature of 1100 K, the melt can be saturated with 5 wt.% water at a pressure of 200 MPa (~8 km depth). When degassing occurs down to 50 MPa (~2 km depth), water solubility decreases to 2.2 wt% and the viscosity increases by about 2.5 log units. With continued equilibrium degassing to the surface, the viscosity can increase by a further 6.5 log units. Results for the dacite are similar. If disequilibrium degassing occurs, where slow homogenous nucleation delays vesiculation until a critical supersaturation is attained, vesiculation and degassing will occur rapidly, causing an extremely abrupt viscosity increase and rheological transition.

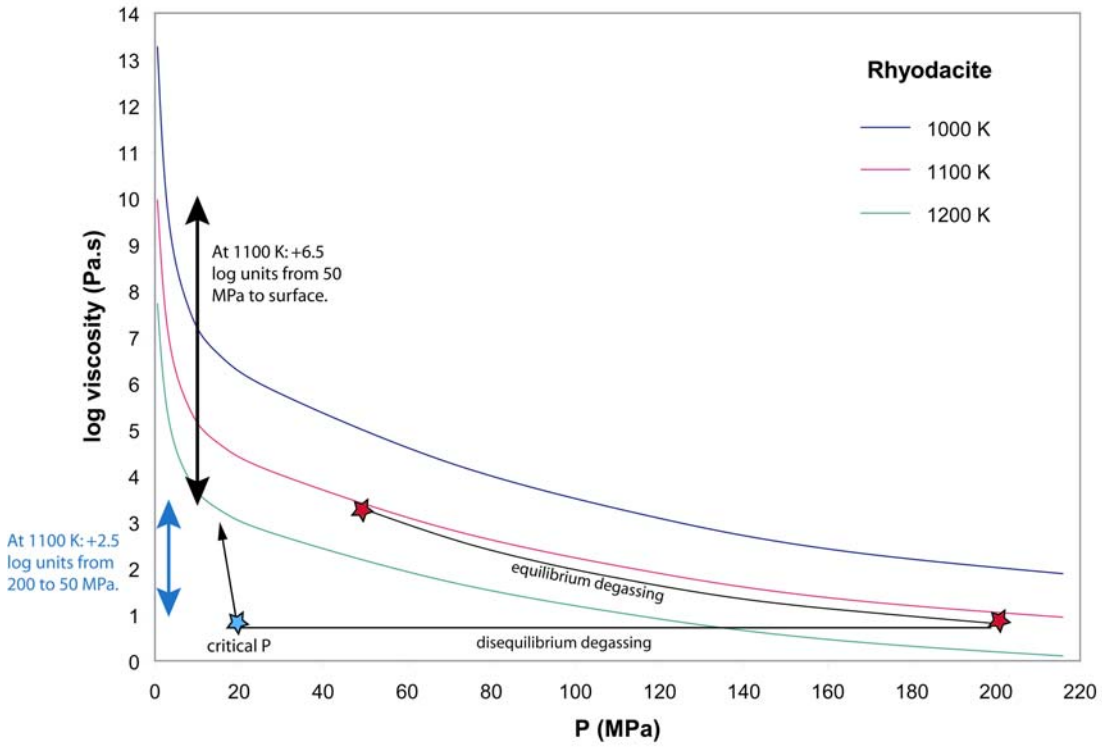

Figure 4.9. Log viscosity as a function of water content for constant temperatures of the rhyodacite. The lines are fitted lines to points calculated from the TVF equations of Table 3.5.

When excessive vesiculation occurs, it can lead to fragmentation when the magma contains about 75% bubbles. The height of fragmentation can be calculated using the equation $P = \rho gh$ where P is pressure, ρ is density, g is gravity (10 m/s^2), and h is the depth below the vent. The dataset from this study can be applied to calculate the height where fragmentation occurs. First, typical magmas at both Santiaguito and Mt. St. Helens contain approximately 0.25 wt.% water at the surface. Using the water solubility diagram show earlier, and the knowledge that the dacites contain 0.25 wt.% water, the saturation pressure (P) is found to be about 10 MPa. The density, ρ, of the magma without bubbles is roughly 2400 kg/m^3, so the density of the magma with 75% bubbles would be about 600 kg/m^3. The height of fragmentation is calculated to be of the order of 1.7 km, which reflects the depth in the magma conduit where the top of fragmentation occurs. Although the summit of Santiaguito is about 2700m above sea level, the dome complex is approximately 600 meters high, so the level of fragmentation should be at least 1 km below its base, but is probably above sea level. The level of fragmentation places a minimum constraint on the depth to the magma chamber.

4.6 Petrological applications 2: Rates of igneous processes

In the following discussion, we will consider likely end-member viscosities for rhyolitic, dacitic and andesitic liquids at 900ºC. Dacitic liquids have viscosities of 10^2 and 10^5 Pa.s for water contents of 5 and 0.5 wt.% respectively, constrained by this study (Figure 4.7c). In contrast, the viscosity of either andesitic or rhyolitic liquids is substantially higher, between $10^{4.5}$ and $10^{7.5}$, for the same water contents (Hess and Dingwell, 1996; Richet et al., 1996; Zhang et al., 2003). Most lavas of dacitic

composition are actually crystal-bearing rhyolitic liquids (e.g. Mt. St. Helens, see Melson, 1983), in which case their viscosities may be even greater.

4.6.1 Stokes Law

Viscosity affects magma differentiation by controlling the terminal settling velocity of crystals, which can float or sink, depending on the relative density of the crystals and the liquid. Stokes Law states that (Stokes, 1851):

$$v = 2r^2 g\Delta\rho/9\eta \qquad (4.6)$$

where v is the terminal velocity of the particles assuming they are smooth spheres, r is the radius of the particles, g is gravity, $\Delta\rho$ is the difference in density between the particle and melt driving the buoyant movement, and η is the viscosity of the magma. Terminal settling velocity is inversely related to viscosity.

In dacite magmas from Santiaguio, plagioclase and orthopyroxene are present as phenocrysts, and liquids are rhyolitic to dacitic at temperatures between 900ºC and 1000ºC, with water contents ranging from 0.5 to 5 wt.%. At 900ºC, the calculated viscosities of the rhyolite, rhyodacite, dacite and andesite are $10^{7.5}$, $10^{5.0}$, $10^{4.8}$, and $10^{7.6}$ Pa.s with 0.5 wt.% water, compared to $10^{4.2}$, $10^{1.0}$, $10^{1.5}$, and $10^{4.4}$ Pa.s with 5 wt.% water, respectively. At 1000ºC, the viscosities are $10^{6.2}$, $10^{3.8}$, $10^{3.6}$, and $10^{6.0}$ Pa.s for 0.5 wt.% water and $10^{3.5}$, $10^{0.5}$, $10^{0.8}$, and $10^{3.5}$ Pa.s for 5 wt.% water, respectively. The average density of plagioclase is around 2.7 g/cm^3 depending on the temperature and chemical composition, while the densities for the rhyolite, rhyodacite, dacite, and andesite range from 2.35 to 2.5 g/cm^3, dependent primarily on water content and temperature. The density difference between crystals and liquid therefore varies by a factor of 2 over the range of temperature and water content considered here.

Using the ranges for viscosity and density, and assuming a constant crystal size, one finds that crystal settling occurs 2 orders of magnitude faster in dacites than in rhyolites or andesites for a water content of 0.5 wt.% water. For melts containing 5 wt.%, settling occurs 3 orders of magnitude faster in dacites, at either 900 or 1000ºC. At all temperatures, plagioclase is denser and will therefore sink.

4.6.2 Critical Dike Width

Dike width is another important parameter controlled by viscosity. The less viscous a magma is, the narrower the minimum dike width necessary to prevent thermal lock up during melt flow, given by (Petford et al., 1993, 1994):

$$w_c = 1.5[c(T_{sol}-T_w)^2/L(T_{liq}-T_{sol})]^{3/4}(\eta kH/g\Delta\rho)^{1/4} \quad (4.7)$$

where w_c is the critical dike width, c is the specific heat, T_{sol} is the temperature at which a magma near the dike wall becomes mobile, T_w is the far-field wall rock temperature, T_{liq} is the initial temperature of the liquid, L is the latent heat of crystallization, η is the viscosity, k is the thermal diffusivity, H is the dike length, g is the gravity, and $\Delta\rho$ is the change in density between the wall rock and the magma. The viscosity in this case has a fourth root relationship to the dike width. As the viscosity increases, the critical dike width also increases.

Using the values discussed in section 4.6.1 for water contents of 0.5 and 5 wt.%, and holding everything other than density difference and viscosity constant, critical dike widths for different liquids can be compared. The difference in density between the wall rock (assumed to be 2.7 g/cm^3 (Scaillet et al., 1996)) and the magma ranges from 0.2 (andesite) to 0.4 g/cm^3 (haplogranite). With a viscosity range of 4 orders of magnitude, the critical width will vary by only 1 order of magnitude, which explains why most dikes

of igneous rock compositions are 10 cm to 10 m in width. Other variations ($\Delta\rho$, T, etc.) can be similar in magnitude to the effect of viscosity on the effect of dike width.

4.6.3 Ascent rate in dikes

The next process to be considered here is magma emplacement and the time that it can take for this to occur. The general form of this equation is (Petford et al., 1994):

$$V_{ave} = g\Delta\rho w^2/12\eta \quad (4.8)$$

where V_{ave} is the average velocity of the magma flow, g is the gravity, $\Delta\rho$ is the difference in the density between the magma and wall rock, w is the dike width, and η is the viscosity. Magma flow rate is inversely related to viscosity, so that as the viscosity increases, the emplacement of a given amount of magma must take a longer amount of time. As discussed in section 4.6.2, the minimum dike width is larger for more viscous magmas.

Magma emplacement can be estimated for Caliente, the active vent on Santiaguito Dome, using measured parameters and the results of this study. The ring fracture of Caliente is estimated to be 100 m in diameter with the magma conduit being 50 m in diameter (Bluth and Rose, 2004). The density of the dacitic glass in this study was 2441 kg/m^3 for 1 wt.% water at 900ºC, and the wall rock was estimated to be 2670 kg/m^3, making a density difference of 229 kg/m^3. Assuming that the magma in the conduit contains approximately 1 wt.% water at 900ºC, the liquid viscosity would be 10^4 Pa.s. Using these values, the calculated velocity of magma ascent is 48 m/s. This value is unrealistically high.

Using the same equation, the effective viscosity can be calculated from estimated extrusion rates. Bluth and Rose (2004) estimated the average extrusion rate through a 50

m conduit as 0.2 m^3/s, making the ascent velocity of the magma 10^{-4} m/s. Using the same parameters as above, the viscosity is estimated to be $10^{9.6}$ Pa.s. Based on the results of this study, this relatively high viscosity would be consistent with dacite liquid at 800ºC with 0.2 wt.% water. The actual lavas at Santiaguito have a rhyolitic liquid matrix containing about 40% crystals and 0.25 wt.% water (Anderson et al., 1995). Using the Hess and Dingwell (1998) model, the temperature can be approximated with these parameters and the estimated viscosity of $10^{9.6}$ Pa.s. The 40% crystal content will increase the viscosity about 2 log units calculated using the Einstein-Roscoe equation, and the temperature at which a rhyolite has a viscosity of $10^{7.6}$ Pa.s is calculated to be 1198.5 K, or 925ºC. Magma storage temperatures at Mt. St. Helens were calculated to be ~940±20ºC prior to the 1980 Plinian eruption based on oxide thermometry (Anderson et al., 1995).

4.6.4 Reynolds Number

Besides influencing the velocity of a lava, viscosity can also influence whether the lava flow is turbulent or laminar. The nature of the flow can be determined by the Reynolds number, which is the ratio of inertial and viscous forces acting on a fluid, given by:

$$\mathrm{Re} = Ud\rho/\eta \qquad (4.9)$$

where U is the velocity of the flow at a specific depth (height above the base of the flow, d), ρ is the density and η is the viscosity. The transition from laminar to turbulent flow in a pipe occurs when the Re increases above 2300. Low Re numbers mean that viscous forces dominate over inertial forces and the flow is laminar, which is favored when the magma has a high viscosity, while turbulence is favored by low viscosity magmas.

Silicate melts typically are laminar due to their high viscosity and relatively low flow velocities. At 1000ºC a dacitic liquid containing 5 wt.% water has a density of 2450 kg/m^3 and viscosity of 10 Pa.s. For U=0.5m/s and a d=10 m, the Reynolds number is 1225, falling in the laminar regime. Using the same velocity and depth, the viscosities of both andesite and rhyolite at 1000ºC is $10^{3.5}$ Pa.s, giving a Reynolds number of 4. Viscosity calculated for all of these compositions show that they are laminar, even at the highest likely temperatures and water contents. Hydrous dacites have a greater possibility of being turbulent compared to andesite and rhyolite due to their unusually low viscosities, but it is still unlikely. In fact, hydrous dacitic viscosity is similar to that of hot, dry basaltic pahoehoe flows on Hawaii (~10^2 Pa.s, Shaw, 1969).

4.6.5 Lava Flows

Viscosity is also a major control on the velocity of lava flows. The velocity can be calculated by (Francis and Oppenheimer, 2004):

$$v = \rho g t^2 / B\eta \sin\alpha \qquad (4.10)$$

The critical thickness for a flow to advance is given by:

$$t = \tau / \rho g \tan\alpha \qquad (4.11)$$

v is the velocity, ρ is the density of the lava, g is the gravity, B is a constant depending on how flat the surface is, η is the viscosity, τ is the yield strength and α is the topographic slope of the land surface. This equation again shows that viscosity is inversely related to the velocity.

The dacite lava flows at Santiaguito Dome complex travel extremely slowly due to their high viscosity. Typical average water contents found at Santiaguito Dome Complex as well as at Mt. St. Helens are about 0.25 wt.% water (Anderson et al., 1995).

The predicted viscosity for the rhyolite, rhyodacite, dacite and andesite with 0.25 wt.% water at 800ºC are $10^{9.4}$, $10^{7.2}$, 10^{7} and $10^{10.2}$ Pa.s, respectively. Note that surface flows and domes are cooler than pre-eruptive magma, and their temperatures extend down to ambient conditions. To understand the relative relationships between the compositions and velocity of the flow, all variables except density and viscosity are held constant in the following discussion. The density is similar for all compositions and has a minor effect on the velocity compared to viscosity, because it varies by less than 10% (equivalent to 0.04 log units).

With 0.25 wt.% water, the velocities of rhyolitic and andesitic flows are about 3 orders of magnitude slower than dacitic compositions. For strictly anhydrous liquids, the andesite will have the highest velocity, followed by the dacite and rhyodacite, and the rhyolite being the slowest. The rhyodacite and dacite velocity is more drastically affected by its water content. Compared to their anhydrous equivalents, 0.25 wt.% water will decrease the viscosity in dacitic liquids by 3 orders of magnitude, by only 2 orders of magnitude for rhyolitc liquids and only 1 order of magnitude for andesitic liquids. The velocities for all of these are typically less than 1 m/s. The Santiaguito lava flows advance very slowly, so that movement cannot be detected during observations on hour to day time scales.

As discussed above, viscosity is a controlling factor on the rates of many magmatic processes. Variable temperature and water content can have drastic effects on the viscosity. Though the lava flows at Santiaguito are rhyolitic liquids with crystals, the magma within the conduit is probably dacitic in nature. The results of this study show

that if the lava flows were dacitic, without crystals, the flow velocity would be significantly faster.

4.7 Summary

- Various parameterizations of hydrous melt viscosities were tested using data for dacitic liquids of this study, but none of them could satisfactorily reproduce the measured data.
- Calculated water solubilities of the rhyodacite, dacite, haplogranite, and andesite are similar at 1100 K, and increase with pressure.
- Previous studies of water speciation in dacites show that initial water dissolution is primarily as hydroxyl groups, followed by dissolution primarily as molecular water at larger total water contents. At about 3.8 wt.% water, both species are present in roughly equal concentrations in the glass. This is similar to other aluminosilicate compositions, including rhyolite and andesite liquids.
- Vesiculation and degassing are important processes that play a role in explosive volcanism. The rhyodacite can be saturated with 5 wt.% water at 200 MPa (6-8 km depth), but with only 2.3 wt.% water at 50 MPa (1.5-2 km depth), leading to a viscosity increase of 2.5 log units from $10^{1.0}$ to $10^{3.5}$ Pa.s at 1100K. If degassing continues to the surface, the liquid viscosity will increase drastically, to 10^{10} Pa.s.
- The results of this study have direct applications to common igneous processes. The rates of processes such as Stoke's Law crystal settling, magma ascent in a conduit, and the flow of lava, are inversely proportional to viscosity, and therefore can vary by orders of magnitude depending on changing water content, temperature and bulk composition. Critical dike width varies with the fourth root

of viscosity, and hence is much less affected by viscosity, so that similar dike widths are observed from granite and basaltic magmas with a wide range in temperature and volatile content. Processes such as Stoke's Law settling and magma ascent also depend on magma density, which varies only slightly with water content, temperature and bulk composition.

Chapter 5 will state the main conclusions from this study regarding the effects of water content, fluorine content, and variable composition on the viscosity of dacitic and rhyodacitic liquids.

CHAPTER 5 – CONCLUSIONS

5.1 Conclusions

Viscosity is one of the most important parameters affecting volcanic activity and is dominantly controlled by temperature, volatile content and melt composition. The purpose of this project was to determine the effects of water content, fluorine content, and variable composition on the viscosity of rhyodacitic and dacitic compositions. Synthetic dacite and rhyodacite glasses were made based on compositions from Santiaguito Dome Complex and their viscosity was measured using both parallel plate viscometry and concentric cylinder viscometry.

Viscosity measurements show that dacitic liquids behave in a non-Arrhenian manner. Dacitic liquids are more viscous than andesites and other depolymerized melts, but less viscous than rhyolites. Viscosity variations between different anhydrous melts are small at high temperatures (0.6 log units at 1200ºC), and more significant at lower temperatures (2 log units at 800ºC).

Typical magmas can contain up to 5 wt.% dissolved water, which decreases the viscosities of silicic melts. Liquids containing 1 and 5 wt.% dissolved water are about 5 and 7 orders of magnitude less viscous than anhydrous liquids, respectively. Dissolved water reduces the viscosity of dacites more than on andesites, but less than for rhyolites, indicating that highly polymerized liquids are more sensitive to dissolved water than less polymerized liquids.

Two series of glasses were prepared to determine the effects of slight variations in composition. Variable MgO and SiO_2 contents, and consequently polymerization states, were shown to affect liquid viscosity to a smaller degree relative to changing temperature

and water content, at least over the NBO/T range 0.10 to 0.31, for liquids with similar ratios of alkalis to alkaline earths. The viscosity decreases by less than 2 orders of magnitude at 1100 K when changing the NBO/T from 0.10 to 0.31, while 1 wt.% water decreases the viscosity by almost 5 orders of magnitude. This emphasizes the fact that determining the effect of volatile content is more important than slight compositional changes for dacitic and related liquids.

There is currently no reliable model to predict the viscosity of hydrous dacitic liquids. TVF equations were constructed for each of the hydrous samples, allowing estimation of viscosity at magmatic temperatures, but a parameterization for any temperature and water content was not successful.

The results of this study can be directly applied to volcanic processes such as vesiculation and degassing, which control the nature of explosive volcanism. Dacitic liquids can be saturated with 5 wt.% water at 200 MPa (6-8 km depth), but only at 2.3 wt.% water at 50 MPa (1.5-2 km depth), leading to a viscosity increase of 2.5 log units, from $10^{1.0}$ to $10^{3.5}$ Pa.s. If degassing continues to the surface, the liquid viscosity will increase drastically, to 10^{10} Pa.s.

The data measured also applies to rates of processes such as Stoke's Law of crystal settling, magma ascent in a conduit, and the flow of lava. All of these are inversely proportional to viscosity, and therefore can vary by orders of magnitude depending on the water content, temperature and bulk composition. Critical dike width varies with the fourth root of viscosity, and hence is not much affected by variable water content. Processes such as Stoke's Law of crystal settling and magma ascent also depend on magma density, which varies only slightly with water content, temperature and bulk

composition. Santiaguito lava flows actually have a slightly higher viscosity than predicted because the liquid is rhyolitic, not dacitic, and contains between 30 and 40% crystals with 0.25 wt% water. Using the Hess and Dingwell (1998) model, the temperature can be approximated with these parameters and the estimated viscosity of $10^{9.6}$ Pa.s. The 40% crystals will increase the viscosity about 2 log units (using the Einstein-Roscoe equation), so the temperature at which a rhyolite has a viscosity of $10^{7.6}$ Pa.s is calculated to be 925ºC, similar to pre-eruptive temperatures of Mt. St. Helens dacite. The magma chamber beneath Santiaguito may contain both dacitic liquid and crystal-bearing rhyolite. A trend of decreasing SiO_2 content may reflect tapping of deeper levels of this chamber (Harris et al., 2003),which would suggest lava flows will move faster and travel further as the current eruptive cycle/phase continues.

REFERENCES

Adam, G. and Gibbs J.H., 1965. On the temperature dependence of relaxation phenomena in glass-forming liquids. Journal of Chemical Physics, 43, 139-146.

Anderson, S.W., Fink, J.H., and Rose, W.I., 1995. Mount St. Helens and Santiaguito lava domes; the effect of short-term eruption rate on surface texture and degassing processes. Journal of Volcanology and Geothermal Research, 69, 105-116.

Angell, C. A., 1985. Strong and fragile liquids. In Relaxations in Complex Systems. (ed. K. L. Ngai and G. B. Wright) pp. 3–11, U.S. Department of Commerce National Technical Information Service.

Angell, C. A., 1991. Relaxation in liquids, polymers and plastic crystals - strong/fragile patterns and problems. Journal of Noncrystalline Solids, 131–133, 13–31.

Aoki, K., Ishikawa, K., and Kanisawa, S., 1981. Fluorine geochemistry of basaltic rocks from continental and oceanic regions and petrogenetic application. Contributions to Mineralogy and Petrology, 76, 53–59.

Bagdassarov, N., and Dingwell, D. B., 1993. Deformation of foamed rhyolites under internal and external stresses: An experimental investigation. Bulletin of Volcanology, 55, 147-154.

Bailey, J. C., 1977. Fluorine in granitic rocks and melts: A review. Chemical Geology, 19, 95–98.

Baker, D. R., 1998. Granitic melt viscosity and dike formation. Journal of Structural Geology, 20, 1395-1404.

Baker, D.R. and Vaillancourt, J., 1995. The low viscosity of F+H_2O-bearing granitic melts and implications for melt ex-traction and transport. Earth and Planetary Science Letters, 132, 199-21 1.

Behrens, H., 1995. Determination of water solubilities in high viscosity melts; an experimental study on $NaAlSi_3O_8$ and $KAlSi_3O_8$ melts. European Journal of Mineralogy, 7, 905-920.

Behrens, H., Romano, C., Nowak, M., Holtz, F., Dingwell, D.B., 1996. Near infrared spectroscopic determination of water species in glasses of the system $MAlSi_3O_8$ (M=Li, Na, K); an interlaboratory study. Chemical Geology, 128, 41-63.

Bluth, Gregg J. S. and Rose, William I, 2004. Observations of eruptive activity at Santiaguito volcano, Guatemala. Journal of Volcanology and Geothermal research, 136, 297-302.

Bottinga, Y., and Weill, D.F., 1972. The viscosity of magmatic liquids: a model for calculations. American Journal of Science, 272, 438-475.

Bouhifd, A., Whittington, A., Roux, J., and Richet, P., 2006. Effect of water on the heat capacity of polymerized aluminosilicate glasses and melts. Geochimica et Cosmochimica Acta, 70, 711-722.

Bowen, N.L., 1928. The Evolution of the Igneous Rocks. Princeton University Press, 332 pp.

Burnham, C. W., 1975. Water and magmas; a mixing model. Geochimica et Cosmochimica Acta, 39, 1077-1084.

Burt, D. M., Sheridan M. F., Bikun J. V., and Christiansen E. H.,1982. Topaz rhyolites distribution, origin and significance for exploration. Economic Geology, 77, 1818–1836.

Carroll, M.R., and Holloway, J.R., 1994. Volatiles in Magmas. Reviews in Mineralogy, 30, 517 pp.

Carroll, M. R. and Webster, J. D., 1994. Solubilities of sulphur, noble gases, nitrogen, chlorine and fluorine in magmas. Reviews in Mineralogy, 30, 231–279.

Congdon, R. D. and Nash, W. P., 1988. High-fluorine rhyolite: An eruptive pegmatite magma at the Honeycomb Hills, Utah. Geology, 16, 1018–1021.

Congdon, R. D. and Nash, W. P., 1991. Eruptive pegmatite magma: Rhyolite of the Honeycomb Hills, Utah. American Mineralogist, 76, 1261–1278.

Conway, M. F., Diehl, J. F., Rose, W. I., and Matias, O., 1994. Age and magma flux of Santa Maria Volcano, Guatemala; correlation of paleomagnetic wave forms with the 28000 to 25000 year B. P. Mono Lake excursion. Journal of Geology, 102, 11-24.

Dingwell, D. B., 1987a. The structure and properties of fluorine-rich magmas: A review of experimental studies. In Recent Advances in the Geology of Granite-Related Mineral Deposits (eds. R. P. Taylor and D. F. Strong), Mining Metal 39, 1–12. Washington, DC: Carnegie Institution of Washington.

Dingwell, D. B., 1987b. Melt viscosities in the system $NaAlSi_3O_8$-H_2OF_2O. 1. In Magmatic Processes: Physicochemical Principles (ed. B. O. Mysen), Geochemical Society Special Publication, 1, 423–433.

Dingwell, D. B., 1989. Effect of fluorine on the viscosity of diopside liquid. American Mineralogist, 74, 333–338.

Dingwell, D. B., 1995. Viscosity and anelasticity of melts. AGU Reference Shelf, 2, 209-217.

Dingwell, D. B. and Mysen, B.O., 1985. The effect of water and fluorine on the viscosity of albite melt at high pressure: A preliminary investigation. Earth and Planetary Science Letters, 74, 266–274.

Dingwell, D. B. and Webb, S. L., 1992. The fluxing effect of fluorine at magmatic temperatures (600–800°C): A scanning calorimetric study. American Mineralogist, 77, 30–33.

Dingwell, D. B. and Hess, K. U., 1998. Melt viscosities in the system Na-Fe-Si-O-F-Cl: Contrasting effect of F and Cl in alkaline melts. American Mineralogist, 83, 1016–1021.

Dingwell, D. B., Scarfe, M. C., and Cronin, D. J., 1985. The effect of fluorine on viscosities in the system Na_2O-Al_2O_3-SiO_2: Implications for phonolites, trachytes and rhyolites. American Mineralogist, 70, 80–87.

Dingwell, D. B., Knoche, R., and Webb, S. L., 1993. The effect of F on the density of haplogranite melts. American Mineralogist, 78, 325–330.

Dingwell, D. B., Bagdassarov, N.S., Bussod, G.Y., and Webb, S.L., 1993. Magma Rheology. In: Short course handbook on experiments at high pressure and applications to the Earth's mantle, Mineralogical Association of Canada Short Course, 21, 131-196.

Dingwell, D. B., Romano, C., and Hess, K.U., 1996. The effect of water on the viscosity of a haplogranitic melt under P-T-X conditions relevant to silicic volcanism. Contributions to Mineralogy and Petrology, 124, 19-28.

Dingwell, D. B., Holtz, F., and Behrens, H., 1997. The solubility of water in peralkaine and peraluminous granitic melts, American Mineralogist, 82, 434-437.

Dingwell, D.B., Hess, K-U. and Romano, C., 1998a. Viscosity data for hydrous peraluminous granitic melts: comparison with a metaluminous model. American Mineralogist, 83, 236-239.

Dingwell, D.B., Hess, K-U. and Romano, C. 1998b. Extremely fluid behaviour of hydrous peralkaline rhyolites. Earth and Planetary Science Letters, 158, 31-38.

Duncan T. M., Douglass D. C., Csenscits R., and Walker K. L., 1986. Study of fluorine in silicate glasses with 19F nuclear magnetic resonance spectroscopy. Journal of Applied Physics, 60, 130–136.

Fierstein, J., and Hildreth, W., 1992. The plinian eruptions of 1912 at Novarupta, Katmai National Park, Alaska. Bulletin of Volcanology, 54, 646-684.

Francis, P., and Oppenheimer, C., 2004. Volcanoes, Oxford University Press: Oxford, 521 pages.

Fugii, T. and Kushiro, I., 1977. Density, viscosity, and compressibility of basaltic liquid at high pressure, Carnegie Institution Washington Yearbook, 76, 419-424.

Fulcher, G. S., 1925. Analysis of recent measurements of the viscosity of glasses. Journal of American Ceramic Society, 8, 339-355.

Giordano, D., and Dingwell, D.B., 2003a. Viscosity of hydrous Etna basalt: implications for Plinian-style basaltic eruptions. Bulletin of Volcanology, 65, 8-14.

Giordano, D., and Dingwell, D.B., 2003b. Non-Arrhenian multicomponent melt viscosity: a model. Earth and Planetary Science Letters, 208, 337-349.

Giordano, D., Dingwell, D.B., Romano, C., 2000. Viscosity of a Teide phonolite in the welding interval. Journal of Volcanology and Geothermal Research, 103, 239–245.

Giordano, D., Romano, C., Dingwell, D.B., Poe, B., and Behrens, H., 2004. The combined effects of water and fluorine on the viscosity of silicic magmas. Geochimica et Cosmochimica Acta, 68, 5159-5168.

Giordano, D., Nichols, A. R., and Dingwell, D. B., 2005. Glass transition temperatures of natural hydrous melts: a relationship with shear viscosity and implications for the welding process. Journal of Volcanology and Geothermal Research, 142, 105-118.

Harris, A.J.L., Flynn, L.P., Matías, O. and Rose, W. I., 2002. The thermal stealth flows of Santiaguito: implications for the cooling and emplacement of dacitic block lava flows. GSA Bulletin, 114(5), 533-546.

Harris, A.J.L., Flynn, L.P. and Rose, W.I., 2003b. Temporal trends in Lava Dome Extrusion at Santiaguito 1922-2000. Bulletin of Volcanology, 65, 77-89.

Harris, A.J.L., Flynn, L.P., Matias, O., Rose, W.I., and Cornejo, J., 2004. The evolution of an active silicic lava flow field: an ETM+ perspective. Journal of Volcanology and Geothermal Research, 135, 147-168.

Head, J.W.I., and Wilson, L., 1987. Lava fountain heights at Pu'u 'O'o, Kilauea, Hawaii: Indicators of amount and variation of exsolved magma volatiles. Journal of Geophysical Research, 92, B13, 13715-13719.

Hess, K-U. and Dingwell, D.B., 1996. Viscosities of hydrous leucogranitic melts: A non-Arrhenian model. American Mineralogist, 81, p. 1297-1300.

Hess, K.-U., Dingwell, D. B., and Webb, S. L., 1995. The influence of excess alkalis on the viscosity of a haplogranitic melt. American Mineralogist, 80, 297–304.

Holtz, F., Dingwell, D. B., and Behrens, H., 1993. Effects of F, B_2O_3, P_2O_5 on the solubility of water in haplogranitic melts compared to natural silicate melts. Contributions to Mineralogy and Petrology, 113, 492–501.

Holtz, F., Dingwell, D. B., Behrens, H., and Johannes, W.,1995. H_2O solubility in haplogranitic melts: Compositional, pressure, and temperature dependence. American Mineralogist, 80, 94-108

Holtz, F., Roux, J., Ohlhorst, S., Behrens, H. and Schulze, F., 1999. The effects of silica and water on the viscosity of hydrous quartzofeldspathic melts. American Mineralogist, 84, 27-36

Huppert, H.E., Sparks, R.S.J., Turner, J.S., 1982. Effects of volatiles on mixing in calc-alkaline magma systems. Nature, 297, 554-557.

Johnson, J. B., Harris, A., Sahetepy-Engel, S., Wolf, R., and Rose, W. I., 2004. Explosion dynamics of pyroclastic eruptions at Santiaguito Volcano. Geophysical Research Letters, 31.

Kohn, S. C., Dupree, R., and Smith, M. E, 1989. Proton environments and hydrogen bonding in hydrous silicate glasses from proton NMR. Nature, 337, 539–541.

Kohn, S. C., Dupree, R., and Mortuza, M. G., 1992. The interaction between water and aluminosilicate magmas. Chemical Geology, 96, 399–409.

Kohn, S. C., Smith, M. E., Dirken, P. J., Van Eck, E. R. H., Kentgens, A. P. M., and Dupree, R., 1998. Sodium environments in dry andhydrous albitic glasses: Improved 23Na solid state NMR data and their implications for water dissolution mechanisms. Geochimica et Cosmochimica Acta 62, 79–87.

Kortemeier, W. T. and Burt, D. M., 1988. Ongonite and topazite dykes in the Flying W ranch area, Tonto Basin, Arizona. American Mineralogist, 73, 507–523.

Kushiro, I., Yoder, Jr., H.S. and Mysen, B.O., 1976. Viscosities of basalt and andesite melts at high pressures. Journal of Geophysical Research, 81, 6351-6356.

Lange, R.A., 1994. The effect of H_2O, CO_2 and F on the density and viscosity of silicate melts. In: Carroll, M.R. and Holloway, J.R. (editors), Volatiles in magmas. Reviews in Mineralogy, 30, p. 331-369.

Lejeune, A.M., 1994. Rheologie des magmas: influence des cristaux et des bulles en suspension. These, Universitt Paris 7, Paris, 216 pp.

Liebske, C., Behrens, H., Holtz, F., and Lange, R.A., 2003. The influence of pressure and composition on the viscosity of andesitic melts. Geochimica et Cosmochimica Acta, 67, 473-485.

Luth, R. W., 1988a. Raman spectroscopic studies of the solubility mechanisms of F in glasses in the system $CaO \cdot CaF_2$-SiO_2. American Mineralogist, 73, 297–305.

Luth, R. W., 1988b. Effects of F on phase equilibria and liquid structure in the system $NaAlSiO_4$-$CaMgSi_2O_6$-SiO_2. American Mineralogist, 73, 306–312.

Mangan, M., and Sisson, T., 2000. Delayed, disequilibrium degassing in rhyolitic magma: Decompression experiments and implications for explosive volcanism. Earth and Planetary Science Letters, 183, 441-455.

Mangan, M., and Sisson, T., 2004. Gas evolution in eruptive conduits: Combining insights from high temperature and pressure decompression experiments with steady-state flow modeling. Journal of Volcanology and Geophysical Research, 129, 23-36.

Mangan, M., and Sisson, T., 2005. Evolution of melt-vapor surface tension in silicic volcanic systems: Experiments with hydrous melts. Journal of Geophysical Research, 110, BO1202.

Marsh, B., 1981. On the crystallinity, probability of occurrence and rheology of lava and magma. Contributions to Mineralogy and Petrology, 78, 85-98.

Mastin, L. G., and Ghiorso, M. S., 2000. A Numerical Program for steady state flow of magma gas mixtures through vertical eruptive conduits, USGS Open-File Report 00-209.

Maxwell, J.C., 1867. On the dynamical theory of glasses. Philos. Transactions of the Royal Society of Edinburgh A: Math and Physical Science, 157, 49– 88.

McBirney, A.R., and Murase, T.,1984. Rheological properties of magmas. Annual Review of Earth and Planetary Sciences, 12, 337-357.

Melson, W. G., 1983. Monitoring the 1980-1982 eruptions of Mt. St. Helens compositions and abundances of glass. Science, 221, 1387-1391.

Mourtada-Bonnefoi, C.C., Mader, H.M., 2003. Experimental observations of the effect of crystals and pre-existing bubbles on the dynamics and fragmentation of vesiculating flows. Journal of Volcanology and Geothermal Research, 129, 83–97.

Mysen, B.O., 1988. Magmatic silicate melts: Relations between bulk composition, structure and properties. In: Mysen, B.O. (ed.), Magmatic Processes: Physicochemical Principles. Geochemical Society, Special Publication 1, p. 375-399.

Mysen, B. O., 1988. Structure and Properties of Silicate Melts, Elsevier, Amsterdam.

Mysen, B. O. and Virgo, D., 1985a. Interaction between fluorine and silica in quenched melts on the joints SiO_2-AlF_3 and SiO_2-NaF determined by Raman spectroscopy. Physics and Chemistry of Minerals, 12, 77– 86.

Mysen, B. O. and Virgo, D., 1985b, Structure and properties of fluorine-bearing aluminosilicate melts. The system Na_2O-Al_2O_3-SiO_2-F at 1 atm. Contributions to Mineralogy and Petrology, 91, 205–220.

Mysen, B. O. and Cody, G. D., 2001. Silicate-phosphate interation in silicate glasses and melts. II Quantitative, high temperature structure of P-bearing alkali aluminosilicate melts. Geochimica et Cosmochimica Acta, 65, 2413-2431.

Mysen, B. O., and Richet, P., 2005. Silicate glasses and Melts: Properties and Structure, Developments in Geochemistry, 10, Elsevier.

Mysen, B. O., Cody, G. C., Smith, A., 2004. Solubility mechanisms of fluorine in peralkaline and meta-aluminous silicate glasses and in melts to magmatic temperatures. Geochimica Cosmochimica et Acta, 68, 2745-2769.

Neuville, D.R., and Richet, P., 1991. Viscosity and mixing in molten (Ca, Mg) pyroxenes and garnets. Geochimica et Cosmochimica Acta, 55, 1011-1019.

Neuville, D.R., Courtial, P., Dingwell, D.B., and Richet, P., 1993. Thermodynamic and rheological properties of rhyolite and andesite melts. Contributions to Mineralogy and Petrology, 113, 572-581.

Nowak, M. and Behrens, H., 1995. The speciation of water in haplogranitic glasses and melts determined by in situ near-in-frared spectroscopy. Geochimica et Cosmochimica Acta, 59, 3445-3450.

Ohlhorst, S., Behrens, H., Holtz, F., 2001. Compositional dependence of molar absorptivities of near-infrared OH- and H_2O bands in rhyolitic to basaltic glasses. Chemical Geology, 174, 5 –20.

Persikov, E.S., Zharikov, V.A., Bukhtiyarov, P.G. and Pol'skoy, S.F., 1990. The effect of volatiles on the properties of mag-matic melts. European Journal of Mineralogy, 2, 621-642.

Persikov, E. S., 1991. The viscosity of magmatic liquids: Experiment generalized patterns, a model for calculation and prediction, applications. In Physical Chemistry of Magmas, Advances in Physical Chemistry (eds. L. L. Perchuk and I. Kushiro), 1−40. Springer, Berlin, Germany.

Petford, N., Kerr, R. C., and Lister, J. R., 1993. Dike transport of granitoid magmas. Geology, 21, 845-848.

Petford, N., Lister, J. R., and Ker, R. C., 1994. The ascent of felsic magmas in dykes. Lithos, 32, 161-168.

Pichavant, M., Valencia Herrera, J., Boulmier, S., Brique, L., Joron, J.-L., Juteau, M., Marin, L., Michard, A., Sheppard, S. M. F., Treuil, M., and Vernet, M., 1987. The acusani glasses, SE Peru: Evidence of chemical fractionation in peraluminous magmas. Geochemistry Society Special Publication, 1, 359–373.

Pinkerton, H. and Stevenson, R.J., 1992. Methods of determining the rheological properties of magmas at subliquidus temperatures. Journal of Volcanology Geothermal Research., 53, 47-66.

Richet, P., 1984. Viscosity and configurational entropy of silicate melts. Geochimicha et Cosmochimica Acta, 48, 471-483.

Richet , P., and Neuville, D.R., 1992. Thermodynamics of silicate melts; configurational properties. Advances in Physical Geochemistry, 10, 132-161.

Richet, P., and Y. Bottinga, Y., 1995. Rheology and configurational entropy of silicate melts. Reviews in Mineralogy, 32, 67-93.

Richet, P., Lejeune, A. M., Holtz, F., and Roux, J., 1996. Water and the viscosity of andesite melts. Chemical Geology, 128, 185-197.

Richet, P., Whittington, A., Behrens, H., Holtz, F., Ohlhorst, S., and Wilke, M., 2000. Water and the density of silicate glasses. Contributions to Mineralogy and Petrology, 138, 337-347.

Robert, E., Whittington, A., Fayon, F., Pichavant, M., and Massiot, D., 2001. Structural characterization of water-bearing silicate and aluminosilicate glasses by high-resolution solid-state NMR. Chemical Geology, 174, 291–305.

Romano C., Hess K-U., Mincione V., Poe B., and Dingwell D.B., 2001. The viscosities of hydrous $XAlSi_3O_8$ (X=Li, Na, K, $Ca_{0.5}$, $Mg_{0.5}$) melts. Chemical Geology, 174, 115-132.

Romano, C., Poe, B. T., Mincione, V., Hess, K. U., and Dingwell, D. B., 2001. The viscosities of dry and hydrous $XALSi_3O_8$ (X = Li, Na, K, $Ca_{0.5}$, $Mg_{0.5}$) melts. Chemical Geology, 174, 15-132.

Romano, C., Giordano, D., Papale, P., Mincione, V., Dingwell, D.B., Rosi, M., 2003. The dry and hydrous viscosities of alkaline melts from Vesuvius and Phlegrean Fields. Chemical Geology, 202, 23–38.

Rose, W.I., 1972b. Santiaguito volcanic dome, Guatemala, GSA Bulletin, 83, 1413-1434.

Rose, W.I., 1978a. Volcanic activity at Santiaguito Volcano, 1976-1984. In Fink, J.H., (ed.), The Emplacement of Silicic Domes and Lava Flows, GSA Special Paper, 212, 17-28.

Russell J. K., Giordano D., and Dingwell D. B., 2003. High-temperature limits on viscosity of non-Arrhenian silicate melts. American Mineralologist, 88, 1390–1394.

Scaillet, B., Holtz, F., Pichavant, M. and Schmidt, M., 1996. Viscosity of Himalayan leucogranites: implications for mechanisms of granitic magma ascent. Journal of Geophysical Research, 101, 27691-27699.

Scholze, H., 1956, Der Einbaudes Wassers in Glasem, 4th International Congress on Glass, 424-429.

Schulze F., Behrens H., Holtz F., Roux J., and Johannes W., 1996. The influence of H_2O on the viscosity of a haplogranitic melt. American Mineralogist, 81, 1155–1165.

Schulze F., Behrens H., and Hurkuck W, 1999. Determination of the influence of pressure and dissolved water on viscosity of high viscous melts. Application of a new parallel-plate viscometer. American Mineralogist, 84, 1512-1520.

Shaw, H.R., 1963. Obsidian-H_20 viscosities at 1000 and 2000 bars in the temperature range 700” to 900°C. Journal of Geophysical Research, 68, 6337-6343.

Shaw, H.R., 1969, Rheology of basalt in the melting range. Journal of Petrology, 10, p. 510-535.

Shaw, H.R., 1972. Viscosities of magmatic silicate liquids; an empirical method of prediction. American Journal of Science, 272, 870-893.

Shen A. and Keppler H., 1995. Infrared spectroscopy of hydrous silicate melts to 1000°C and 10 kbar: Direct observation of H_2O speciation in a diamond-anvil cell. American Mineralogist, 80, 1335-1338.

Silver, L.A., Ihinger, P.D., and Stolper, E., 1990. The influence of bulk composition on the speciation of water in silicate glasses. Contributions to Mineralogy and Petrology, 104, 142-162.

Sparks, R. S. J., Barclay, J., Jaupart, C., Madar, H. M., and Phillips, J. C., 1994. Physical aspects of magmatic degassing in: M.R. Carroll, J.R. Hollaway (Eds.), Volatiles in magmas, Mineralogical Society of America, 412-445.

Sparks, R. S. J., Bursik, M. I., Carey, J. S., Gilbert, J. S., Glaze, L. S., Sigurdsson, H., and Woods, A. W., 1997. Volcanic Plumes. John Wiley and Sons, Chichester, 574 pages.

Spera, F. J., 1974. A thermodynamic basis for predicting water solubilities in silicate melts and implications for the low velocity zone. Contributions to Mineralogy and Petrology, 145, 175-186.

Spera, F.J., 2000. Physical properties of magmas. In Encylopedia of Volcanoes, 171–90.

Stein, D. J., and Spera, F. J., 2002. Shear viscosity of rhyolite-vapor emulsions at magmatictemperatures by concentric cylinder rheometry. Journal of Volcanology and Geothermal Research, 113, 243-258

Stevenson, R.J., Bagdassarov, N.S., Dingwell, D.B., and Romano, C., 1998. The influence of trace amounts of water on the viscosity of rhyolites. Bulletin of Volcanology, 60, 89-97.

Stokes, G.G., 1851. On the effect of the internal friction of fluid on the motion of pendulums. Transactions of Cambridge Philosophical Society, 9: 8ff. (Reprinted in Mathematical and physical papers, vol III, pp 1±141. Cambridge University Press, 1901)

Stolper, E., 1982. Water in silicate glasses: An infrared spectroscopic study. Contributions to Mineralolgy and Petrology, 81, 1–17.

Sykes, D. and Kubicki, J. D., 1993. A model for H_2O solubility mechanisms in albite melts from infrared spectroscopy and molecular orbital calculations. Geochimica et Cosmochimica Acta, 57, 1039 –1052.

Sykes, D. and Kubicki, J. D., 1994. Reply to the comment by Kohn, S.C., Smith, M.E. and Dupree, R. on “A model for H2O solubility mechanisms in albite melts from infrared spectroscopy and molecular orbital calculations.” Geochimica et Cosmochimica Acta 58, 1381–1384.

Tammann, G., and Hesse, W., 1926. Die Abhängigkeit der Viskosität von der Termperatur bei unter kühlten Flüssigkeiten, Zeitschrift fuer anorganische und allgemeine Chemie, 156, 245-257.

Thomas, N., Jaupart C, and Vergniolle, S., 1994. On the vesicularity of pumice. Journal of Geophysical Research, 99, 15633-15644.

Van Groos, K., and Wyllie, P. J., 1967. Melting relationships in the system $NaAlSi_3O_8$-NaF-H_2O to 4 kb pressure. Journal of Geology, 76, 50-70.

Vogel, H., 1921. Das Temperaturabhängigkeitsgesetz der Viskosität von Flüssigkeiten. Physikalische Zeitschrift, 22, 645-646.

Whittington, A., Richet, P., and Holtz, F., 2000. Water and the viscosity of hydrous depolymerized aluminosilicate melts. Geochimica et Cosmochimica Acta, 64, 3725-3736.

Whittington, A., Richet, P., Linard, Y., and Holtz, F., 2001. The viscosity of hydrous phonolites and trachytes. Chemical Geology, 174, 209-224.

Whittington, A.G., Richet, P., Behrens, H., Holtz, F., and Scaillet, B., 2004. Experimental temperature-X(H_2O)-viscosity relationship for leucogranites, and comparison with synthetic silicic liquids. Transactions of the Royal Society of Edinburgh: Earth Sciences, 95, 59-72.

Wilding, M., Webb, S.L., Dingwell, D.B., 1995. Evaluation of a relaxation geospeedometer for volcanic glasses. Chemical Geology, 125, 137– 148.

Wyllie, P. J., and Tuttle, 1961. Experimental investigation of silicates containing two volatile components. II The effects of NH_3 and HF in addition to H_2O on the melting temperature of granite and albite. American Journal of Science, 259, 128-143.

Yamamoto K., Nakanishi T., Kasahara H., and Abe K., 1983. Raman scattering of SiF_4 molecules in amorphous fluorinated silicon. Journal of Non-Crystalline Solids, 59/60, 213–216.

Zhang, Youxue, Xu, Zhengjiu, and Liu, Yang, 2003. Viscosity of hydrous rhyolitic melts inferred from kinetic experiments and a new viscosity model, American Mineralogist, 88, 1741-175.

APPENDIX A – NIST STANDARD DATA TABLES AND CERTIFICATES

Table A.1. Low temperature viscosities of 717a borosilicate test run

Temp (K)	log η (Pa.s)
791.8	12.19[b]
792.4	12.27[a]
801.9	11.80[b]
802.4	11.89[a]
816.8	11.22[b]
817.0	11.30[a]
826.8	10.88[b]
827.0	10.92[a]
841.7	10.42[a]
842.0	10.35[b]
856.8	9.96[a]
857.2	9.87[b]
872.2	9.42[b]
872.2	9.50[a]
881.8	9.18[b]
883.6	9.15[a]

[a,b]For the standard, superscripts indicate measurements on 2 different cylinders

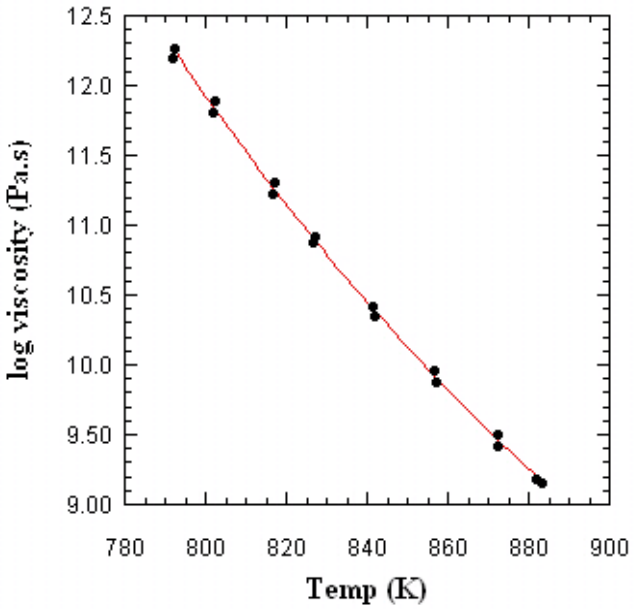

Figure A.1 Log viscosity as a function of temperature for 717a borosilicate glass. The points are measured data and the line is a fitted TVF equation. The equation for the average of runs A and B is: log η = [-2.26 + 4883.7/(T(K) – 455.7)]. The TVF equation for run A is: log η = [-2.28 + 4972.3/(T(K) – 448.9)] and for run B is: log η = [-2.23 + 4785.5/(T(K) – 462.9).

Table A.2
Accuracy and Precision determination

Temp (K)	Ref. TVF	TVFavg	Avg-Ref	TVF A	TVF B	A-B
792.05	12.30	12.26	0.04	12.21	12.31	0.10
802.10	11.86	11.84	0.02	11.80	11.88	0.08
816.85	11.25	11.26	0.01	11.23	11.29	0.06
826.85	10.87	10.90	0.03	10.88	10.92	0.04
841.80	10.34	10.39	0.05	10.38	10.40	0.02
856.98	9.84	9.91	0.07	9.90	9.91	0.01
872.19	9.37	9.47	0.09	9.47	9.46	0.00
882.65	9.07	9.18	0.11	9.18	9.17	0.01
		$AAD_{avg-ref}$:	**0.05**		**AAD_{A-B}:**	**0.04**

[1]$AAD_{avg-ref}$ is the absolute average deviation of the average of runs A and B subtracted from the reference TVF value (relates to the accuracy)
[2]AAD_{A-B} is the absolute average deviation of run A subtracted from run B (relates to the precision)

National Institute of Standards & Technology

Certificate

Standard Reference Material® 717a

Borosilicate Glass

This Standard Reference Material (SRM) is intended primarily to check test methods and to calibrate equipment for the determination of the viscosity of glass in accordance with ASTM Procedure C 965-81 [1]. A unit of SRM 717a consists of a borosilicate glass block with nominal dimensions: 40 mm x 40 mm x 150 mm, and a nominal mass of 570 g.

The certified viscosity values as a function of temperature were obtained from the results of seven cooperating laboratories, used to calculate a consensus fit of the Fulcher equation as follows:

$$\log_{10} [\text{viscosity (Pa·s)}] = -2.5602 + 4852.2/(t - 192.462)$$

where t is the temperature expressed in °C.

Expiration of Certification: This SRM has an indefinite room temperature shelf life. The certification of this SRM is deemed to be indefinite, provided the SRM is handled in accordance with information provided under the Cautions to User section. However, the certification will be nullified if the SRM is remelted, contaminated, or otherwise modified.

Cautions to User: This SRM, like many borosilicates, is susceptible to volatilization at high temperature, especially above 1400 °C. Care should be taken to ensure that the SRM not be exposed for prolonged periods of time to temperatures near or above 1400 °C since there may be some time dependence to the volatilization. Experience has shown that volatilization will also occur with repeated remelting of the glass, remelting will invalidate the certification.

The glass for this SRM was obtained from Corning Inc., Corning, NY. The interlaboratory measurements leading to certification were performed under the auspices of ASTM Subcommittees C14.04 on Physical and Mechanical Properties of Glass and C14.91 on Glass Reference Materials.

Technical coordination of the certification of this SRM was performed by M.J. Cellarosi of the NIST Ceramics Division with the support of A.E. Siefert, ASTM C14.91 Research Associate.

Statistical evaluation was performed by L.M. Gill of the NIST Statistical Engineering Division.

The support aspects involved in the certification and issuance of this SRM were coordinated through the Standard Reference Materials Program by R.J. Gettings.

Gaithersburg, MD 20899
Certificate Issue Date: September 18, 1996
(Revision of certificate dated 8-7-95)

Thomas E. Gills, Chief
Standard Reference Materials Program

From the consensus fit of the Fulcher equation on page 1, the certified viscosity values versus temperature were calculated and are listed below in Table 1. The certified uncertainties are the 95 % simultaneous confidence intervals for the Fulcher equation. Noncertified viscosity values for the temperature range of 834 °C to 540 °C and borosilicate glass fixpoint temperatures are given for information only in Tables 2 and 3.

Table 1. Certified Viscosity

$\log_{10}$ [viscosity (Pa·s)][a]	Temperature (°C)
1.00 ± 0.06	1555
1.25 ± 0.06	1466
1.50 ± 0.07	1388
1.75 ± 0.08	1318
2.00 ± 0.10	1256
2.25 ± 0.11	1201
2.50 ± 0.12	1151
2.75 ± 0.13	1106
3.00 ± 0.14	1065
3.25 ± 0.14	1028
3.50 ± 0.15	993
3.75 ± 0.15	961
4.00 ± 0.16	932
4.25 ± 0.16	905
4.50 ± 0.17	880

[a]The SI unit for viscosity is Pa·s [2]. To convert to poise from Pa·s multiply by ten. The viscosity in Table 1 is expressed in the customary manner as $\log_{10}$ viscosity. If $\log_{10}$ [viscosity (Pa·s)] = 1.0 ± 0.06 then $\log_{10}$ [viscosity (poise)] = 2.0 ± 0.06.

INFORMATION VALUES

The following laboratory data provided by one of the round robin participants is given for information purposes and is not certified. Fulcher fit of beam bending [3] and parallel plate viscometry [4] data using a 5 °C/min heating rate for the range 1 x 10^{13} Pa·s through 1 x 10^{5} Pa·s was:

$$\log_{10}[\text{viscosity (Pa·s)}] = -3.012 + 5495.3/(t\text{-}148.1)$$

From the fit to that laboratory data, the following viscosity values were calculated:

Table 2. Noncertified Viscosity

$\log_{10}$ [viscosity (Pa·s)]	Temperature (°C)
5	834
6	758
7	697
8	647
9	606
10	570
11	540

The fixpoint temperatures as measured by ASTM Test Methods C 336 [5], C 338 [6], and C 598 [7] are:

Table 3. Fixpoint

Fixpoint	Temperature (°C)
Softening Point	719 ± 5
Annealing Point	513 ± 6
Strain Point	470 ± 9

The uncertainties given for the fixpoint temperatures are the 95 % confidence intervals of the interlaboratory mean temperatures.

Table 4. Glass Nominal Composition

Element	Mass Fraction (%)
SiO_2	68.0
B_2O_3	18.5
K_2O	8.0
Na_2O	1.0
Al_2O_3	3.5
Li_2O	1.0

Index of Refraction $N_D = 1.487$

Cooperating Laboratories:

Corning Inc., Corning, NY
Ferro Corp., Independence, OH
Monarch Analytical Laboratories Inc., Toledo, OH
OSRAM/Sylvania Inc., Danvers, MA
Owens Corning Fiberglass, Granville, OH
PPG Industries Inc., Pittsburgh, PA
Schuller Corp., Littleton, CO

REFERENCES

[1] ASTM Standard C 965-81, "Standard Practice for Measurement of Viscosity of Glass Above the Softening Point," Annual Book of ASTM Standards, Vol. 15.02, ASTM, Philadelphia, PA, (1990).

[2] Taylor, B.N., Guide for the Use of the International System of Units (SI), NIST Special Publication 811, 1995 Ed., (April 1995).

[3] Hagy, H.E., "Experimental Evaluation of Beam-Bending Method of Determining Glass Viscosities in the Range 10^8 to 10^{15} Poise," J. Am. Ceram. Soc., **46 (2)**, p. 93, (1963).

[4] Fontana, E.H., "A Versatile Parallel-Plate Viscometer for Glass Viscosity Measurements to 1000 °C," Bull. Am. Ceram. Soc., **49 (6)**, p. 594, (1970).

[5] ASTM Standard C 336-71, "Standard Test Method for Annealing Point and Strain Point of Glass by Fiber Elongation," Annual Book of ASTM Standards, Vol. 15.02, (1991).

[6] ASTM Standard C 338-93, "Standard Test Method for Softening Point of Glass," Annual Book of ASTM Standards, Vol. 15.02, (1993).

[7] ASTM Standard C 598-93, "Test Method for Annealing Point and Strain Point of Glass by Beam Bending," Annual Book of ASTM Standards, Vol. 15.02, (1993).

National Institute of Standards & Technology

Certificate

Standard Reference Material 710a

Soda-Lime-Silica Glass

This Standard Reference Material (SRM) is primarily intended to check test methods and to calibrate equipment for the determination of the viscosity of glass in accordance with ASTM Procedure C965. The SRM is a soda-lime-silica glass 100 x 100 x 40 mm (4 x 4 x 1.5 inches).

The certified viscosity is based on results from ten cooperating laboratories. Fitted results from eight laboratories were used to calculate a consensus fit of the Fulcher equation given below and the certificate viscosity-temperature values.

The certified $\log_{10}$ viscosity values versus temperature are:

Log_{10} Viscosity (poise)	Temperature, T (°C)
2.00 ± .015	1464
2.10 ± .014	1432
2.25 ± .012	1387
2.50 ± .010	1319
2.75 ± .008	1259
3.00 ± .008	1205
3.25 ± .008	1157
3.50 ± .009	1113
4.00 ± .011	1037
4.50 ± .013	973
5.00 ± .016	918

The consensus fit to the Fulcher equation is:

$$\text{Log}_{10}\ \text{Viscosity (poise)} = -1.729 + \frac{4560.}{(T\ °C - 240.8)}$$

The certified Softening Point temperature as measured by ASTM Test Method C338 is:

Softening Point = 730.6 ± 1.3 °C ($\log_{10}$ viscosity poise = 7.6)

Note: $10^{7.6}$ poise = $10^{6.6}$ Pa•s

The uncertainties stated above are two standard deviations of the listed values.

NIST measurements and technical coordination for this SRM were performed by M.J. Cellarosi, NIST Ceramics Division. Statistical analysis was performed by R.C. Paule, NIST Statistical Engineering Division. The support aspects involved in the certification, and issuance of this SRM were coordinated through the Standard Reference Materials Program by R.L. Gladhill.

March 20, 1991
Gaithersburg, MD 20899

William P. Reed, Acting Chief
Standard Reference Materials Program

SUPPLEMENTAL INFORMATION

The glass for this standard was donated by Schott Glass Technologies Inc., Duryea, Pennsylvania. The annealing and strain points as defined in ASTM Test Methods C336 and C338 were measured by several of the participating laboratories. These values are not certified, but provided for information only.

Annealing Point = 545 °C
Strain Point = 504 °C

Index of Refraction N_D = 1.5231
Dispersion V_D = 58.5

Glass Nominal Composition

Element	Wt. %
SiO_2	67.55
Al_2O_3	2.10
Na_2O	8.05
K_2O	9.30
CaO	8.50
ZnO	3.60
TiO_2	0.40
As_2O_3	0.05
Sb_2O_3	0.20

The interlaboratory comparison measurements leading to certification were performed under the auspices of ASTM Subcommittee C14.04 on Physical and Mechanical Properties of Glass, H.E. Hagy, Chairman. The laboratories that cooperated in the measurements are:

Alfred University, Alfred, New York
Anchor Hocking Corp., Lancaster, Ohio
Brockway Glass Co., Brockway, Pennsylvania
Corning Inc., Corning, New York
Ferro Corp., Independence, Ohio
National Inst. of Standards & Technology, Gaithersburg, MD
Owens-Corning Fiberglas Corp., Granville, Ohio
Owens-Illinois Inc., Toledo, Ohio
PPG Industries Inc., Pittsburgh, Pennsylvania
Schott Glass Technologies Inc., Duryea, Pennsylvania

List of References

1) ASTM Designation C965, Measuring Viscosity of Glass Above the Softening Point.
2) ASTM Designation C338, Softening Point of Glass.
3) ASTM Designation C336, Annealing Point and Strain Point of Glass by Fiber Elongation.
4) ASTM Designation C162, Standard Definitions of Terms Relating to Glass and Glass Products.
5) ASTM Designation C598, Annealing Point and Strain Point of Glass by Beam Bending.